INL/RPT-24-76187
Revision 0

Startup Physics Testing of Advanced Reactors

January 2024

A Survey of Historical Practices

S. E. Bays, M. K. H. Jaradat, F. N. Gleicher, I. Trivedi,
R. H. Stewart, N. P. Martin, S. G. Weir, J. Rymer
Idaho National Laboratory

A. Weitzberg
Private Consultant

NRIC | INL Idaho National Laboratory

INL is a U.S. Department of Energy National Laboratory operated by Battelle Energy Alliance, LLC.

DISCLAIMER

REVISION LOG

Revision No.	Date	Affected Pages	Description

Page intentionally left blank

EXECUTIVE SUMMARY

This report documents the startup physics testing from initial fuel loading through ascension to full power for past advanced reactor startup physics testing programs. The review includes an assessment of what nuclear physics data was measured, why this data was measured, how the measurement was made, and the agreement with predictive reactor performance calculations of that time. The purpose of this review is to establish historical precedence for test inclusion for consideration by future advanced reactors planned for demonstration in the National Reactor Innovation Center. The historical review includes reactor designs considered to be significantly different from current light-water reactor designs or using simplified, inherent, passive, or other innovative means to accomplish their safety functions.

Several measurement types are mutually consistent across all reactor designs assessed irrespective of reactor type, time, or country:

- Inverse multiplication (1/M) approach to critical mass
- Quantification of control rod (or drum) reactivities
- Reactor power or neutron flux levels using in-core and ex-core detectors
- Temperature and power coefficients of reactivity
- Power and temperature response to changes in coolant flow

There are several principal observations that provide background to the purpose of these tests. The observations are consistent for all reactors reviewed in this report and are also generally true of other startup physics testing reports found in literature but not covered in this report. There is one observation common to all reactors, whether they have control rods or drums installed during fuel loading. They all have operating instrumentation and control systems that can insert negative reactivity by mechanical means or injecting poison, sufficient to terminate any inadvertent criticality or potential reactivity insertion accidents.

- Some of the reactors did not have all control rods installed during fuel loading. However, those rods that were installed had an adequate shutdown margin for fuel loading and could be inserted given a scram signal.

- For all reactors, except Fort St. Vrain, the fuel was loaded in a subcritical state with control rods (or drums) inserted. These control rods (or drums) would then be fully withdrawn after each loading to quantify the shutdown margin. The process was repeated until the critical fuel loading (i.e., the critical mass) was achieved.
- For all fuel loadings, operators ensured that the instrumentation and control system included neutron detectors that are sufficiently sensitive during the loading sequence and could initiate a scram signal to the operable control rods used to ensure shutdown during fuel loading. All reactors used one or more neutron sources with sufficient activity to give a statistically meaningful count rate at the startup detectors.
- All reactors measured control rod (or drum) reactivities started from a critical state then withdrew the rod (or drum) to be measured to make the core supercritical on a positive period. The inverse kinetics method was then used to convert a stable period to a reactivity worth.
- Some reactors used subcritical methods, such as the pulsed source and modified source multiplication methods, in addition to the inverse kinetics method.
- All reactors, except SNAP10A, assessed control rod interference effects by moving rods individually and by moving neighboring rods together.
- All reactors except the Molten Salt Reactor Experiment used in-core activation monitors or flux detectors to measure flux or power distributions. Frequently, these measurements were also used to calibrate the flux detected in ex-core detectors with the core average fission rate.

There are several lessons learned mentioned in the original startup physics test reporting. These are included here as supplemental information to current and future reactor developers:

- The Fort St. Vrain reactor did not load to critical mass. Instead, cans of boron carbide were loaded into control rod holes at certain points in the fuel loading to ensure a prescribed subcriticality margin. Not all control rods were installed. Those that were installed were connected to actuators in the fully removed (i.e., uncontrolled) position. These control rods could be inserted given a scram signal. The test resulted in a concave up 1/M plot.
- Fort St. Vrain also performed a 1/M measurement using control rods. This measurement was performed with a fully loaded core and resulted in a nonconservative concave down 1/M plot. This nonconservative plot led to the discovery that differences in control rod insertions between inner and outer control rod banks would cause the ex-core detectors to not indicate the true reactor power. As a result, administrative controls were placed on control rod motion.

- The High Temperature Engineering Test Reactor (HTTR) mispredicted the critical mass, as measured by the 1/M approach to critical process. Later it was realized that nitrogen impurities in the fuel blocks and boron impurities in the graphite dummy blocks were not accurately characterized in the predictive computer models.
- During the non-nuclear tests, prior to loading fuel, the HTTR found that cold helium bypass flow for cooling the control rod standpipes in the vessel head was insufficient. This caused excessive heating of the biological shield above the core. The bypass coolant system was redesigned to ensure proper cooling.
- During the rise-to-power tests, the HTTR discovered that the temperature of the core support plate was significantly greater than predicted. Further analysis allowed the temperature limit to be increased.
- The Molten Salt Reactor Experiment measurements showed the significance of delayed neutrons to core reactivity. Critical mass and control rod worths were quantified for both flowing and non-flowing fuel.
- The System for Nuclear Auxiliar Power and the Experimental Breeder Reactor II both performed startup physics testing with and without the liquid metal coolant.
- The System for Nuclear Auxiliary Power, Experimental Breeder Reactor II, and HTTR benefited from extensive zero-power critical assembly tests, which were prototypic of the actual reactor. These testbeds were used to validate simulation and design codes. In some instances, the zero-power critical assemblies were used to predict measurements in the actual startup physics test program. Though the zero-power assemblies were a predictive asset, they were not part of the actual startup physics testing program.
- The Superphénix control rod reactivity worths were significantly less than designed. Transport equivalent cross sections were developed to correct for inaccuracies in the modeling software. Effectively, the calculated reactivity values were calibrated to the measured values.

ACKNOWLEDGEMENTS

This document was sponsored by the National Reactor Innovation Center (NRIC). NRIC is a national program funded by U. S. Department of Energy's Office of Nuclear Energy and is dedicated to the demonstration and deployment of advanced nuclear energy.

Page intentionally left blank

CONTENTS

FIGURES

TABLES

Page intentionally left blank

ACRONYMS

1/M	inverse multiplication
ARE	Aircraft Reactor Experiment
C/E	Computed divided by experimentally measured value
CFR	Code of Federal Regulations
DOE	U. S. Department of Energy
EBR-II	Experimental Breeder Reactor II
FS	Flight System
FSV	Fort St. Vrain
FTC	fuel temperature coefficient
HEU	highly enriched uranium
HTGR	high-temperature gas reactor
HTTR	High Temperature Engineering Test Reactor
ITC	isothermal temperature coefficient
JTC	Joint Test Group
LEU	Low Enriched Uranium
LMFBR	Liquid Metal Fast Breeder Reactor
LMR	liquid-metal reactor
LWR	light-water reactor
MSM	modified source multiplication method
MSRE	Molten Salt Reactor Experiment
MTC	moderator temperature coefficient
NRC	Nuclear Regulatory Commission
NRIC	National Reactor Innovation Center
ORNL	Oak Ridge National Laboratory
PCRV	prestressed concreate reactor vessel
PWR	pressurized-water reactor
RG	Regulatory Guide
RPF	radial peaking factor
SCA	SNAP Critical Assembly
SNAP	System for Nuclear Auxiliary Power
SNR	startup notification report
SPND	self-powered neutron detector
SSC	systems, structures, and components
TRISO	tristructural isotropic

VHTRC	Very High Temperature Reactor Critical Assembly
ZPR	Zero-Power Reactor

Page intentionally left blank

Startup Physics Testing of Advanced Reactors

INTRODUCTION

Reactors are considered advanced if they have design features significantly different from light-water reactors (LWRs) or use simplified, inherent, passive, or other innovative means to accomplish their safety functions. All reactors undergo startup physics testing to provide evidence that the as-built reactor conforms to design expectations.

To ensure safety, such novel design features need to be verified prior to their application in hazard mitigation during operation of the reactor. This verification is done through a process known as startup physics testing. In startup physics testing, systems, structures, and components (SSCs) are tested when the reactor is at a power level sufficiently low that reactor safety is not reliant on the successful demonstration of the SSC to perform its safety function. Upon completion of the test, the reactor is considered ready to be operated at a greater power level, hotter temperature, and higher coolant pressure. The startup physics test plan is organized into a series of hold points of increasing power, temperature, and pressure. Each hold point verifies that the SSCs are ready to mitigate hazards at the next energetic hold point.

The Startup Physics Test Program

Startup physics testing is a normal part of new reactor commissioning. Extensive testing is done prior to normal operation of all reactors. A subset of this testing is performed following maintenance and refueling outages. Regardless of reactor type, there is a common cadence of the startup physics testing. Startup test programs will vary from the general list based on design-specific features. Tests are performed at power levels and state points appropriate to the specific design. A list of common measurements is:

- Hot functional tests
- Fuel loading
- Control element worths and calibration
- Excess reactivity and shutdown margin
- Kinetics parameters
- Reactivity coefficients
- Power, temperature, and flow distributions
- Natural circulation, if applicable
- Reactor stability
- Response during pump startup and coast down.

More details of startup physics testing guidance are offered by the U.S. Nuclear Regulatory Commission (NRC) Regulatory Guide (RG) 1.68. This document is largely focused on LWR startups, but the genesis of this document precedes the NRC and was originally drafted to support liquid-metal reactors (LMRs) or high-temperature gas reactors (HTGRs). RG-1.68 does contain guidance for first-of-a-kind testing for plants licensed under 10 Code of Federal Regulations (CFR) 50 or 10 CFR 52. The American National Standard Institute and American Nuclear Society standard ANSI/ANS-19.6.1, “Reload Startup Physics Tests for Pressurized Water Reactors,” also identifies best practices for nuclear measurements following core refueling in pressurized-water reactors (PWRs). The measured quantities in ANS-19.6.1 are nearly universal in all reactors. However, some of the test methods listed in ANS-19.6.1 are specific to PWRs.

Appendix A of this report provides a tutorial review of startup physics testing fundamentals. The tutorial provides context to why various reactor parameters are measured during startup physics testing.

Regulatory Expectations for Startup Physics Testing

Different sections of the CFR describe the requirement to test nuclear reactors prior to full-power operation in similar language. In every instance, the language generally describes the need to gain verifiable knowledge of the behavior of all SSCs deemed necessary to safe and reliable operation prior to approval by the applicable regulatory body.

Two-Step Licensing

The two steps of licensing pursuant to 10 CFR 50 are obtaining a construction permit and obtaining an operating license. Upon a satisfactory review of the Preliminary Safety Analysis Report and the Environmental Assessment, and antitrust statements, the NRC issues a construction permit. The applicant then applies for an operating license, which the NRC grants only after it is satisfied that the plant design will perform safely and with acceptable environmental impacts at the chosen site as documented in the Final Safety Analysis Report.

For design certifications under 10 CFR 50, the applicant's license will be approved if "performance of each safety feature of the design has been demonstrated through either analysis, appropriate test programs, experience, or a combination thereof," as stated in 10 CFR 50.43(e)(1)(i). Also, it will be approved if "sufficient data exist on the safety features of the design to assess the analytical tools used for safety analyses over a sufficient range of normal operating conditions, transient conditions, and specified accident sequences, including equilibrium core conditions," as stated in 10 CFR 50.43(e)(1)(iii). From 10 CFR 50.43(e)(2), "if a prototype plant is used to comply with the testing requirements, then the NRC may impose additional requirements on siting, safety features, or operational conditions for the prototype plant to protect the public and the plant staff from the possible consequences of accidents during the testing period."

Combined Operating and Construction Licenses

The combined license process, pursuant to 10 CFR 52, combines the construction permit and operating license, with certain conditions, into a single license. An application for a combined license may include a standard design certification, an early site permit, both, or neither. The approach is intended to allow for early resolution of safety and environmental issues. Operation of the nuclear reactor is still conditional upon verification via inspections, tests, analyses, and acceptance criteria.

Standard design certifications under 10 CFR 52 may be approved with either separate effects or integral system tests, prototype tests, or a combination of tests, analyses, and operating experience. Such a priori testing (i.e., prior to startup physics testing) implements the NRC's policy on "proof of performance" testing for all advanced reactors with the goal of resolving all safety issues before authorizing construction, see RG-1.68. From 10 CFR 52.47(b)(1) and 10 CFR 52.54(a)(5), the Commission may issue a standard design certification in the form of a rule for the design that is the subject of the application if:

> The proposed inspections, tests, analyses, and acceptance criteria that are necessary and sufficient to provide reasonable assurance that, if the inspections, tests, and analyses are performed and the acceptance criteria met, a facility that incorporates the design certification has been

> constructed and will be operated in conformity with the design certification, the provisions of the Act, and the Commission's rules and regulations.

For reactor designs that are not evolutionary modifications of LWRs, 10 CFR 52.47(c)(2):

> An application for certification of a nuclear power reactor design that differs significantly from the light-water reactor designs described in paragraph (c)(1) of this section or uses simplified, inherent, passive, or other innovative means to accomplish its safety functions must provide an essentially complete nuclear power reactor design except for site-specific elements such as the service water intake structure and the ultimate heat sink, and must meet the requirements of 10 CFR 50.43(e).

Department of Energy

The Department of Energy (DOE) operates nuclear facilities, both reactor and non-reactor, regulated by 10 CFR 830. Reactors that are not regulated by DOE are those regulated by the NRC, Navy nuclear propulsion, or activities related to launch approval and actual launch of reactors into space per 10 CFR 830.2.

For DOE-regulated nuclear facilities, the contractor responsible for a nuclear facility must, "establish and maintain the safety basis for the facility" and "identify and analyze the hazards associated with the work," see 10 CFR 830, Subpart B.

10 CFR 830.3 defines surveillance requirements as "requirements relating to test, calibration, or inspection to ensure that the necessary operability and quality of safety SSCs and their support systems required for safe operations are maintained, that facility operation is within safety limits, and that limiting control settings and limiting conditions for operation are met."

Acceptance testing is defined by DOE-STD-1189-2016, Integration of Safety into the Design Process, Section 4.5.4: "Inspections, tests, and acceptance criteria shall be developed by the design organization for validating that functional requirements and performance criteria are met for all [Systems, Structures, Components] SSCs important to safety."

Startup physics test planning serve an important part of readiness reviews per DOE O 425.1D, Verification of Readiness to Startup or Restart Nuclear Facilities, Section 4.f, to ensure: "a program is in place to confirm and periodically reconfirm the condition and operability of Vital Safety Systems. This includes examinations of records of tests and calibration of these systems. The material condition of all safety, process, and utility systems is adequate to support the safe conduct of work."

For capital asset projects, DOE G 413.3-23, "Nuclear Facilities Commissioning," offers a phased checkout, testing, and commissioning plan in preparation for the acceptance and turnover of the SSCs produced by the project before startup. This guide document recommends forming a Joint Test Group (JTG), comprised of key stakeholder organizations, including operations, engineering, environmental, quality assurance, design authority, and DOE. The JTG provides oversight of the commissioning test program and works with stakeholders to ensure a timely resolution of related issues. This guide endorses NRC RG-1.68 as providing acceptable test requirements. The JTG actively contributes to the management of test requirements.

Idaho National Laboratory Processes

Idaho National Laboratory uses management control process, MCP-9902, to ensure the appropriate type of readiness review is completed per DOE O 425.1D. A readiness review is required for the initial startup of a newly constructed nuclear facility or restart following the

conversion of an existing nuclear facility. This readiness review needs to be presented following template TEM-9902-A at least 12 months prior to the planned startup or restart date. A startup notification report (SNR) must be prepared and updated every three months using TEM-9902-B as a template. The SNR is updated quarterly to reflect changes in scope, revised readiness review type, revised schedules, and completion dates.

The SNR is issued before fuel is loaded. The startup physics test plan is typically reviewed as part of the readiness review. Review of non-nuclear tests of SSCs may be part of the readiness review. After startup physics testing begins, test results that do not meet acceptance criteria require a safety pause or timeout. The test results and the source of the error are then evaluated, such as design calculation, core configuration, fuel tolerances, nuclear instrumentation error. If the source of the error cannot be adequately resolved or if the reactor configuration is not conformant to the safety basis, DOE is notified, and appropriate corrective actions are taken to ensure the safe operability of the reactor. Such a corrective action could entail a potential inadequacy of the documented safety analysis, though not necessarily depending on the safety margin of the missed acceptance criteria.

Report Organization

This report documents the startup physics testing programs from initial fuel loading through ascension to full power for past advanced reactors. The review includes an assessment of what nuclear physics data was measured, why this data was measured for those specific designs, how the measurement was made, and the agreement with predictive reactor performance calculations. The purpose of this review is to establish historical precedence for test inclusion for future advanced reactors planned for demonstration in the National Reactor Innovation Center (NRIC) facilities. The historical review includes reactor designs considered to be significantly different from current LWR designs or using simplified, inherent, passive, or other innovative means to accomplish their safety functions. Four chapters detailing six past reactor test programs are included:

- SNAP-2/8/10A—The System for Nuclear Auxiliary Power (SNAP) program developed compact, lightweight, and reliable nuclear reactors (and isotope power sources) for use in space, sea, and land. This reactor test program is selected to represent microreactors or fission batteries.
- Molten Salt Reactors—The Molten Salt Reactor Experiment (MSRE) demonstrated the practicality and reliability for developing a full-scale breeder reactor based on molten fuel salt. Such testing demonstrated the effect of flowing fuel salt and associated delayed neutron precursor removal on the reactor's kinetic behavior and dynamic temperature feedback.
- FSV & HTTR—These two HTGRs are not part of the same reactor program. Fort St. Vrain (FSV) demonstrated tristructural isotropic (TRISO) fuel in prismatic blocks in the United States in the 1970s and early 1980s. The Japanese High Temperature Test Reactor (HTTR) also utilized TRISO fuel in prismatic blocks. HTTR's reactor commissioning began in the late 1990s, and the reactor is still operating today. HTTR's primary purpose is to demonstrate very-high-temperature operation (>900°C). These two reactors are chosen to represent small modular HTGR reactors that are designated as passively safe.
- EBR-II—The Experimental Breeder Reactor II (EBR-II) demonstrated advanced fast neutron fuels and materials, plutonium breeding and recycling, and the passive heat removal safety case that became the foundation of the LMR technology family. This reactor program is selected to represent microreactors and small modular LMRs that are designated passively safe.

- Superphénix—This very large LMR was the largest fast reactor ever built. The technology leveraged a series of smaller sodium-cooled fast reactor prototypes: Rapsodie, France's first experimental fast reactor, and Phénix, a small-scale prototype of Superphénix. The Superphénix commissioning tests are well documented in a series of journal articles in Nuclear Science and Engineering and will be summarized in this report. This reactor was chosen to represent advanced reactors too large to be considered small modular reactors.

MICROREACTOR AND FISSION BATTERY

The SNAP Reactors

The SNAP Program was conducted from 1955 through 1973, primarily by the Atomic Energy Commission. Its objective was to develop compact, lightweight, reliable nuclear electric devices for space, sea, and land uses. The even-numbered SNAP systems were nuclear reactors, and the odd-numbered systems were radioisotope thermoelectric generators.

The most well known SNAP reactors were the family of sodium-potassium eutectic (NaK) cooled, uranium-zirconium-hydride-fueled SNAP 2, SNAP 8, and SNAP 10A systems. They shared a common technology development and testing program, including criticality experiments and test reactors. Six reactors were operated as shown in Table 1, including the Flight System (FS) 4 reactor which was the only reactor launched into space by the United States. Additionally, three SNAPTRAN (SNAP 10A transient reactor) tests [1] [2] were conducted at the National Reactor Test Station, now Idaho National Laboratory, and the TSF-SNAP (10A) reactor was operated at 10 kW at the Oak Ridge National Laboratory (ORNL) Tower Shield Facility.

Table 1. SNAP reactor test experience [3].

	SNAP 2 Experimental Reactor (SER)	SNAP 2 Developmental Reactor (SDR)	SNAP 8 Experimental Reactor (S8ER)	SNAP 10A Flight System (FS-3)	SNAP 10A Flight System (FS-4)	SNAP 8 Developmental Reactor (S8DR)
Critical	September 1959	April 1961	May 1963	January 1965	April 1965	June 1968
Shutdown	December 1960	December 1962	April 1965	March 1966	May 1965	December 1969
Thermal power	50 kwt	65 kwt	600 kwt	38 kwt	43 kwt	600/1000 kwt
Thermal energy	225,000 kwt-hr	273,000 kwt-hr	5.1×10^6 kwt-hr	382,944 kwt-hr	41,000 kwt-hr	4.3×10^6 kwt-hr
Electric power	-	-	-	402 watts	560 watts	-
Electric energy	-	-	-	4028 kw-hr	574 kw-hr	-
Time at power & temperature	1800 hr AT 648°C 3500 hr ABOVE 482°C	2800 hr AT 648°C 7700 hr ABOVE 482°C	1 yr AT 704°C 400-600 kwt	10,005 hr (417 days)	43 days	7500 hr

SNAP-4 [4] [5] [6] was a multiyear mission application and system design program using the NaK-cooled, uranium-zirconium-hydride-fueled reactor technologies and did not proceed further. A few SNAP-6 [7] design studies are mentioned in the literature, but no details are readily available. SNAP-4 addressed hardened military bases, and the objectives shown in Table 2 closely resemble those of today's transportable microreactors. Several other SNAP-related mission studies were also conducted.

Table 2. SNAP objectives [8].

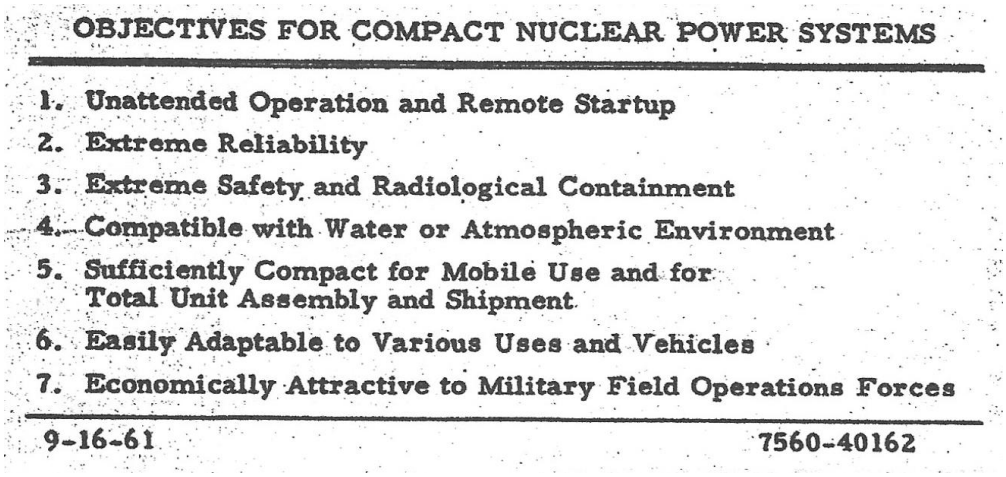

A complete summary of the zirconium hydride NaK SNAP program activities performed by the Atomics International Division of North American Aviation [9] provides more programmatic details as well as some of the technical information that will be presented in the following sections.

The SNAP program also included the SNAP-50/SPUR lithium-cooled refractory metal system [3] work performed by Pratt and Whitney Aircraft, the technology of which formed the basis of the SP-100 program of the 1980s and 90s.

Because the SNAP-10A flight reactors were the only complete reactor, heat transport, power conversion, and heat rejection systems operated in the program, while benefitting from the prior nuclear and non-nuclear testing activities, they will be the basis for assessing the fuel loading and reactor startup physics testing of the SNAP reactors.

SNAP-10A

Reactor Design Summary

SNAP-10A was designed to be assembled at Atomics International's facilities at the Santa Susannah Field Laboratory in Chatsworth, California, followed by qualification and acceptance testing prior to truck transport to Vandenberg Air Force Base for launch. Primary requirements were to reliably produce 500 watts of electricity for 1 year with automatic startup and no active control after 30 days and to meet safety requirements for ground testing and launch to and operation in a stable orbit. A schematic of the SNAP-10A FS is shown in Figure 1.

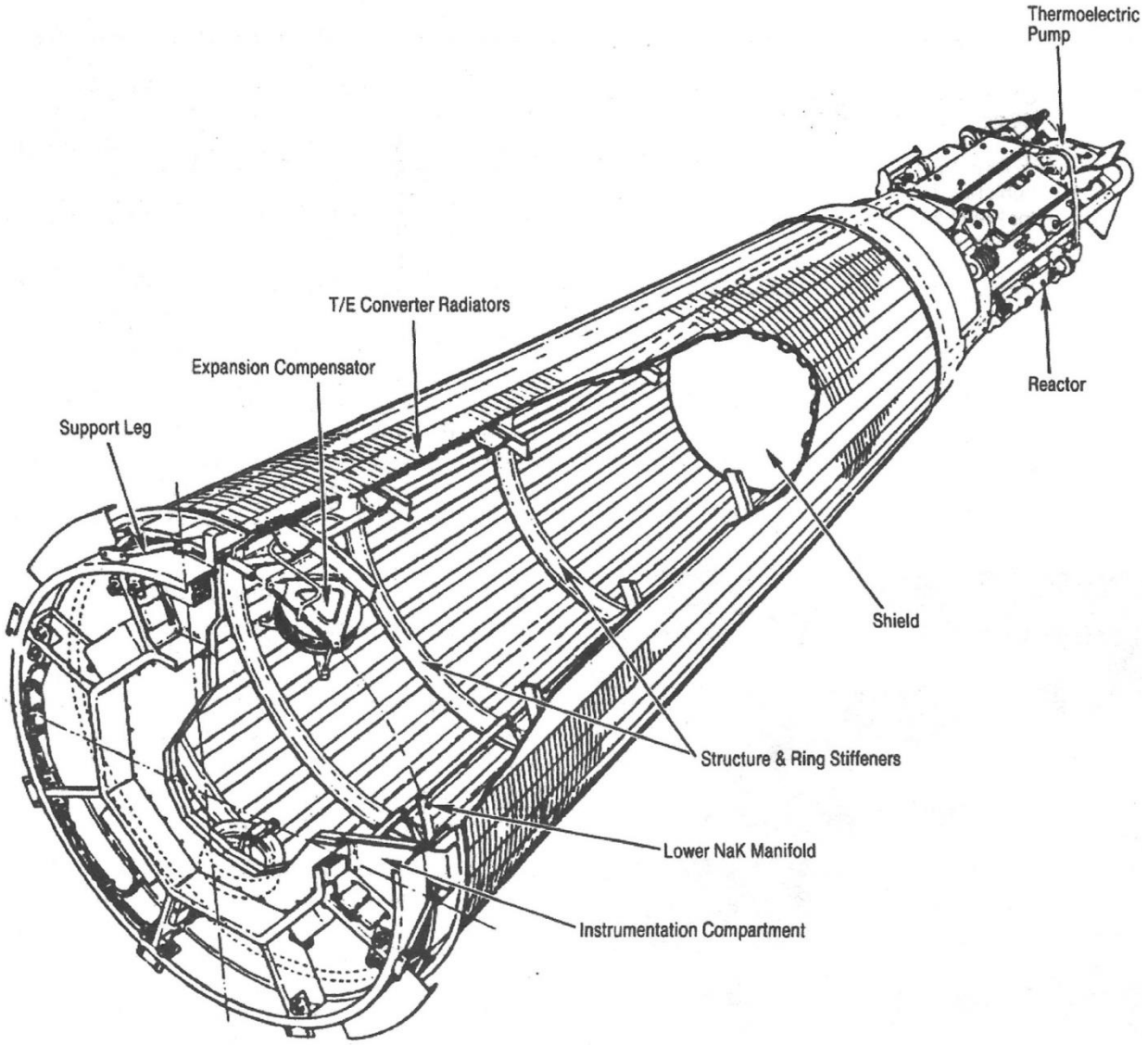

Figure 1. SNAP-10A system [10].

The fuel was an alloy of zirconium-10 w/o uranium, hydrided to a hydrogen density of 6.35 × 10^{22} atoms/cc with a U-235 enrichment of approximately 93.2%. Fuel cladding was Hastelloy-N, and the remainder of the primary coolant boundary and core grid plates was 316 stainless steel. To reduce hydrogen loss from the fuel, the internal surface of the fuel cladding was coated with 2–4 mils of ceramic (Solaramic) that included nominal loadings of 8.0 ± 0.8 mg/inch of burnable poison samarium oxide to reduce the required control swing during operation. The core contained 37 1.25-inch-diameter fuel elements in a hexagonal array with beryllium inserts placed between the outer ring of fuel elements and the reactor vessel.

The cylindrical reactor vessel was surrounded by a beryllium annulus reflector approximately 2 inches thick. There were four 3½-inch-diameter cylindrical cutouts spaced 90 degrees apart on the periphery to house the rotating beryllium control drums. The two fine control and two coarse control drums were 2-inch-thick minor segments of a 3½-inch diameter cylinder, with provision for adding up to three 1/8-inch-thick beryllium plates to adjust control worth. The coarse control drums were activated by snap-in springs. Note that the reactor was controlled by leakage and

not by rotating poison. Figure 2 shows the reflector assembly including the removable void blocks used to prevent drum motion during reactor handling and movement.

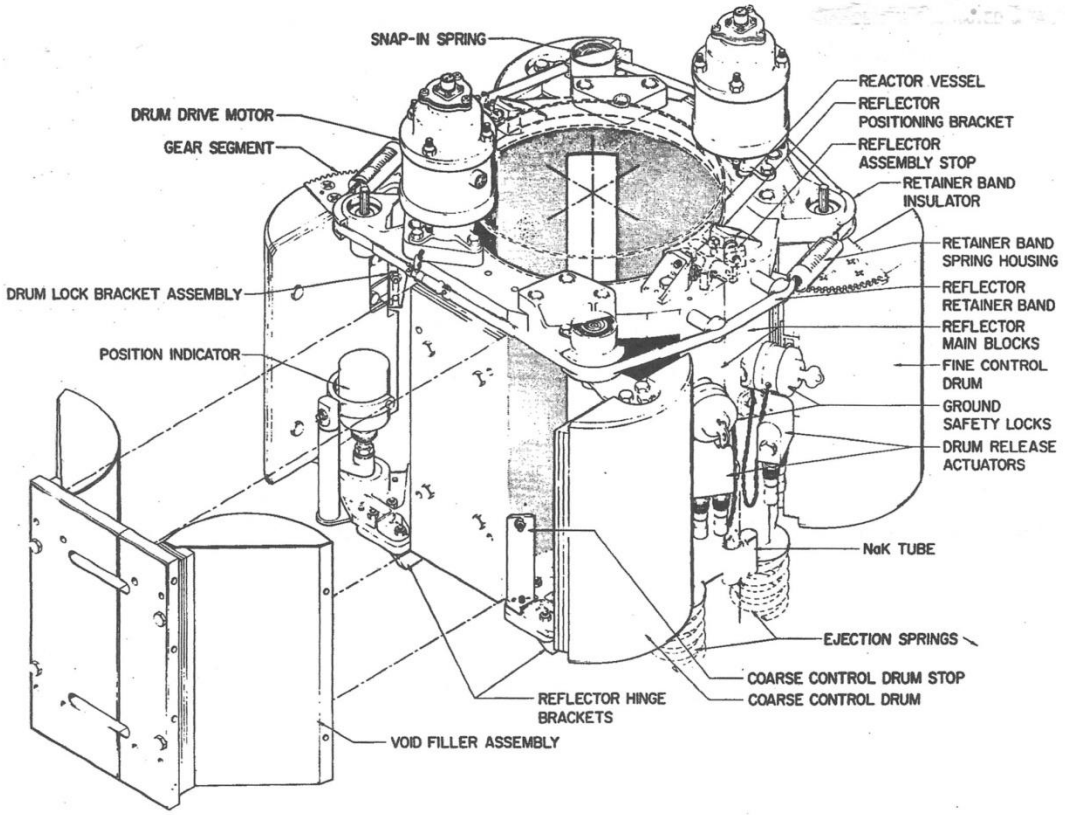

Figure 2. SNAP-10A reactor reflector assembly [11].

Because the control drive motors were unshielded, their lifetime in the radiation field was uncertain, and the system was therefore designed to operate passively after the control system was deactivated after 30 days. Power would decay slowly over the year because of the combination of U-235 burnup, fission product buildup, hydrogen diffusion through the fuel cladding, and degradation of the thermoelectric power conversion elements.

The reactor core was cooled by a single loop that passed though the core, a direct current thermoelectric-electromagnetic pump and then through the hot side of thermoelectric elements that were conductively coupled to the conical radiator. Because the pump was cooled directly by radiating to space, pumping power was provided as long as the NaK remained at elevated temperatures. To ensure the NaK did not freeze in space prior to startup and that adequate pumping was available during startup, the reactor was encased in a thermal blanket during launch and a small direct current battery provided pumping power before the reactor produced adequate sensible heat.

A summary of the SNAP 10A design parameters is given in Table 3.

Table 3. SNAP-10A reactor design summary [11].

Nominal Operating Conditions	
Reactor thermal power (kwt)	39.5
Net electrical power (watt) – Minimum	525
Operating life	1 yr
NaK outlet temperature (°F)	987
NaK inlet temperature (°F)	859
NaK operating pressure (psia)	5
Maximum fuel temperature (°F)	1058
Maximum cladding temperature (°F)	1037
Reactor Design	
Fuel elements	
Number	37
Fuel alloy (wt % U in Zr)	10
Degree of hydriding N_H (10^{22} atom/cm^3)	6.35
Cladding material	Hastelloy-N
Fuel diameter (in.)	1.210
Cladding diameter (OD, in.)	1.25
Cladding thickness (in.)	0.015
Active fuel length (in.)	12.25
Core Vessel	
Material	316 SS
Internal diameter (in.)	8.875
Length (in.)	15.6
Minimum wall thickness (in.)	0.032
Inlet plenum grid plate (lower)	
Material	316 SS
Thickness (in.)	1/2 (sandwich construction)
Outlet plenum grid plate (upper)	
Material	316 SS
Thickness (in.)	1/8
Reflector	
Material	Be
Configuration	Cylindrical sleeve
Nominal thickness (in.)	2
Reflector control elements	
Number	4
Material	Be
Nominal thickness (in.)	2
Internal reflectors	
Material	Be
Cladding	None
Nuclear Parameters	
Average core thermal flux (n/cm^2-sec)	2.5×10^{11}
Mean fission energy (ev)	0.12
Isothermal temperature coefficient at nominal operating conditions (¢/°F)	-0.29
Uranium loading (kg U^{235})	4.75
Effective delayed neutron fraction	0.008
Mean prompt neutron lifetime (μ-sec)	6.5
Burnable poison	
Material	Sm_2O_3
Prepoison reactivity worth ($)†	-1.60
Initial cold excess reactivity ($)†	+3.00
Total lifetime reactivity loss ($)†	-2.58
Xenon equilibrium	-0.17
Samarium burnout	+0.17
Temperature and power defect	-2.25
Hydrogen loss	-0.03
Hydrogen redistribution	-0.20
Burnup and fission product poisons	-0.10
Contingency ($)†	+0.42
Total control drum worth with no shims ($)†	8.60
Total shim capability ($)†	1.26
Shield Parameters	
Material	LiH (cold pressed)
Dimensions	
Maximum diameter (in.)	21.08
Minimum diameter (in.)	17.56
Height (in.)	27.47
Shield casing	
Material	316 SS
Minimum thickness (in.)	0.032
Integrated radiation doses below shield for 1 year of full power operation (fast neutrons and gammas)	
Mating plane (NPU-Booster)	
Center of plane r = o	8.6×10^{12} nvt 7.3×10^{6} r
Inner edge of instrumentation compartment (max) (r = 13-3/4 in.)	1.6×10^{13} nvt 9.6×10^{6} r
Outer edge of instrumentation compartment (max) (r = 24-1/2 in.)	3.8×10^{14} nvt 1.1×10^{7} r
Reference plane (17-1/2 ft below core)	
Center of plane r = 0	2.6×10^{12} nvt 1.9×10^{6} r
Outer edge of plane (max) (r - 30 in.)	3.8×10^{13} nvt 2.8×10^{6} r
Weight Summary	
Reactor core and vessel assembly (lb)	167
Reflector-control assembly (lb)	107
Shield assembly (lb)	217
Electronic equipment (lb)	8
Total nuclear system (lb)	499

†One dollar = 0.008 Δk/k

Startup Physics Test Program

When compared with the customary requirements for the fuel loading and startup testing of terrestrial reactors, SNAP startup testing requirements were complicated by the additional requirements to withstand launch environments followed by autonomous startup and operation for 1 year in Earth orbit. The testing required to satisfy the additional requirements was mitigated by the availability of sufficient nuclear infrastructure to support a comprehensive series of nuclear and non-nuclear tests of systems and components, including full system mockups and the startup and ground testing of a duplicate full-up system prior to the actual startup in space. Figure 3 shows the major milestones of the SNAP 10A Program. The extensive testing program is not directly analogous to those for a stationary terrestrial reactor and is well beyond the capability of today's infrastructure.

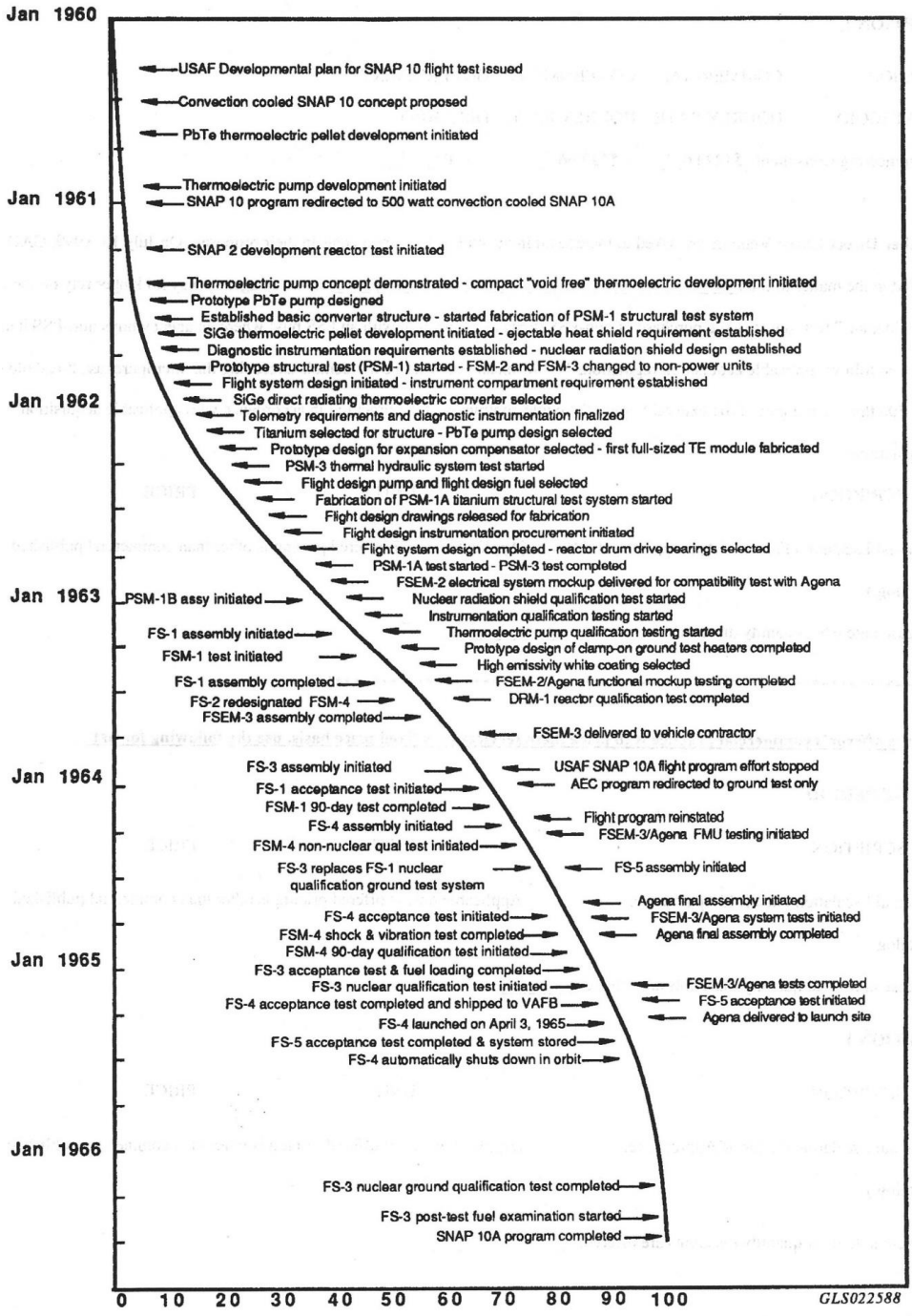

Figure 3. Significant SNAP-10A program milestones [10].

During technology development activities that preceded the SNAP-10A program activities, critical experiments were conducted and the SNAP-2 Experimental Reactor and SNAP-2 Developmental Reactor were operated as previously shown in Table 1. The nuclear-related SNAP-10A test activities have been separated into four categories: critical experiments, transient reactor experiments, prototype experiments, and FS experiments. Information from all of these experiments was essential to ensuring that the FS would meet its design requirements.

CRITICAL EXPERIMENTS

Initial SNAP-10A nuclear criticality experiments were performed in the SNAP Critical Assembly (SCA) and were designated SCA-4A [12], SCA-4B [13], and SCA-4C [14]. The primary objective of SCA-4A experiments was to determine the optimum beryllium reflector, both radially and axially. Additionally, the reactivity worths of various possible core and cladding materials were measured and flux mappings illustrated the differences in the flux profiles from center to corner and center to flat as well as the flux behavior near an open drum. In the SCA-4B experiments, reactor cores and assemblies were subjected to water flooding and reflection conditions that simulated possible transportation and launch accidents. SCA-4C reactor assembly experiments yielded extensive reactivity information for the SNAP-10A flight reactor core design, external reflector worth, and shutdown margin, demonstrating that changes in hydrogen and beryllium in the fuel region could be used to control the excess reactivity of the system without excessive flux perturbations. Actual FS fuel was used in these experiments. Additionally, other core parameters and various component and human mockups were studied to determine reactivity worths and possible environmental effects on the system.

TRANSIENT REACTOR EXPERIMENTS

As part of the Aerospace Safety Program, three transient reactor tests were conducted [1] [2]. Criticality experiments were conducted as part of the fuel loading and startup testing of the SNAPTRAN-1 and SNAPTRAN-2 reactors. The nondestructive SNAPTRAN-1 tests studied the prompt neutron kinetics of the SNAP 10A core with a beryllium reflector. The control drives were modified to allow the rapid insertion and removal of reactivity, and the reactor assembly was encased in a furnace to permit the measurements of temperature effects. Figure 4 shows the SNAPTRAN-1 reactor.

The SNAPTRAN-2 test provided information on the behavior of a SNAP 10A type reactor during a destructive transient. The test was an extension of the SNAPTRAN-1 tests, providing kinetics and reactivity feedback information at a higher power and temperature levels and over shorter periods than could be achieved with a nondestructive transient.

The SNAPTRAN-3 test was a single destructive test of a SNAP 10A reactor core fully flooded and immersed in a water tank to simulate a launch or transportation accident. The transient was initiated by the rapid ejection of a poison sleeve, the reactivity effect of which had been determined during the SCA-4B critical experiment tests.

The transient tests were not relevant to terrestrial reactor startup testing. However, they provide information about the level of understanding of the reactor transient behavior that the reactor designers and operators developed before the reactor startup and testing.

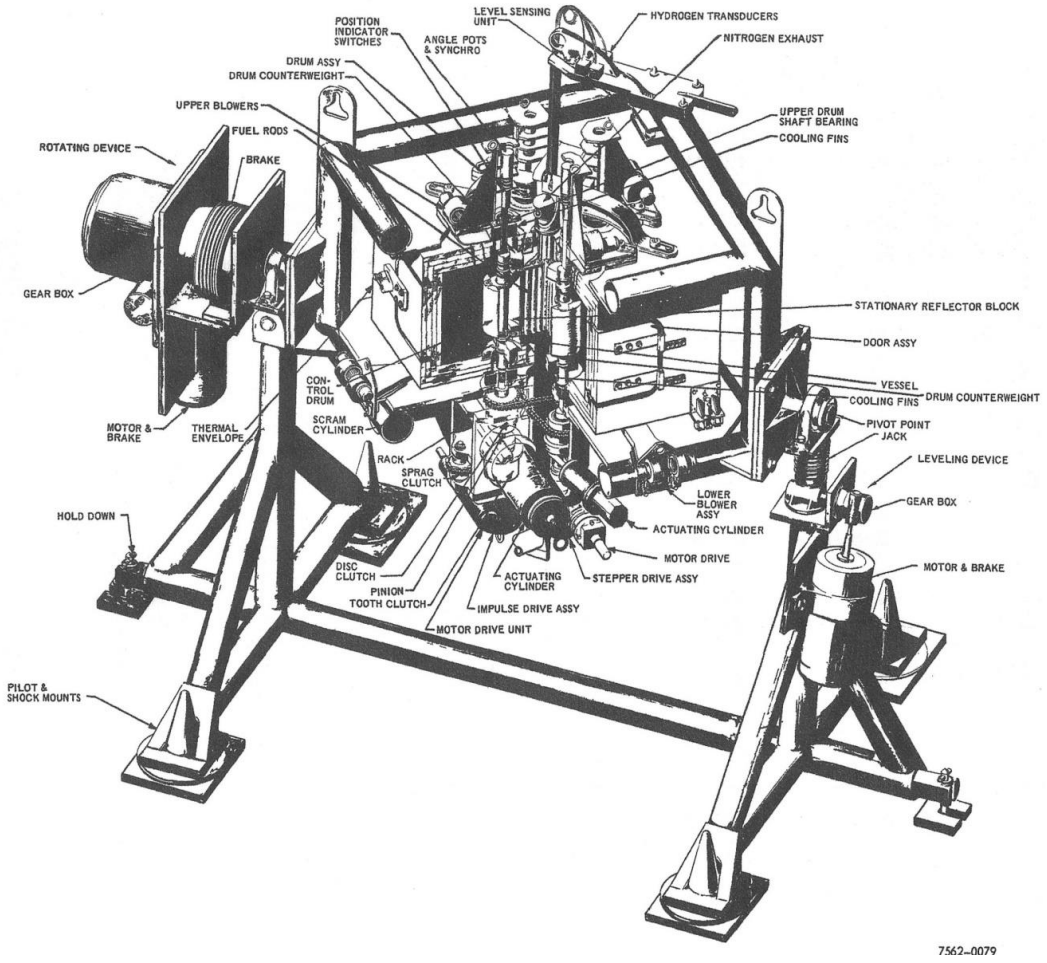

Figure 4. SNAPTRAN-1 reactor [1].

PROTOTYPE EXPERIMENTS

Prototypic system mockups were used to demonstrate that the final FSs would meet their system requirements for power output and lifetime, automatic startup, and stable operation following launch. System thermal performance was demonstrated in non-nuclear FS Mockups 1 and 4 [15]. In these tests, electric heaters replaced the nuclear fuel in the core vessel of a full-up SNAP-10A FS. Nuclear characteristics of the final FS design were confirmed in the FS-1 test [16]. They were determination of minimum critical loading, approach to critical with full core fuel loading, control drum calibration, NaK loading, and wet criticality.

FLIGHT SYSTEM TESTING

FS-3 was used for the complete qualification and acceptance testing of the SNAP-10A system prior to the launch of the FS-4 SNAPSHOT reactor. The ground testing for 1 year in a thermal vacuum chamber demonstrated that the system satisfied all operational design requirements [15]. FS-4 fuel loading and dry critical testing were performed at Santa Susannah Field Laboratory, followed by NaK loading and thermal reference testing [17]. The beryllium reflectors were then removed and replaced with a boron-poisoned shipping sleeve for transport to Vandenberg Air Force Base. No nuclear measurements were made at Vandenberg Air Force Base prior to launch.

Experimental Methods and Results

Loading Approach to Dry Critical

It is important to note that in the later SNAP water critical experiments performed by Atomics International, as well as the reactor fuel loadings, the fuel was loaded sequentially as shown in Figure 5, starting adjacent to the reflector. The core was initially filled with Lucite dummy rods approximating the hydrogen density of the fuel and supporting the fuel elements as they were individually placed by hand into the reactor vessel. The SNAPTRAN experiments performed by the Phillips Petroleum Company at the National Reactor Test Station used aluminum dummy rods during fuel loading.

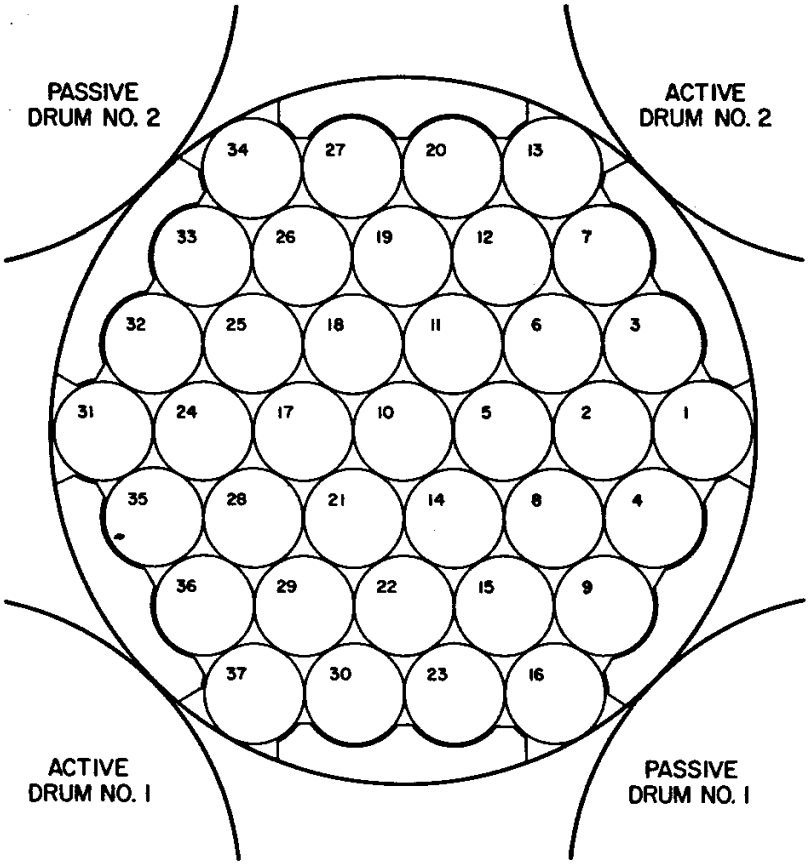

Figure 5. The SCA-4A core loading diagram [12].

The FS-1 loading approach to critical is shown in Figure 6 [16]. Note that the curve is concave downward, which is nonconservative. Critical approaches in prior experiments used loading sequences such as 7, 3, 2, 3, 3, 2, 3, 3, 3, 1, 1, 1 to reach initial criticality, following a loading criteria of ¼ of calculated critical loading, 3/16 of extrapolated critical loading, 1/8 of extrapolated critical loading until critical [14]. Because the fuel element designs were no longer changing, later experiments were able to use fewer loading steps to critical. Three or more fission chambers were used to measure neutron counts.

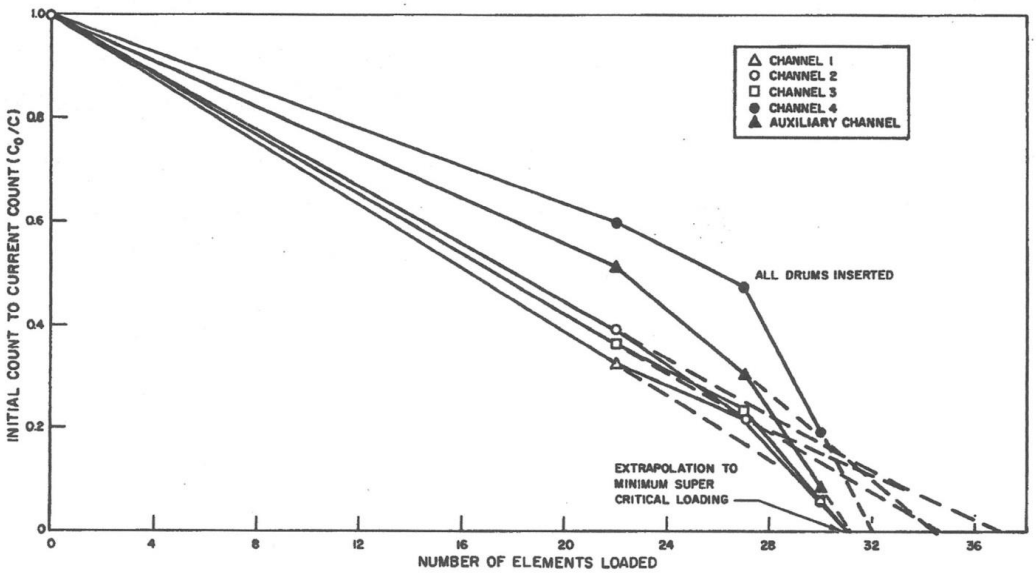

Figure 6. FS-1 loading approach to critical [16].

There is no mention of the use of external neutron sources except in some earlier experiments. The well known ^{9}Be(alpha, ^{1}n) reaction in beryllium can produce sufficient neutrons for criticality determinations and reactor startups. In space, additional neutrons are provided by the high-energy proton reactions on beryllium ^{9}Be(^{1}H, ^{1}n), which obviates the need for a startup source. After criticality was reached, reactivities were calculated using the well known relationship to a stable positive period [18]:

$$\rho = \frac{l^*}{T_P} + \sum_{i=1}^{6} \frac{\beta_i}{1+\lambda_i T_P} \qquad 1$$

where ρ is reactivity, ℓ^* is neutron generation time, T_p is stable period, β_i is *i*th fraction of delayed neutrons, and λi is *i*th precursor decay constant. β_i and λ_i were obtained from ANL-5800. [19] Because the fuel was fully enriched U-235, little error was introduced by ignoring the parameter differences from the delayed neutrons emanating from the U-238 fast fissions.

In the SNAP program, the kinetics parameters (i.e., delayed neutron fraction and prompt neutron lifetime) were assumed to be that of U-235. Following initial criticality, remaining fuel elements were incrementally loaded, control drums were calibrated, and the worth of the control drums was determined.

Control Drum Calibration and Worth

The drums were calibrated using the period bump method in which one drum is rotated in from the steady-state critical configuration, resulting in a measurable stable period [14]. The second drum is then rotated out until a steady-state condition is reached. Each drum movement is then assigned a reactivity value using Equation 1 and their measured period. Pulsed neutron decay and inverse multiplication methods were also used, but these were not relied upon for accurate measurements. FS-1 drum calibrations are shown in Figure 7. The very similar FS-3 drum calibration curves, shown in Figure 8, illustrate consistency between the different flight systems and their nuclear characteristics.

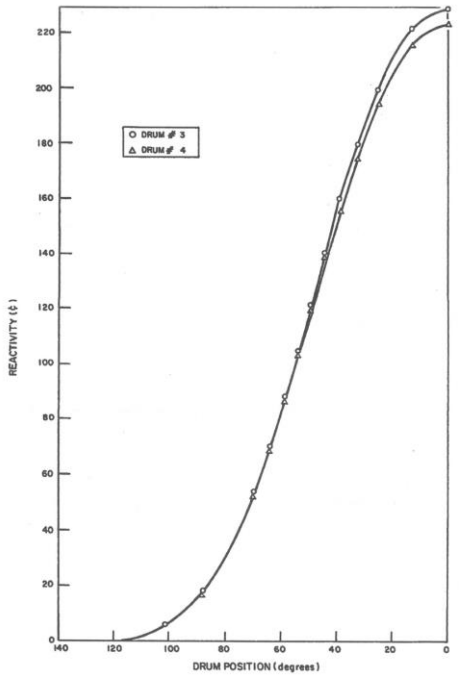

Figure 7. FS-1 drum calibration [16].

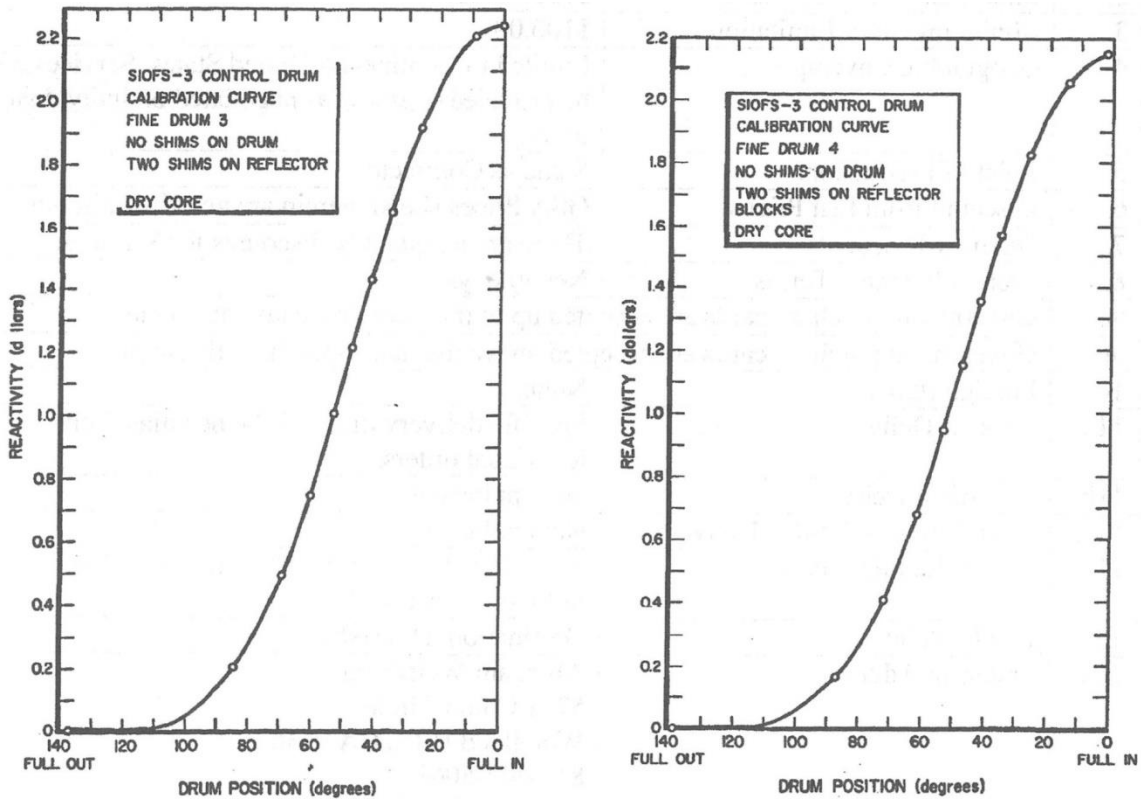

Figure 8. FS-3 drum calibration [16].

NaK Fill and Purity Check

NaK coolant was loaded into FS-3 [20] from the bottom, and the coolant level was raised slowly to displace gas voids in the system. The NaK was purified by circulating through the system and the loading cart that contained a cold trap to precipitate the impurities. Purity was confirmed by three runs demonstrating plugging temperatures under the required 20°F. The plugging temperature is when the NaK solidifies, which is related to the impurity content. A wet criticality check followed the NaK fill.

Reactivity Coefficients

The isothermal temperature defect for FS-3 was measured by using electric heaters on the coolant inlet lines to increase the reactor temperature while the reactor power was held constant at about 0.1 watt [21]. The results of FS-3 dry and wet critical checks and startup losses from the thermal reference test are shown in Table 4.

Table 4. Results of dry and wet critical checks and startup losses for FS-3 [21].

	S10FS-3 (1 shim) ($)
Excess reactivity at cold, dry critical	2.64
Excess reactivity at cold, wet critical	2.95
Isothermal temperature defect 80 to 1010°F	2.12
Reactivity inserted to reach full power	1.92
Excess reactivity at full power	1.02
Reactivity inserted (control drums) during active control period	0.49
Excess reactivity at end of active control period	0.53

The top grid plate temperature coefficient was measured in the SCA-4C reactor assembly with the internal beryllium unattached to the steel top grid plate [14]. The grid plate was heated by a heater cable and was insulated from the fuel, air, and core vessel. Temperatures over 550°F were reached before fuel heating became significant. The data in Figure 9 yielded an effective temperature coefficient of reactivity of -0.026 ¢/°F over 75°F–575°F for fuel movement resulting from grid plate thermal expansion.

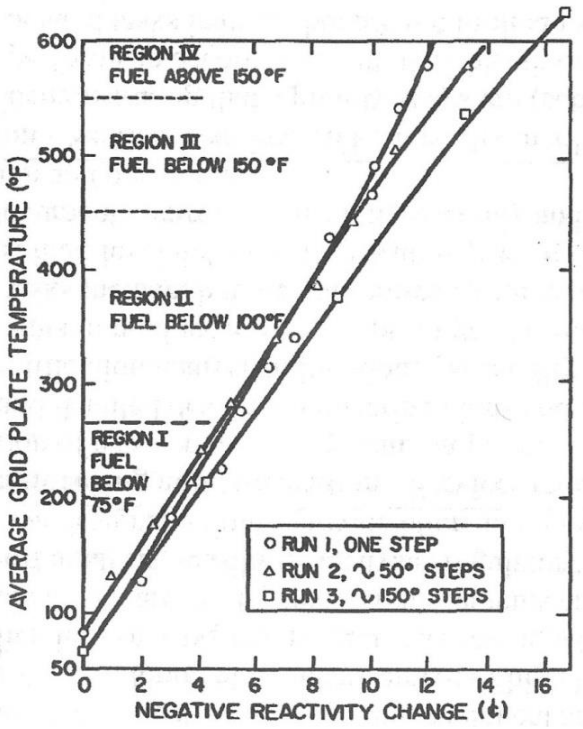

Figure 9. SCA-4C grid plate temperature coefficient [14].

Kinetics Parameters

The ratio of the effective delayed neutron fraction to prompt neutron lifetime was measured during several SNAP experiments using the frequency analysis of the reactor noise spectra. In SCA-4C [14], a value of 1107 sec^{-1} was obtained for β/ℓ^*, corresponding to a prompt lifetime of 7.2 μsec, if a value of 0.008 is taken for β. Noise measurements were also made in some of the SCA-4B water flooded and moderated critical experiments, one yielding prompt a neutron lifetime of 14 μsec [22].

The mean prompt neutron lifetime, ℓ^*, was measured in the SNAPTRAN-1 reactor [23]. Noise analysis techniques were used to determine the magnitude of the reactor transfer function over the frequency range of 10–80,000 cps while the reactor was operated in a low-power, source-free, critical mode. Details of the measurement technique are presented in Reference [24]. The reactor noise signals for a source-free, two-region critical reactor is shown in Figure 10 together with a plot of the analytical model. The fractional standard deviation was 1.8%, which can be considered an excellent fit. Solving the four differential equation yields:

$\beta/\ell^* = 1280\ sec^{-1}$
$(\beta + \beta_7)/\ell^* = 76{,}500\ sec^{-1}$
$\ell^* = 6.25$ μsec — average prompt neutron lifetime, assuming β = 0.008
$\ell_c = 0.83$ μsec — average core neutron lifetime
$\ell_r = 96.8$ μsec — average time neutrons spend in reflector
$\beta_7 = 0.056$ — fraction of neutrons in core appearing from reflector

Note that lifetime values differ by only 13% and that the core and reflectors systems were very similar but not identical.

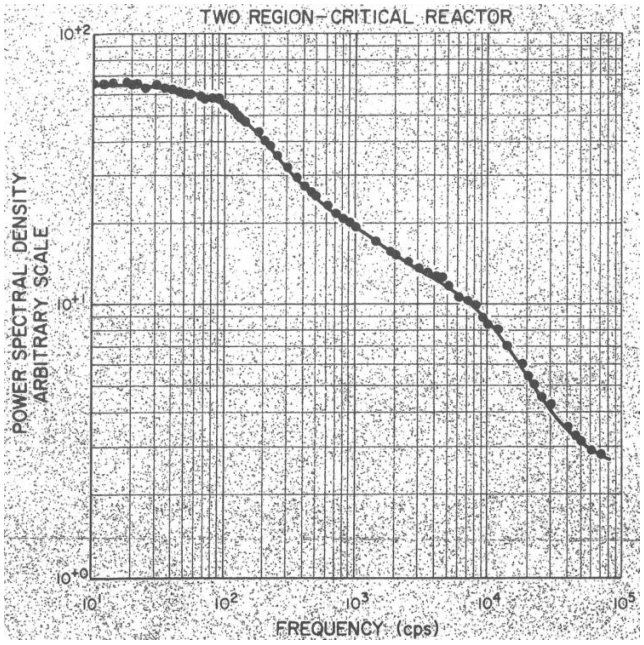

Figure 10. Power spectral density of high-frequency reactor noise signals for a source-free, two-region critical reactor (three break frequency fit) [24].

Thermal Testing

Reactor power, coolant flow rate, and coolant outlet temperature were measured during the FS-3 startup transient [21]. Detailed information on the development and testing of the SNAP-10A pumps is given in Reference [25], including the testing of the FS-3 and FS-4 flight system pumps.

The satisfactory comparison of measurements with calculations at low power, as shown in Figure 11, confirms the operability of the reactor at higher power.

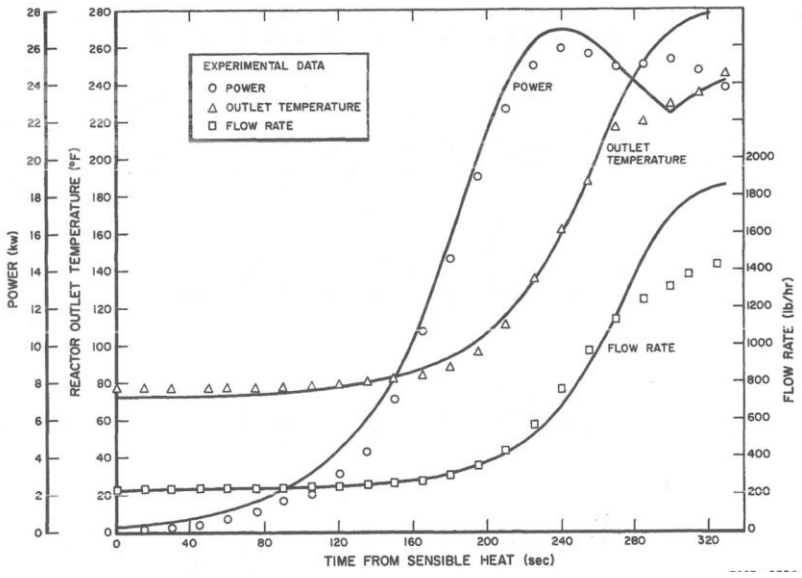

Figure 11. Comparison of calculated and observed FS-3 startup transients [21].

Flux Mapping and Power Distribution

During the SCA-4C critical experiments, relative flux distributions were measured for different drum configurations and partial core loadings, with some fuel having lower hydrogen loading (N_H) to determine whether reflector shimming or loss of hydrogen in the central fuel positions had significant effect on core leakage [14]. As shown in Figure 12, some elements had 1 cm^2 U-235 foils taped at the locations shown to provide axial and radial traverses.

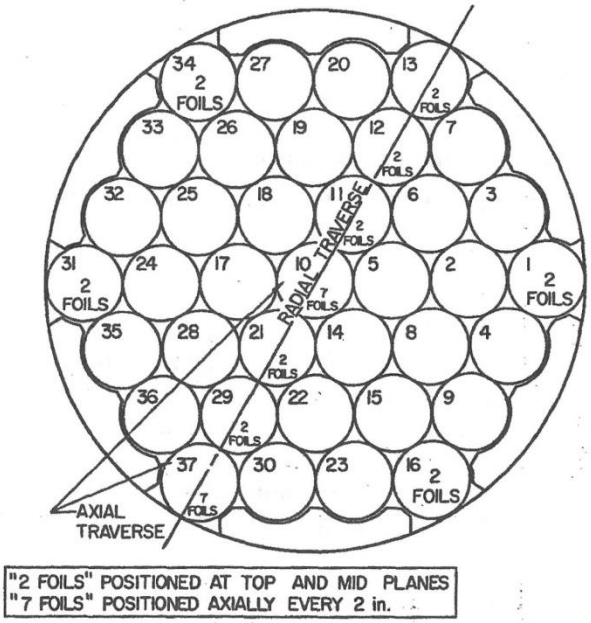

Figure 12. SCA-4C foil irradiation positions [14].

From the tests, it was concluded that adding shims to the reflector had no significant effect, whereas substituting the low N_H rods into the core resulted in a definite lowering of the peak flux and an increase in the peripheral flux.

Comparison of Predicted and Measured Values

The SNAP documents do not contain any reference to quantitative or qualitative nuclear and thermal-hydraulic acceptance criteria for either the FS-3 or FS-4 startup tests. Because the SNAPSHOT mission required an autonomous rapid startup in space shortly after launch, the startup testing for the SNAPSHOT flight reactor FS-4 was performed on its ground test twin, FS-3. FS-3 was operated for 1 year, starting 72 days before the SNAPSHOT launch on April 3, 1965. Because of the prior measurements of nuclear and thermal-hydraulic parameters in prototypic experiments and mockups, it was only necessary for startup testing to show the functionality of the reactor system components and the core reactivity, control drum worths, and thermal performance were consistent with prior test results. The assembled FS-3 underwent an electrically heated thermal test, and the fuel elements were checked previously in the SCA-4 critical assembly [21]. From the perspective of the startup testing of a space reactor terrestrial twin, the core excess reactivity was known, the two coarse drums had been made operable so that there was sufficient shutdown margin to accommodate any reactivity insertion accident, the negative temperature coefficients were demonstrated in the thermal tests, and the SNAPTRAN tests had previously demonstrated the benefits of the temperature coefficients to limit transients.

As stated in Reference [10]:

The following technical considerations were demonstrated by system development and qualification efforts prior to flight demonstration:

- The complete system had a high probability for surviving the shock and vibration environment for the factory-launch-orbit startup sequence.
- The thermal-hydraulic performance was as predicted and the system would produce the designed electrical power.
- The system, in orbit, could be started up with a high degree of reliability and would be self-regulating.
- The instrumentation, required for data feedback, was expected to transmit more than 75% of the data for a minimum of 90 days.
- The manufacturing, assembly, acceptance test, and checkout procedures proposed for the actual flight units were technically sound, reproducible, and did not degrade or increase the technical uncertainty in the flight units.
- The system would not be abruptly shortened in life or the flight test prematurely terminated due to the operating environment (thermal, vacuum, and radiation).

FS-3 and FS-4 were heavily instrumented. A four-page list of the FS-3 instruments is in Reference [20], with expected values of the readings together with the actual readings over the first 4 months of the ground test. A comparison of the power, outlet temperature, and flowrate information for the first 320 seconds of the FS-3 startup was shown previously in Figure 11.

Table 5 gives a summary of some FS-3 test results compared with design predications. There are some small differences between the results shown in Table 4 and Table 5. There is discussion in Appendix A of Reference [21] about the abnormal reflector movement in FS-3. To safely perform the ground testing, some mechanical modifications were made to the reflector attachments and the coarse drum spring actuators were replaced with functional drive motors. Small reflector movements might account for the observed difference in reactivities. After a 300 second transient test, there was confidence that the fully autonomous first-of-a-kind startup demonstration could proceed.

Table 5. Summary of FS-3 test results [20].

Operating Characteristics	Design Prediction	Experimental Result
System stability	Stable	Stable
Excess reactivity		
At cold, dry critical	$2.70 ± 0.10	$2.67
At cold, wet critical	$2.96 ± 0.11	$2.95
At zero power and at a reactor outlet temperature of 1010 ± 5°F	$0.75 ± 0.10	$0.83
At end of active control period	$0.46 ± 0.28	$0.59
Reactivity inserted during active control period after achieving full power	$0.47	$0.47
NaK coolant reactivity effect	$0.26 ± 0.05	$0.31
Temperature coefficient (isothermal)		
80°F	-0.20¢/F°	-0.22¢/F°
600°F	-0.25¢/F°	-0.23¢/F°
950°F	-0.27¢/F°	-0.30¢/F°
Converter output, normalized to a converter average NaK temperature of 920°F and a vacuum vessel wall temperature of 120°F	442 watts	439 watts
Converter degradation rate		
During first 20 days	5%/500 hr	6%/500 hr
After first 20 days	2.7%/1000 hr	0.95%/1000 hr
NaK pump flowrate, normalized to 1010°F reactor coolant outlet temperature	14.5 gpm	14.6 gpm
NaK pump degradation rate		
During first 30 days	16%/1000 hr	12%/1000 hr
After first 30 days	2.6%/1000 hr	0.28%/1000 hr
Average core coolant temperature decay during first 90 days of power separation	33 ± 25F°	49F°

MOLTEN-SALT REACTORS

The Molten Salt Reactor Program

In the 1950s, the Aircraft Reactor Experiment (ARE) was successfully designed, constructed, and operated at ORNL as the first reactor ever utilizing a flowing liquid fuel [26]. Figure 13 shows vertical cross section of the ARE. The ARE utilized a beryllium oxide (BeO) moderator with fuel dissolved into a fluoride salt of $NaF\text{-}ZrF_4\text{-}UF_4$. It had a target power output of 1–3 MWth. Several experiments were performed with ARE to demonstrate the viability of using liquid fuel, including initial criticality, control rod worth, temperature feedback coefficients, flow effect on reactivity, power ascension, off-gas removal, and xenon buildup [27]. The operation of the ARE proved that a liquid-fueled reactor could be operated safely. It provided a useful source of power and led to the design and operation of the MSRE in the 1960s at ORNL. The MSRE had a target power output of 10 MWth [28] and was the first liquid-fuel salt and graphite moderated reactor. The liquid fuel salt was composed of $LiF\text{-}BeF_2\text{-}ZrF_4\text{-}UF_4$ with U-235 as the fissile component. It was later replaced

with U-233, being used as a fuel for the first time [29] [30]. The main purpose of the MSRE was to demonstrate the practicality of liquid-fuel operation at high temperatures and ensure the safety and reliability for developing the full-scale breeder reactor project [31]. The MSRE was operated for about 10 years.

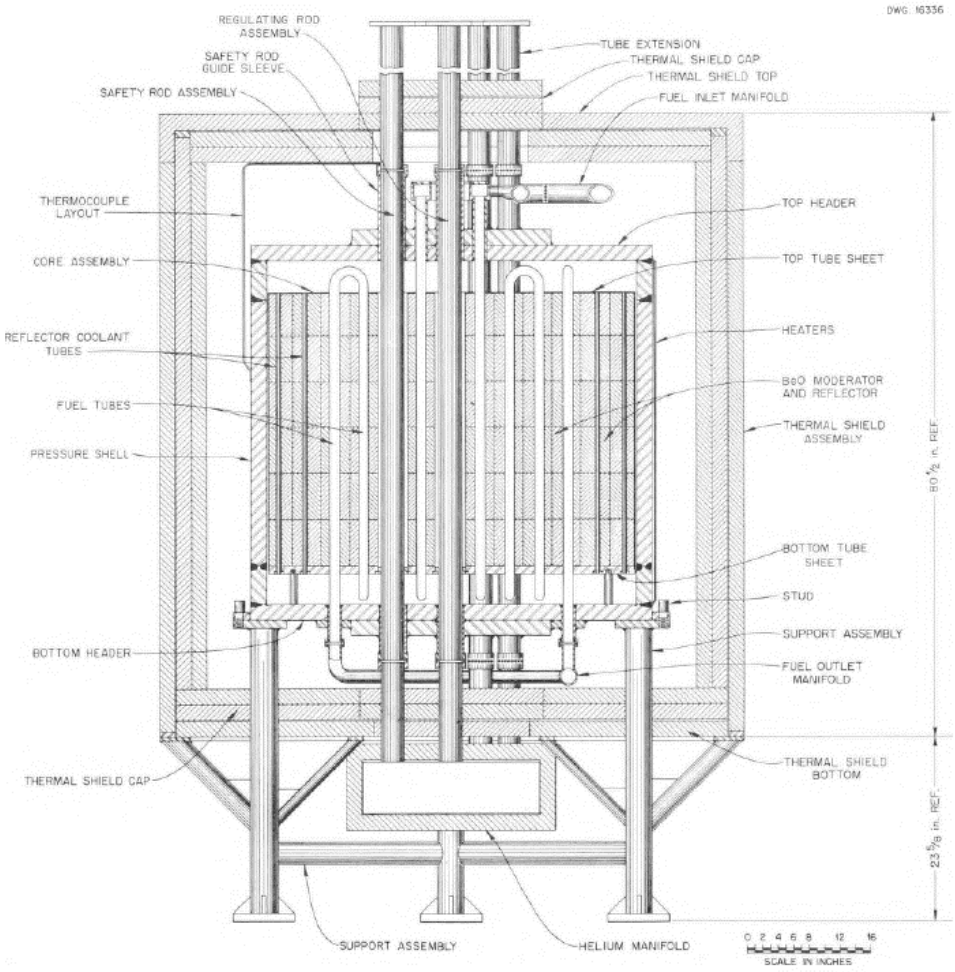

Figure 13. Vertical cross-section of the ARE reactor [26].

Molten Salt Reactor Experiment

Reactor Design Summary

The MSRE was built in 1964 at ORNL as a thermal neutron spectrum reactor with liquid fuel salt flowing through graphite moderator channels. Although the MSRE was designed to be a 10 MWth reactor, in the final stages, the heat extraction in the secondary system was smaller than expected and the maximum power level was restricted to 8.0 MW. MSRE operation started in 1965 and continued until 1968. It was fueled with U-235 (33% enriched), and the salt molar composition was LiF-BeF_2-ZrF_4-UF_4 (65.0 mol% - 29.17 mol% - 5.0 mol% - 0.83 mol%). It was designed to be operated between 908 and 936 K, with a temperature rise of 28 K and core average temperature of 922 K. The total circulation time of the fuel salt in the primary system was about 25 seconds. In 1968, the fuel was replaced with U-233 fuel (91% enriched) with a slightly different molar

composition of 64.5 mol% - 30.18 mol% - 5.19 mol% - 0.13 mol% [32]. See Table 6 for a summary of significant design parameters.

The MSRE reactor vessel had an inner diameter of 58 inches with a wall thickness of 1 inch. The core container was inside the vessel and had an inner diameter of 55.5 inches and a thickness of 0.25 inches. The main function of the container was to support the graphite. All salt-containing components were made from the nickel alloy INOR-8, including the reactor vessel. The MSRE lattice was made of vertical graphite stringers with a 2 × 2 inch cross section and was 67 inches long. The fuel salt flowed through a total of 1,140 rectangular channels (1.2 × 0.4 inch with round corners with a 0.2 inch radius) in the sides of the stringers. The cannel dimensions were chosen to prevent blockage by small objects and to obtain a nearly optimum fuel-to-graphite ratio in the core. Figure 14 shows a schematic representation of the MSRE reactor vessel [32].

The MSRE was designed to be operated with three control rods containing gadolinium in the form of Gd_2O_3-Al_2O_3 (70–30 wt%) ceramic, with a density of 5.78 g/cm^3. Each control rod was made of 38 elements for a 59.4 inch total length of the poison section. Each element consisted of a thin-walled ceramic cylinder with a 1.08 inch outer diameter, 0.84 inch inner diameter, and 0.438 inch length. Figure 15 shows a representation of the control rod lattice arrangement and element geometry.

The MSRE reactor vessel was installed in a thermal shield to reduce the radiation damage to the reactor containment vessel. It serves as biological shielding and provides support for the reactor vessel. The shield was a water-cooled, steel- and water-filled container surrounding the reactor vessel. The thermal shield was 16 inches thick and contained approximately 50% steel and 50% water. The inside of the thermal shield was lined with 6-inch-thick high-temperature insulation. Figure 16 shows a representation of the outer vessel regions, effective core region, and control rod movement level [32] [33].

The primary and secondary system's layout of the MSRE is shown in Figure 17. The fuel salt was circulated by a centrifugal pump, cooled through a shell-and-tube heat exchanger, with heat radiated to the atmosphere [32]. In the heat exchanger, the primary fuel salt flows through the shell side and the secondary coolant salt flows through the tube side. The coolant salt for the secondary system was molten LiF-BeF_2.

Table 6. Characteristics of the MSRE [34] [35] [36].

Thermal power	8 MWth
Fuel composition	LiF-BeF_2-ZrF_4-UF_4
Molar composition	U-235 core (65.0%-29.17%-5.0%-0.83%) U-233 core (64.5%-30.18%-5.19%-0.13%)
Enrichment	U-235 core (33.0%) U-233 core (91.5%)
Fuel inlet/ outlet temperature	1,175°F / 1,225°F
Core height / core diameter	64 inches / 55.25 inches
Total fuel salt transit time	25.2 seconds

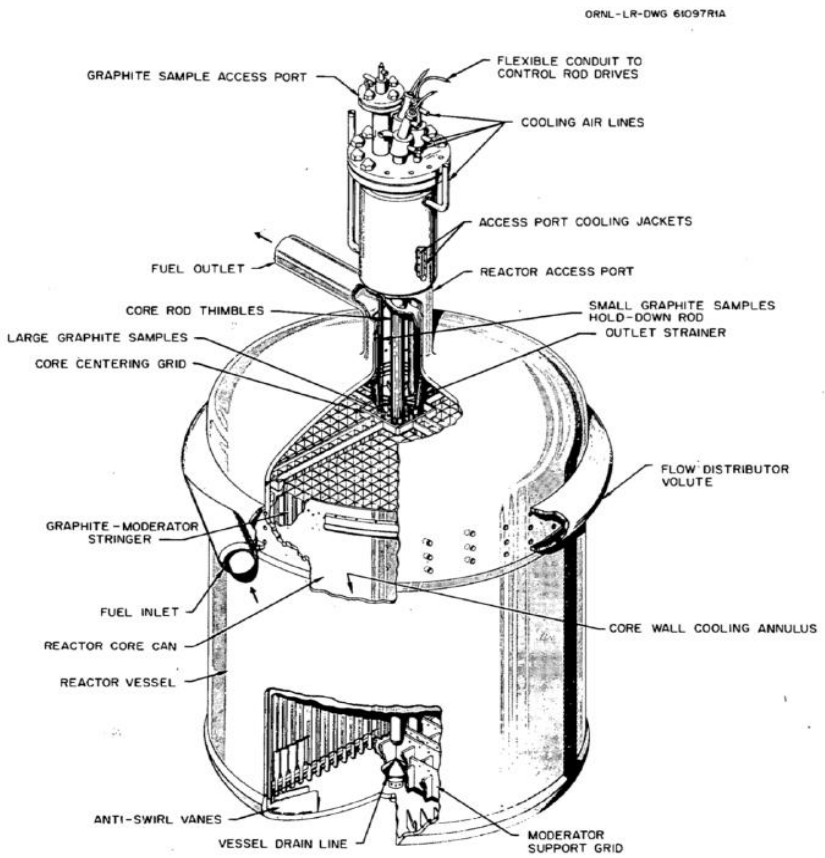

Figure 14. Schematic diagram of MSRE reactor vessel [32] [33].

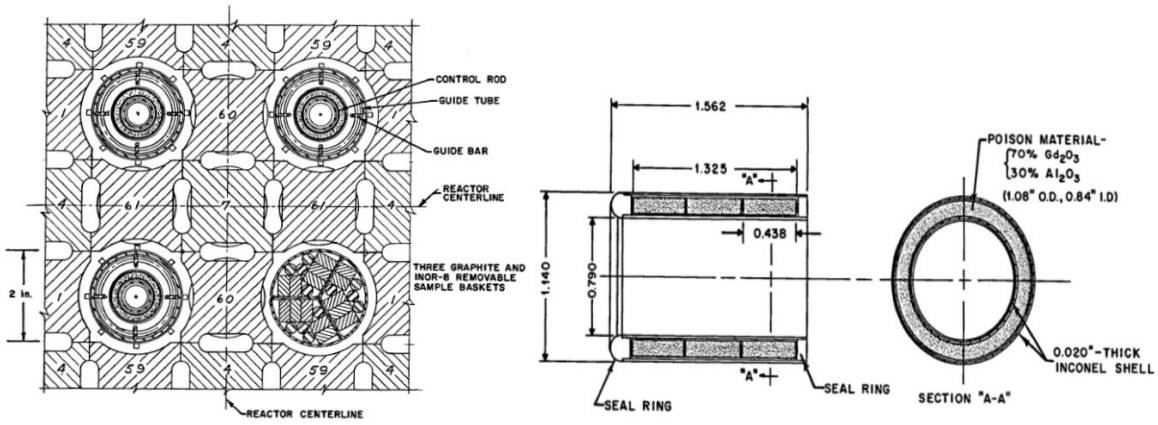

Figure 15. Lattice arrangement of the MSRE control rods (left) geometry and composition of the control rod element (right) (units in inches) [32].

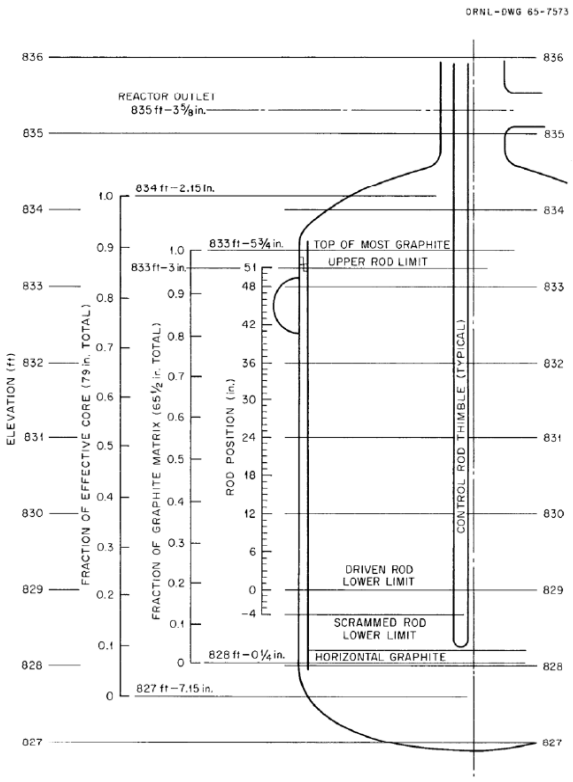

Figure 16. Representation of MSRE control rod level and effective core region [37].

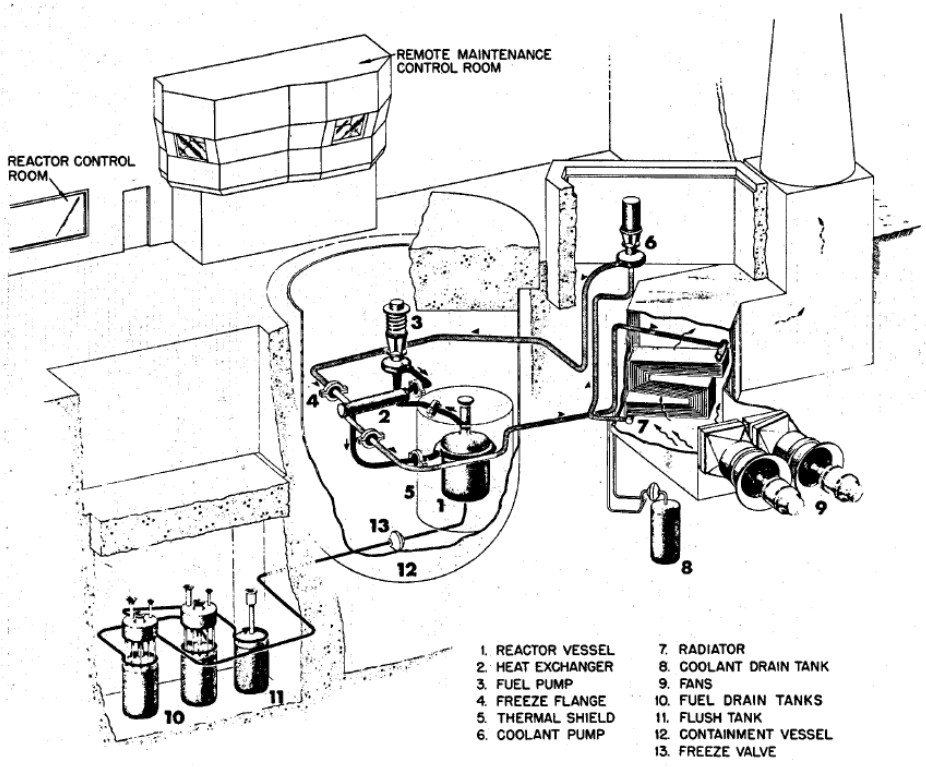

Figure 17. Layout of MSRE primary and secondary systems [32].

Startup Physics Test Program

Tests conducted during commissioning of the MSRE were categorized into three types: prenuclear or non-nuclear tests, zero-power nuclear tests, and full-power nuclear tests. The prenuclear tests were performed to make sure that all systems operated well and there were no unanticipated problems in handling the molten salt. These tests are shown in Figure 18 and include installing and testing the control rods, system flushing, filling the drain tank, and loading and circulating the carrier salt [29] [30].

The zero-power nuclear tests were performed after loading the fuel salt and achieving criticality at a very low power without reaching nominal operating temperatures. These tests were performed from 1964 to 1965 and included fuel salt loading, approach to criticality, control rod worth, rod shadowing, reactivity effects of the fuel circulation, fissile concentration reactivity effects, temperature coefficients, and protected pump transient experiments. The operation history and tests during this period are shown in Figure 18 [30].

The zero-power tests in the kW range showed that the system dynamics were as expected. The ascension to full power started at the beginning of 1966. The full-power nuclear tests were performed from the kW range to the MW range and include power ascension, dynamic tests, thermal convection heat removal, reactivity insertion, xenon stripping experiment, etc. The operation history during 1966–1969 is shown in Figure 19. During that period, all the tests were performed with U-235 in the carrier salt. In 1968, the U-235 was replaced with U-233 and some of the zero-power tests were conducted with U-233 in the carrier salt. These tests included approach to criticality, control rod worth, fissile concentration reactivity effects, and isothermal temperature coefficient.

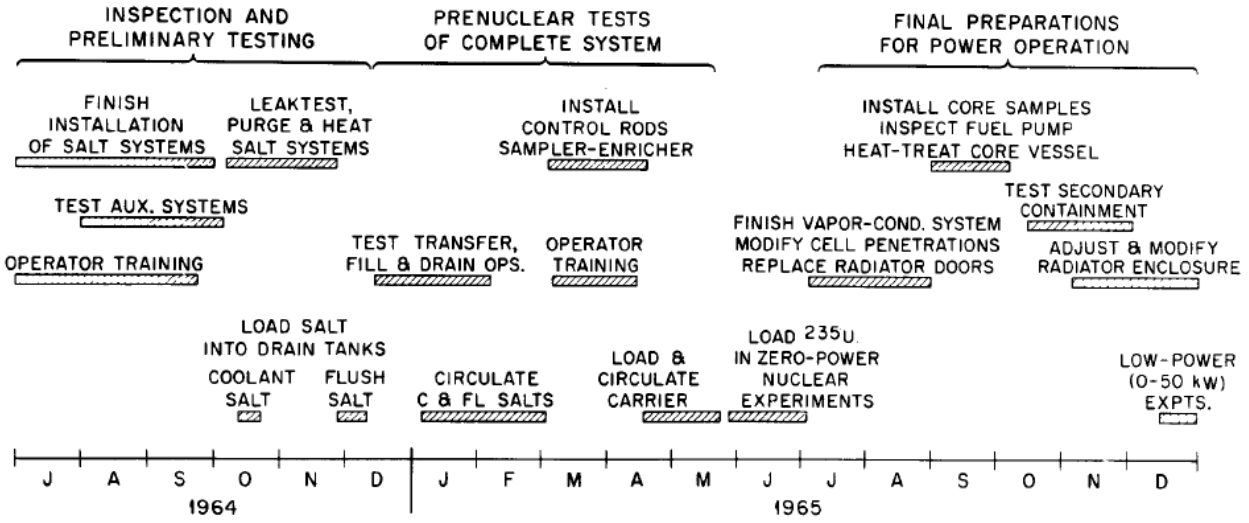

Figure 18. Startup tests and activities of the MSRE from 1964 to 1965 [30].

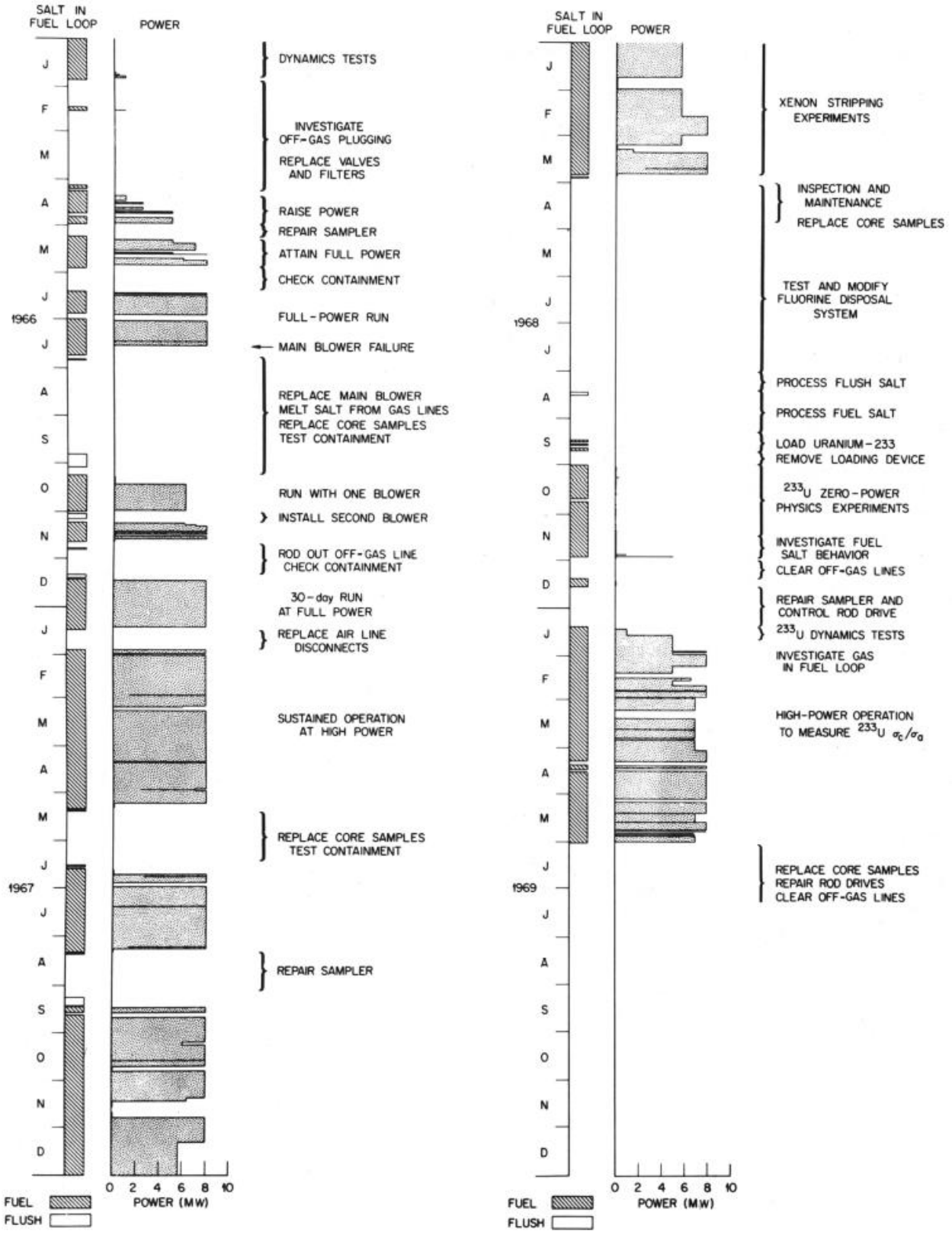

Figure 19. Power operation and activities of the MSRE from 1966 to 1969 [30].

Experimental Methods and Results

Fuel Loading and Initial Criticality

The MSRE initial fuel loading determined the critical concentration of the U-235 in the salt with all control rods fully withdrawn for stationary fuel at isothermal temperature conditions. The fuel salt molar composition specified for power operation was (65.0 mol% - 29.17 mol% - 5.0 mol% - 0.83 mol%). For chemical considerations, the total uranium content would be considerably above the minimum required for criticality if highly enriched uranium (HEU) were used. Therefore, the core was initially filled with depleted uranium salt. Then HEU salt was added incrementally to bring the core to the critical loading. The predicted critical concentration was 0.256% mole $^{235}UF_4$ (0.795% mole total UF_4) considering the temperature of 1200°F. Control rods were fully withdrawn, and the fuel was stationary. The U-235 critical mass was calculated to be 68.7 kg, using the volumetric concentration from the criticality calculations and the volume of salt in the fuel loop and drain tank [37].

Before the HEU-UF_4 was added, the core was incrementally filled with a depleted uranium carrying salt, 73LiF-27UF_4. The critical concentration of U-235 was determined by incrementally adding enriched HEU-UF_4 until criticality was achieved. The salt was prepared in three lots, the beryllium-zirconium-lithium carrier salt, 150 kg of 73LiF-27UF_4, and 90 kg UF_4 [37]. Initially, HEU-UF_4 was added to the carrier salt drain tank before being charged to the primary loop. Later, HEU-UF_4 capsules were added to the primary pump bowl.

The neutron multiplications measurement was performed with the following instrumentation, as shown in Figure 20 [38].

- Neutron Source: ^{241}Am-^{242}Cm-Be source, and an inherent fuel salt source from alpha particles from U-234 interacting with the beryllium and fluorine in the salt.
- Neutron Detectors: Two fission chambers and two BF_3 chambers.

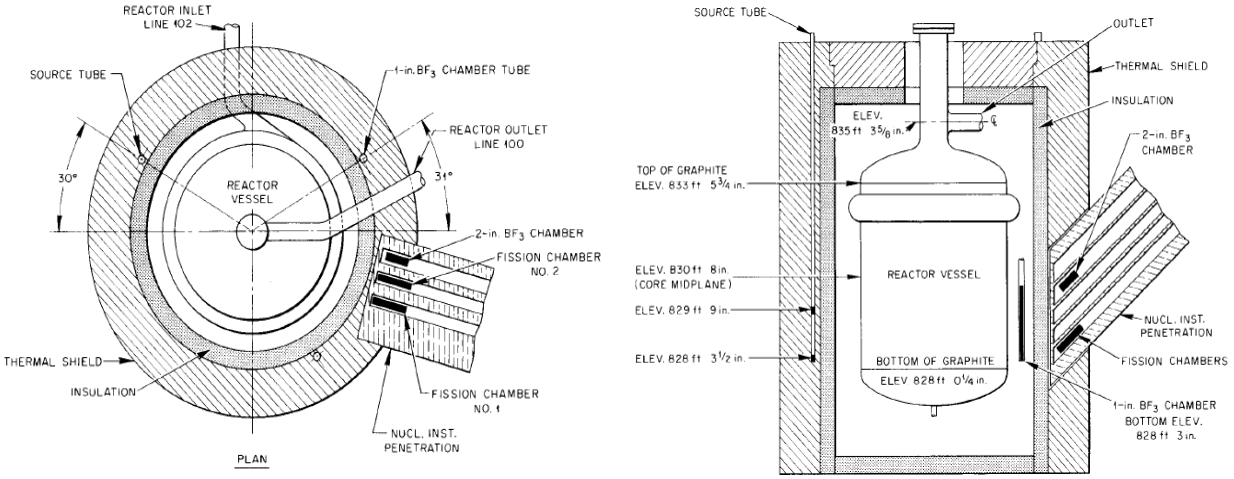

Figure 20. Configuration of source and instrumentation in initial critical experiment of MSRE [37].

This is the procedure followed while loading the enriched salt into the carrier salt:

- The depleted uranium 73LiF-27UF_4 was mixed with the carrier salt in a heated drain tank. Two cans of depleted uranium salt were mixed with 35 cans of carrier salt to fill the drain tank. After mixing, the salt was charged to the primary loop such that the core was filled to

40%, 60%, 80%, and 100% of the graphite moderator height. Count rates were taken after each filling.

- The depleted uranium salt circulated for 10 days in the primary loop before adding the HEU-UF_4.
- The drain tank was then filled with molten salt from the primary loop. Then one can of frozen HEU-UF_4 was added to the heated drain tank before being charged to the primary system. This step was repeated four times. Each step filled the core to 40%, 60%, 80%, and 100% of the graphite moderator height. After each filling, fuel circulation was stopped, the rods were withdrawn, and count rates were measured.
- The fourth addition was 4.38 kg of U-235, which was approximately 1 kg below the critical loading. The inverse of multiplication showed that the loading was within 0.8 kg of the critical loading with all rods fully withdrawn and stationary fuel. The measured count rates and approach to criticality curve are shown in Figure 21.
- At this point, HEU-UF_4 capsules, containing 85 g of U-235, were added through the outer loop pump bowl. After adding seven capsules (595 g of U-235), the inverse of multiplication indicated that, after one more capsule, the reactor could be made critical. When the eighth capsule was added, the total mass of the U-235 salt was 69.6 kg.
- The reactor reached criticality at approximately 6:00 p.m., June 1, 1965, with two rods fully withdrawn and the other inserted to 0.03 of its worth. Criticality was verified with a U-235 loading of 69.6 kg by leveling the power at successively higher levels with the same rod position.

The MSRE internal source (α, ^{1}n) reaction in the beryllium and fluorine was measured to be 3%–5% of the external source, which corresponds to 3×10^5–5×10^5 neutrons/sec. The U-235 mass fraction in the fuel salt was 1.414 ± 0.005 wt% at the time of the initial criticality. The density of the fuel salt at 1200°F, determined after the uranium was added to the fuel drain tank with an average of four measurements, was 145.1 lb/ft^3, with a maximum deviation of 1.1 lb/ft^3. A temperature correction should be applied to the salt density since the core temperature at the time of criticality was 1181°F instead of 1200°F. Based on a fractional change in density of -1.2×10^{-4}/°F, the density at 1181°F would have been 145.3 ± 1.0 lb/ft^3 [37].

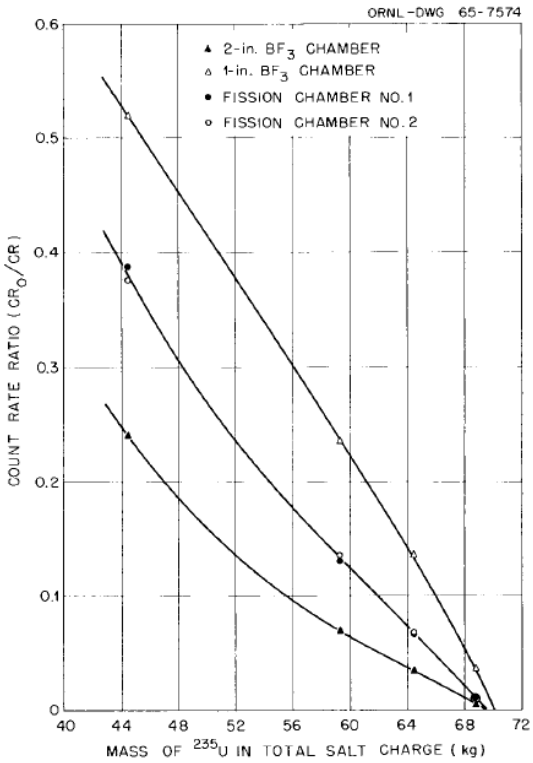

Figure 21. Approach to criticality and count rate ratios after first four additions of U-235 in the MSRE [37].

Control Rod Worth Measurement

After initial criticality was achieved, U-235 was added beyond the minimum critical mass to ensure there was sufficient excess reactivity for full power and long operation. Another eight capsules, 85 g each, were required to maintain the reactor critical at 1200°F with the fuel pump running. This is the consequence of the effective loss of delayed neutrons from precursor decay in the external circulating system. With the new concentration, the worth of the regulating rod was measured using the stable period approach.

The control rod worth was calculated using the in-hour equation, the precalculated kinetics parameters, and the inverse of the measured stable period. The critical position of the regulating control rod was measured after addition of each capsule, with the fuel pump running. At intervals of four capsules, period measurements were made to determine the control rod differential worth with the pump running. Then the pump was turned off, and the same measurement was made. Period measurements were made in pairs. The rod was first adjusted to make the reactor critical at about 10 W. Then it was pulled a prescribed distance away and held there until the power had increased by about 2 decades. The rod was then inserted to bring the power back to 10 W, and the measurement was repeated. The stable period was determined by averaging the slopes of the two curves, which usually agreed within about 2%. Periods observed were generally in 30–150 seconds. For the measurements with the pump off, the standard in-hour equation was used to calculate the reactivity increment corresponding to the observed stable inverse period ($\omega = 1/T$):

$$\rho = \omega\Lambda + \sum_{i=1}^{6} \frac{\omega\beta_i}{\omega+\lambda_i} \qquad 2$$

The calculated value of the mean neutron generation time, Λ, was 2.6×10^{-4} seconds for the initial critical loading. The rod sensitivity measurements show that the in-hour equation was not sensitive to the neutron generation time. The decay constants, λ_i, and the effective delay fractions, β_i, are given in Table 7. Note the importance of delayed neutrons because of their emission at lower energies relative to the prompt fission neutrons.

Table 7. Delayed neutrons data of the MSRE [39].

Group	$\lambda_i\ (sec^{-1})$	$\beta_i(x10^{-5})$
1	0.0124	22.3
2	0.0305	145.7
3	0.1114	130.7
4	0.3013	262.8
5	1.1400	76.6
6	3.0100	28.0

The measured differential worth of the regulating rod with the fuel pump off is shown in Figure 22. Theoretical corrections were applied to differential worth measurements to account for the rod shadowing effect and to adjust the measurements to the initial critical concentration. The approximate correction factors increased linearly with U-235 concentration up to I.087 for the final concentration. The root-mean-square deviation of the data points is about 0.7% of the mean differential worth with a maximum deviation of a single point of 8.7%. The main source of uncertainty in the differential worth was in the reactor period measurement, and the uncertainty of determining the rod position was about ±0.01 inches. Figure 23 shows the integral worth of the regulating rod with the fuel pump off for initial and final U-235 concentrations [37] [38].

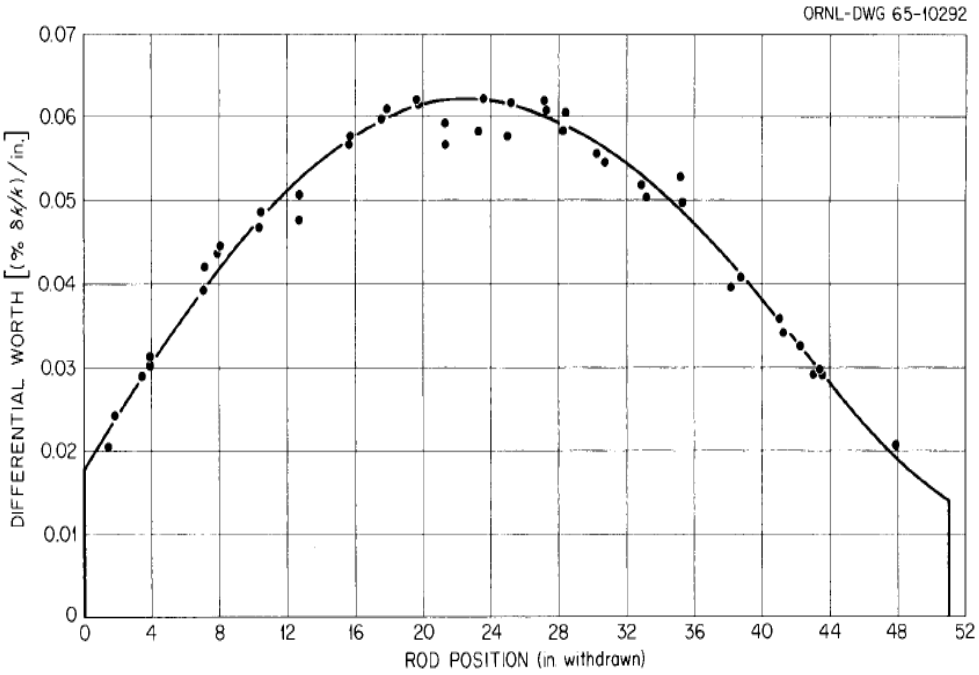

Figure 22. Measured differential rod worth of the regulating rod with stationary fuel in the MSRE [38].

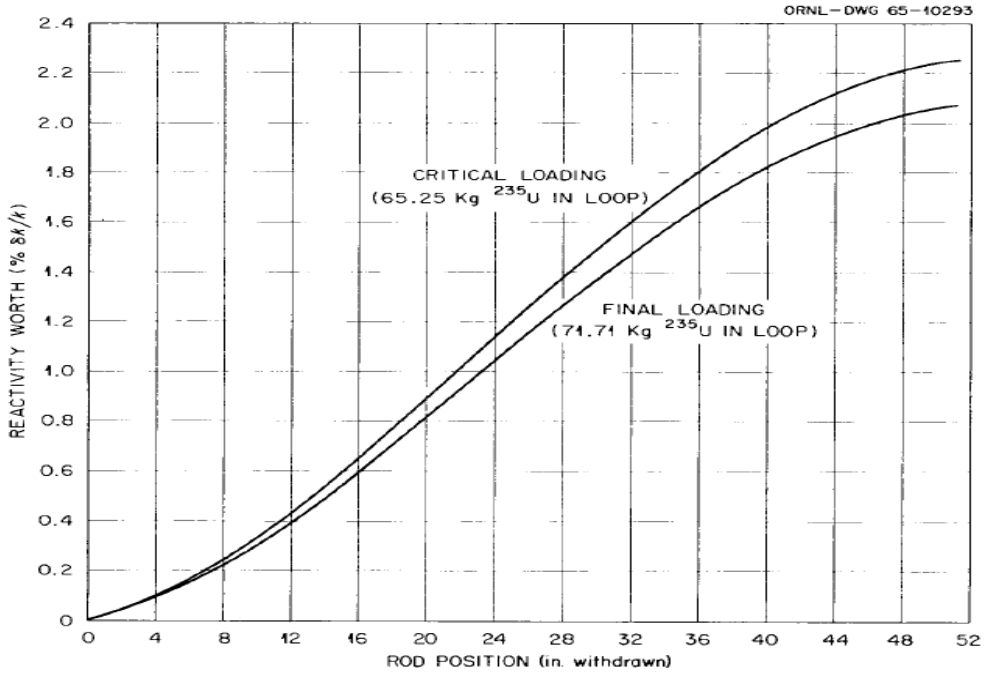

Figure 23. Integral rod worth of the regulating rod with stationary fuel in the MSRE [37].

The measured differential rod worth of the regulating rod with the fuel pump on is shown in Figure 24. The measurements were made using stable periods and the in-hour equation modified for circulating fuel. The variability in the measured values is greater for flowing fuel than it is for stationary fuel, see Figure 22 compared to Figure 24 [38].

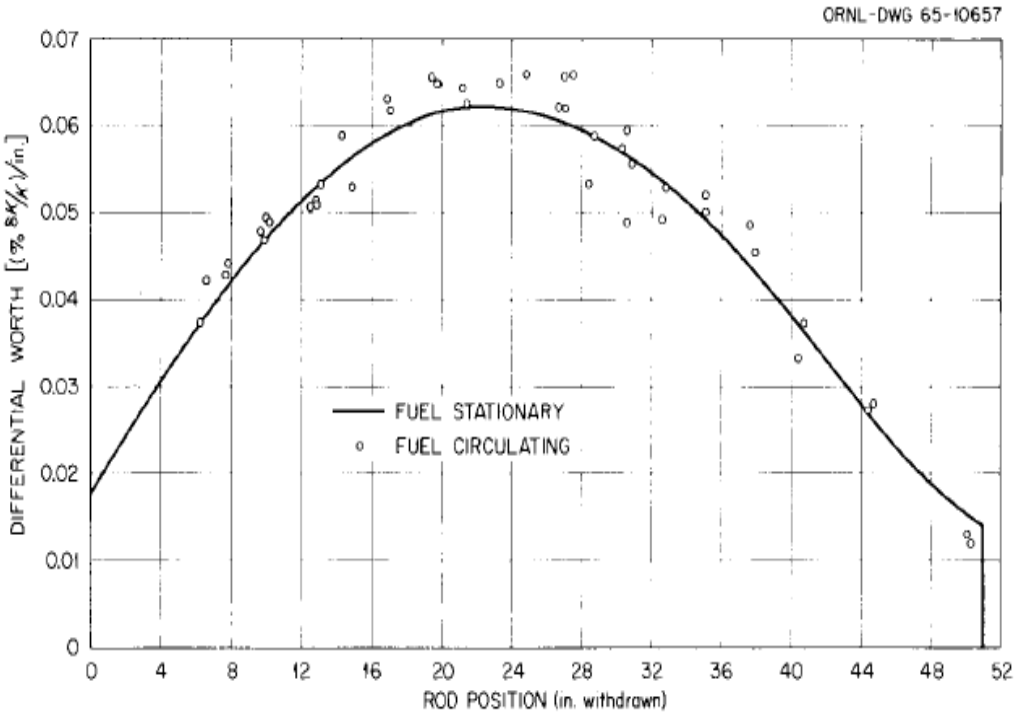

Figure 24. Measured differential rod worth of the regulating rod with circulating fuel in the MSRE [38].

U-235 Concentration Coefficient of Reactivity

The critical position of the control rod was measured with the pump off after every fourth capsule. Critical rod positions at each U-235 level were then converted to reactivity using the integral rod worth curve with a linear correction between the initial and final U-235 concentrations. The reactivity changes of the stationary and circulating fuel at different U-235 loadings are shown in Figure 25. The difference between the two curves provides the net reduction in reactivity due to release of delayed neutrons in the external loop.

The U-235 concentration coefficient of reactivity is given by the ratio of the change in reactivity to the fractional change in U-235 concentration, which was 0.223 $(\delta k/k)/(\delta m/m)$, while the calculated value was 0.234 for the average during the excess uranium additions [37].

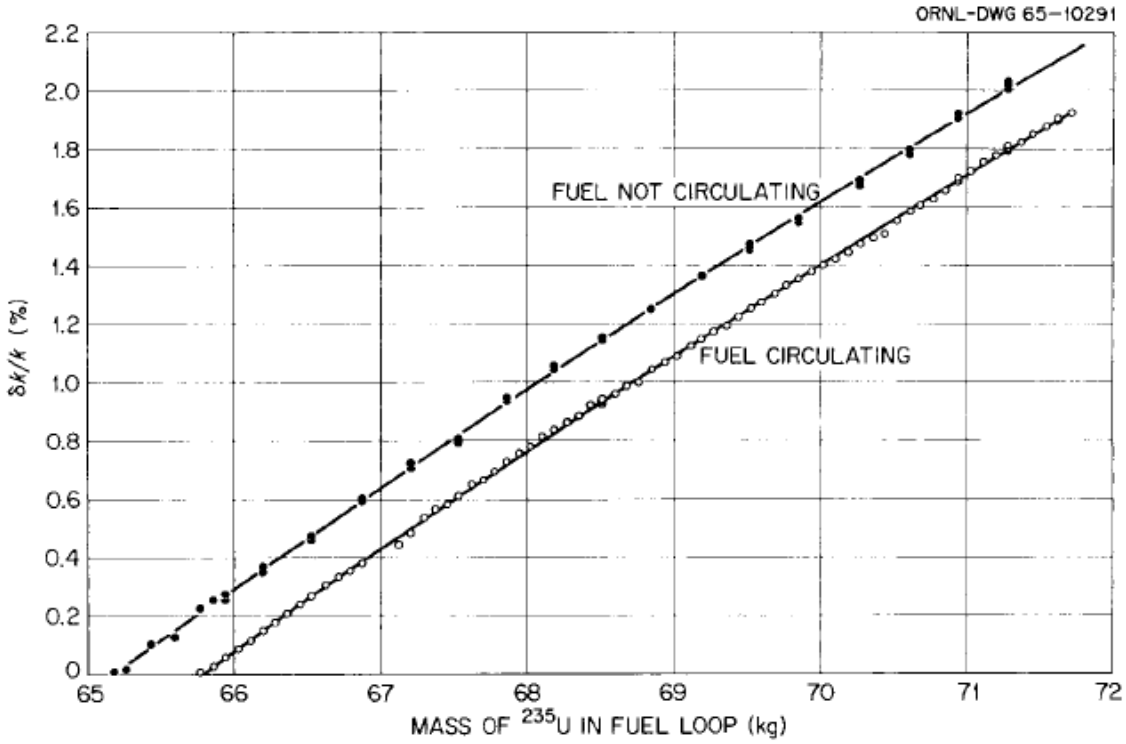

Figure 25. Reactivity change with mass of the U-235 in the MSRE [37].

Rod Shadowing Measurement

After adding U-235 enriching capsules, two separate experiments were performed to explore the change in the critical position of the regulating rod (No. l) while inserting shim rods (No. 2 and No. 3) into the core with the pump running. The first experiment was inserting No. 2 with No. 3 held fully withdrawn. The other experiment inserted No. 2 and No. 3 as a bank. Figure 26 shows the change in the critical rod position of the regulating rod for both experiments considering different U-235 concentrations.

An experimental check was performed to determine if there was any asymmetry in the control rod worths at each U-235 loading and core temperature. The critical positions of each of the three rods were measured and compared with the other two rods held in the fully withdrawn position. The amount of asymmetry in rod worths experiments was negligible because the three control rods were identical [37].

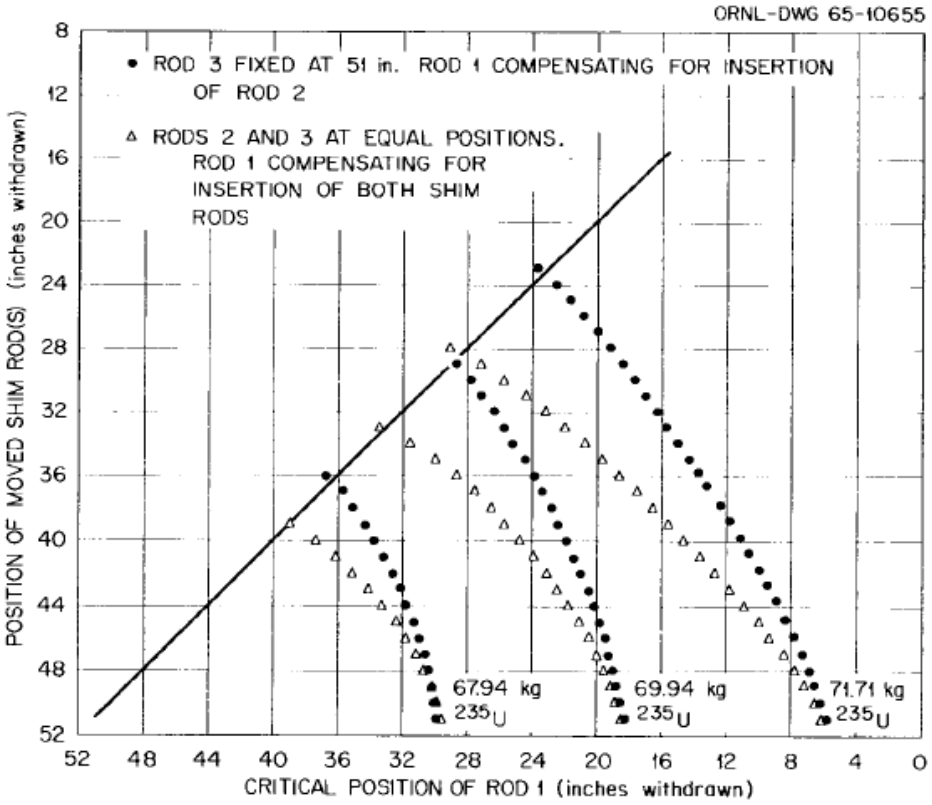

Figure 26. Change in critical position of the MSRE regulating rod No. 1 with the change in shim rod No. 2 and No. 3 positions [37].

Reactivity Effects of Circulating Fuel

The reactivity effect of fuel circulation was determined from the change in the critical rod position of circulating and stationary fuel. It can be obtained directly from the vertical difference between the two lines in Figure 25, which is 0.212% ± 0.004%δk/k. The initial calculated reactivity difference due to fuel circulation, and subsequent change in delayed neutron precursors in the core, was 0.3%δk/k. By extending the calculations to include the contribution of the delayed neutrons emitted while the fuel is in the upper and lower plenums, the calculated reactivity difference due to fuel circulation became 0.222%δk/k. This showed the importance of including the upper and lower plenums in the calculations due to the relatively large fuel volume changes, increased fuel residence times in plenums, and the displaced equilibrium precursor distributions in the upper plenum direction. The measured differential rod worth of the regulating rod with which the fuel is circulating is shown in Figure 24 [37] [38].

Temperature Coefficient Measurement

ISOTHERMAL TEMPERATURE COEFFICIENT

The thermal feedback effects of the MSRE were first determined by measuring the isothermal temperature coefficient, which sums the fuel salt and graphite temperature coefficients. The temperature effects include the thermal expansion of the fuel salt (density changes). The measurement was performed at three different concentrations of the U-235 in the circulating fuel salt where the system temperature was slowly changed (about 15°F/hr) using electric heaters to ensure the fuel salt and graphite are in thermal equilibrium. During the experiment, the critical rod

position was monitored as the temperature changed. The rod position was converted into reactivity using the measured integral worth of the regulating rod. Figure 27 shows the reactivity change about the nominal operating temperature of 1200°F for the three experiments. The temperature was determined from the average of measured values of a set of thermocouples distributed in the system [37].

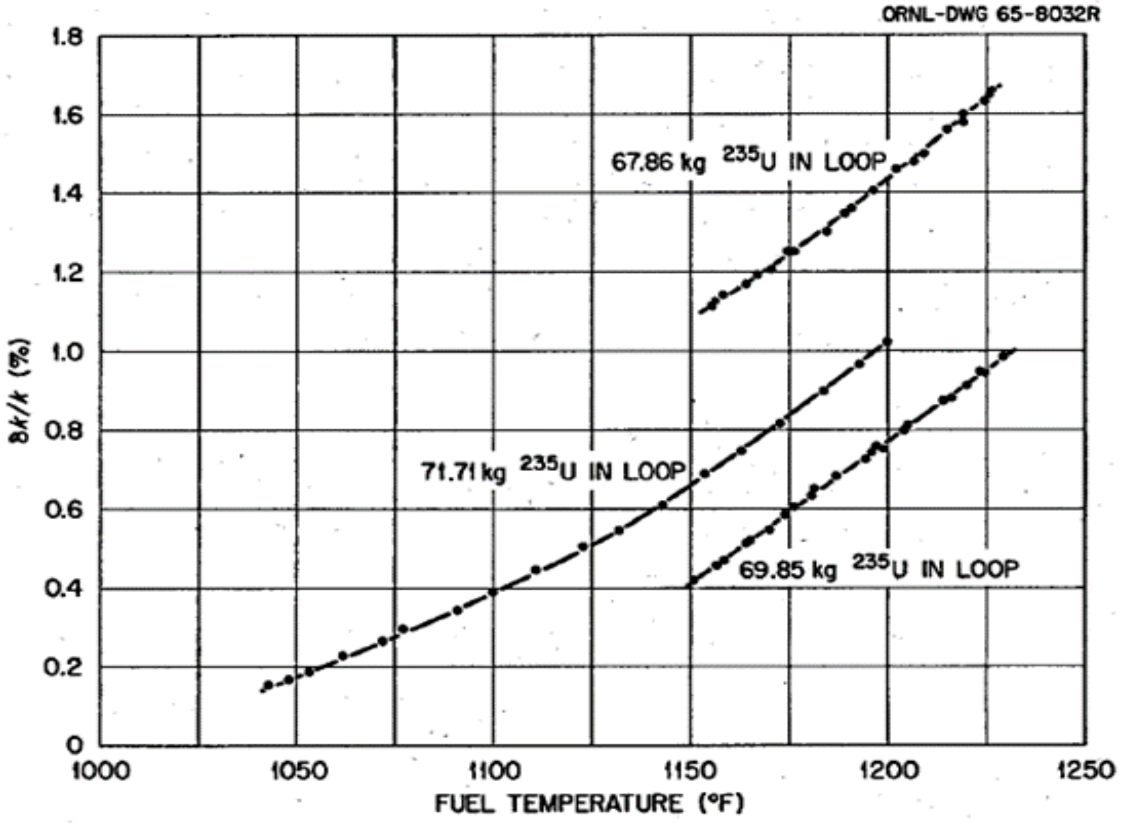

Figure 27. Effect of MSRE core temperature on reactivity [37].

The first two experiments were performed between 1150°F and 1230°F where the last experiment temperature range was 1040°F–1200°F. This observed reactivity change with temperature (i.e., the slope of the 71.7 kg curve in Figure 27) is lower below 1140°F. This is because of the increasing amount of entrained helium bubbles in the circulating salt at lower temperatures[a]. As the temperature was lowered, the fuel salt density increases, which increases reactivity. However, the volume of entrained bubbles increases, thus lowering the coolant density. The reduction in salt density from the bubbles compensates for the increase in salt density due for decreasing temperature, thus reducing the U-235 concentration and corresponding reactivity. The isothermal temperature coefficient (ITC) values derived from these measurements are provided in Table 8. The calculated value of the isothermal temperature coefficient of reactivity was −0.0081%δk/k/°F, with fuel and graphite components being −0.0041%δk/k/°F and −0.0040%δk/k/°F, respectively [37].

[a] A gas stripper in the pump bowl was designed to spray a portion of the salt into the helium purge gas in the pump bowl. The purpose of this device was to purge fission product gases from the molten salt. However, a significant amount of this spray impinged upon the salt's liquid surface causing helium bubble entrainment with the flow pumped back to the core. An equilibrium occurred where the helium entrained would equal the helium purged through the stripper.

Table 8. Measured isothermal temperature coefficient of the MSRE [37].

Experiment No.	U-235	ITC %δk/k/°F
1	67.9	−0.0066 to −0.0083
2	69.9	−0.00724
3	71.7	−0.0073

FUEL TEMPERATURE COEFFICIENT

The fuel salt temperature coefficient was measured by stopping the fuel salt pump and raising the temperature of the circulating coolant salt and stagnant fuel salt in the heat exchanger. Then, the fuel pump was restarted to pass the heated fuel salt through the core. The change in reactivity was attributed entirely to the change in the fuel salt temperature by assuming the graphite remains at its initial temperature.

The measured fuel temperature coefficient (FTC) was -0.0047 ± 0.0007%δk/k/°F. The graphite temperature coefficient was assumed to be equal to the difference between the isothermal temperature coefficient and fuel salt temperature coefficient [37].

Pressure Reactivity Coefficient

The impact of the pressure in the MSRE on reactivity also quantified the worth of undissolved helium in the circulating fuel through the action of the fission product gas stripping device. The volume fraction of gas in the circulating fuel is inversely proportional to the local pressure, which changes with elevation, velocity, and head losses. If the loop pressure is changed rapidly, the mass ratio of undissolved gas to liquid would remain nearly constant. The volume fraction of gas in the loop would decrease as the pressure is increasing, which would give a positive pressure coefficient of reactivity. For very slow increases in pressure, the volume fraction of gas at the pump suction would remain constant, and the volume of gas in the core would increase (i.e., increasing pressure slowing causes more helium to become entrained). The slow increase in entrained helium with increasing pressure produces a small negative pressure coefficient of reactivity.

The pressure reactivity coefficient was measured in three tests with the loop overpressure slowly increased from the normal 5 to 15 psig and then quickly relieved. The first two tests were carried out at the normal system temperature with the normal operating salt level in the fuel pump bowl. No change in the control rod position was recorded, which indicates that there were no helium bubbles circulating with the fuel salt. The third test was performed at an abnormally low pump bowl level, which was obtained by lowering the operating temperature to 1050°F [37].

Protected Pump Experiments

Flow rate transients were performed to obtain fuel flow rate change effects on reactivity. Figure 28 shows the fuel and coolant pump speeds and coolant flow rate changes during startup and coast down transient tests.

For flow rate change effects on reactivity tests, the reactor was operated at a low power level (~10 W), and the fuel flow rate in the primary loop was increased or decreased by adjusting the speed of the fuel pump. Since the reactor was at a low power level, the temperature feedback effects were negligible, and the reactivity changes were mainly due to the flow perturbations. During the test, the control rod position was adjusted to maintain a constant low power level by compensating for the reactivity changes from flow changes and associated redistribution of delayed neutron precursors in the core and their decay outside the core. The recorded control rod

positions during the startup and coast down tests are provided in Figure 29. The recorded control rod positions can be converted into reactivity data using the integral control rod worth curves [37].

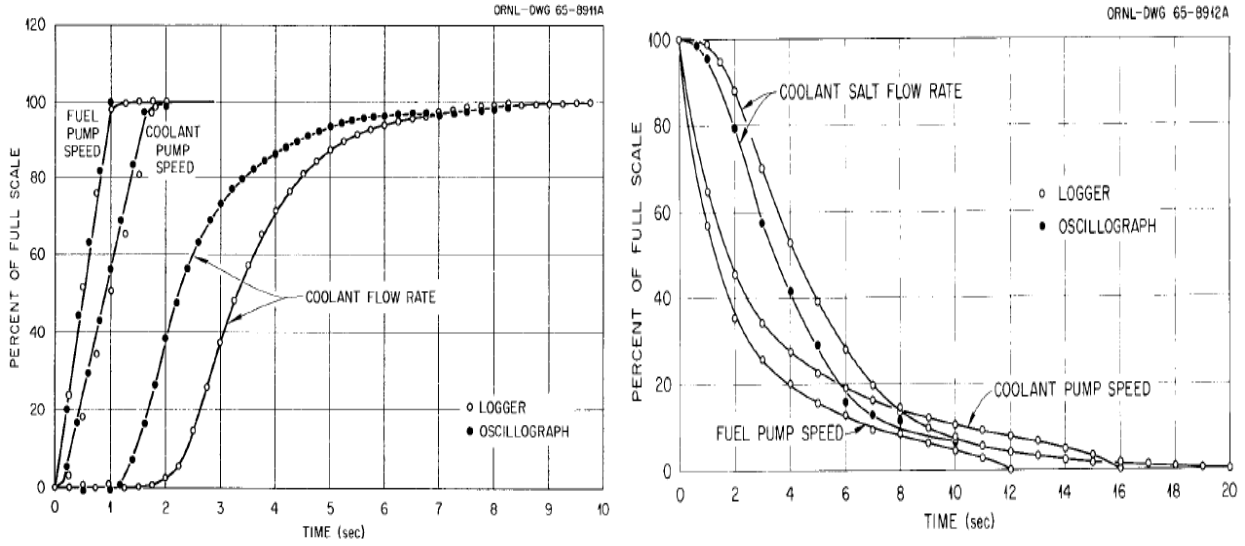

Figure 28. Fuel and coolant pump speeds and coolant flow rate change during MSRE startup (left) and coast down (right) transient tests [37].

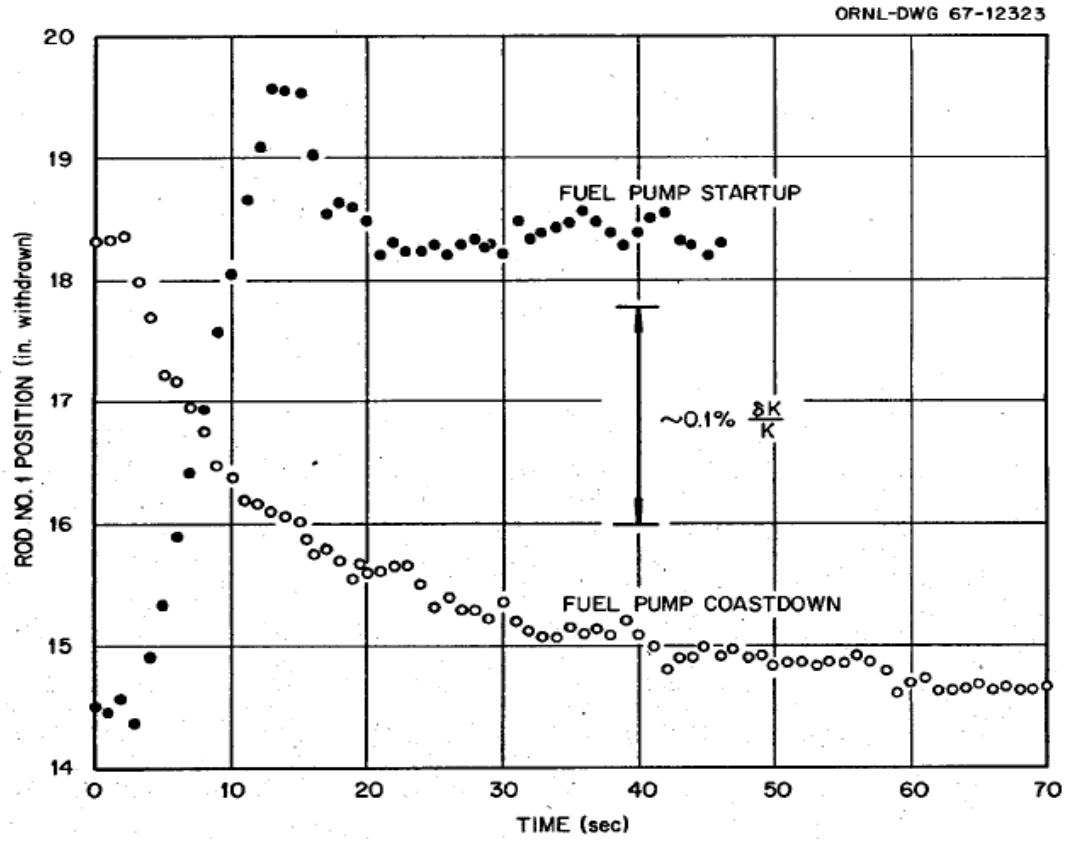

Figure 29. Control rod response to MSRE fuel pump startup and coast down transient tests [37].

Thermal Convection Heat Removal Test

The purpose of this test was to determine the characteristics of heat removal from the MSRE fuel system by natural convection flow of the fuel salt. This test was conducted with U-233 in the carrier salt. At the beginning of the test, the reactor was operated at a low power of about 4.1 kW with a limited fuel flow rate and maintained a forced circulation in the coolant system during the test. The core inlet temperature was then decreased by increasing the heat removal rate in the air radiator in the secondary loop for 6 hours while the reactor was at critical conditions. The reactor was controlled entirely by the inherent thermal feedback of the system during this transient, and no adjustments were made to the control rods. Figure 30 shows the measured reactor power, reactor inlet and outlet temperatures, and coolant inlet and outlet temperatures for the 6 hour period. There are no data recorded for the fuel salt inlet mass flow rate or the heat removal rate by the secondary loop. The reactor power followed the radiator load smoothly and with small oscillations. The maximum power attained was 354 kW while limiting the temperature difference across the reactor vessel to not exceed 75°F [40].

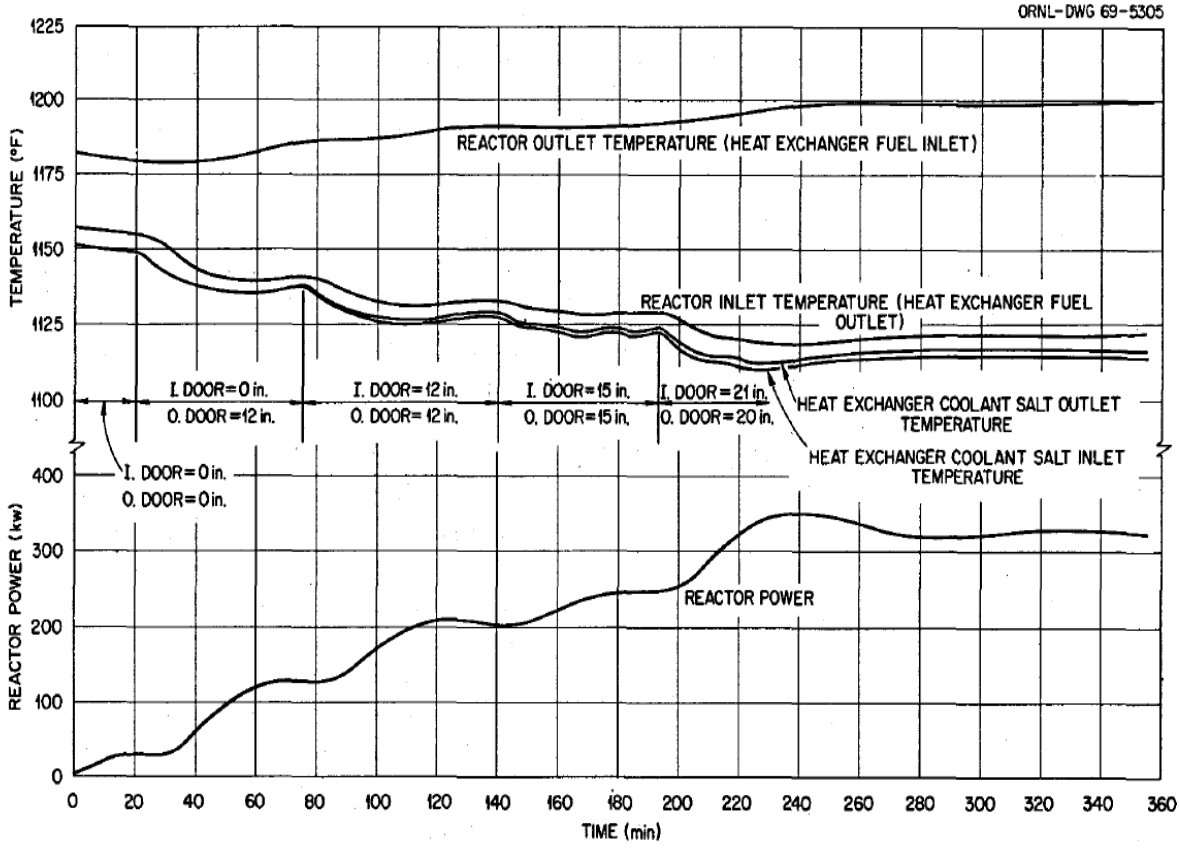

Figure 30. Recorded power and temperatures during natural circulation test of the MSRE [40].

Reactivity Insertion Experiments

During power ascension after loading the U-233 in the salt carrier, step reactivity insertions were introduced into the system by withdrawing the regulating rod from its critical position and observing the time response of the neutron flux. The test was performed at three power levels, 1.0, 5.0, and 8.0 MW, with reactivity insertions of 0.0139, 0.0190, and 0.0248%δk/k, respectively. The main purpose of these tests is to characterize the dynamic response of the system relative to a

step change in reactivity. Figure 31 shows the measured change in the reactor power for each power level with introduced reactivity along with calculation results from ORNL. The dynamic response of MSRE from these tests was characterized as slower responding and more oscillatory at lower power. Compared to the high-power case (8.0 MW), the low-power case (1.0 MW) oscillatory behavior of the system was much longer and the power change relative to the initial power or fractional amplitude of the oscillations was higher. This is related to the thermal feedback of the system and fuel circulation time [41] [42].

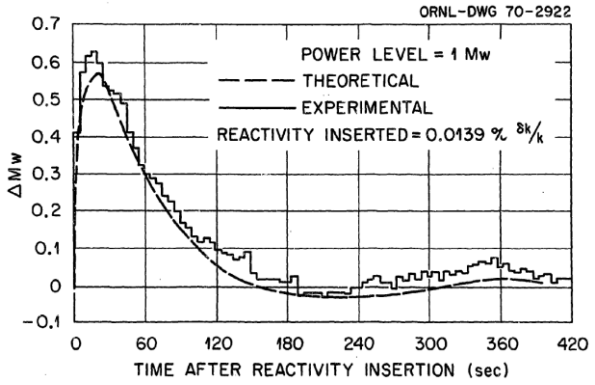

(a) 0.0139%δk/k. initial power of 1.0 MW.

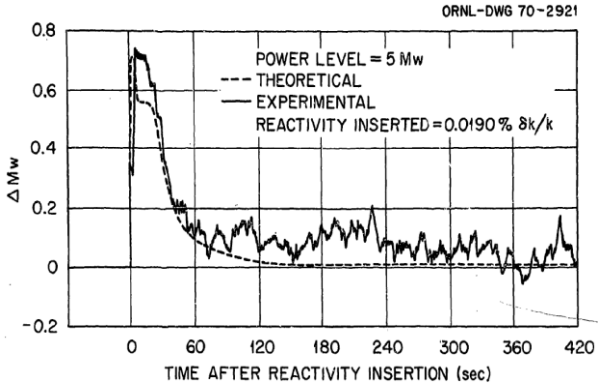

(b) 0.0190%δk/k. initial power of 5.0 MW.

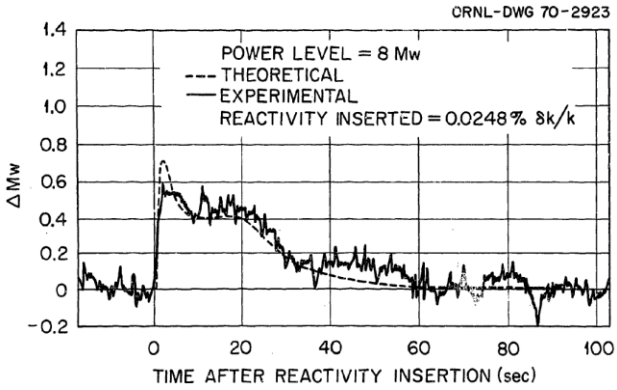

(c) 0.0248%δk/k. initial power of 8.0 MW.

Figure 31. Change in reactor power after step reactivity insertions in the MSRE [41] [42].

Comparison of Predicted and Measured Values

The published MSRE reports do not contain quantitative or qualitative acceptance criteria for startup tests with either U-235 or U-233 fuels. However, a comparison of the ORNL predicted or calculated values and the measured values of the MSRE initial startup tests is provided in Table 9 and Table 10 for U-235 and U-233 fuels, respectively. For all the tests, the predicted values are within 7.0% of the measured values except for the isothermal and FTC of the U-235 fuel case where the differences are 11.0% and 16.5%, respectively.

Table 9. Comparison of the measured and calculated values of the initial startup tests of the MSRE with U-235 fuel [30] [37].

	Test	Unit	Measured Value	Calculated Value	Calculated/ Measured
1	Initial critical concentration in salt	gU/liter	32.85 ± 0.30	33.06	1.0064
2	Reactivity loss due to fuel circulation	% δk/k	0.212 ± 0.004	0.222	1.0472
3	Control rod worth / Rod 1	% δk/k	2.26 ± 0.06	2.11	0.9336
4	Control rod worth / bank	% δk/k	5.59 ± 0.16	5.46	0.9767
5	Isothermal temperature coefficient	%δk/k/°F	-0.0073 ± 0.002	-0.0081	1.1096
6	FTC	%δk/k/°F	-0.0049 ± 0.0023	-0.0041	0.8367

Table 10. Comparison of the measured and calculated values of the initial startup tests of the MSRE with U-233 fuel [30].

	Measured Parameter	Unit	Measured Value	Calculated Value	Calculated/ Measured
1	Initial critical concentration in salt	gU/liter	15.15 ± 0.1	15.30	1.0099
2	Reactivity loss due to fuel circulation	% δk/k	—	0.093	—
3	Control rod worth / Rod 1	% δk/k	2.58 ± 0.07	2.75	1.0659
4	Control rod worth / bank	% δk/k	6.90 ± 0.20	7.01	1.0159
5	Isothermal temperature coefficient	%δk/k /F	-0.0085 ± 0.002	-0.0088	1.0353
6	FTC	%δk/k /F	—	-0.0057	—

HIGH-TEMPERATURE GAS REACTORS

Fort St. Vrain

Reactor Design Summary

The FSV reactor was built by the General Atomics Company and was owned and operated by the Public Service Company of Colorado. FSV began fuel loading in 1973 [43], and electric power generation began in 1976 [44]. The FSV reactor was permanently shut down in 1990 [45]. The rated reactor power was 842 MWth.

The active core had an effective diameter of 19.5 ft and an effective height of 15.6 ft [46] and was an approximate cylindrical array of individual graphite prisms. The side reflector had a thickness of 3.9 ft, and the top and bottom reflector had thicknesses of 3.3 and 3.9 ft, respectively. The active core consisting of 247 vertical columns of fuel elements was distributed over 37 regions, or 1,482 fuel elements stacked in six layers [47, 46]. A layout of the active core is shown in Figure 32, and a vertical view of the core is shown in Figure 33. The layout in Figure 32 identifies the regions of the core.

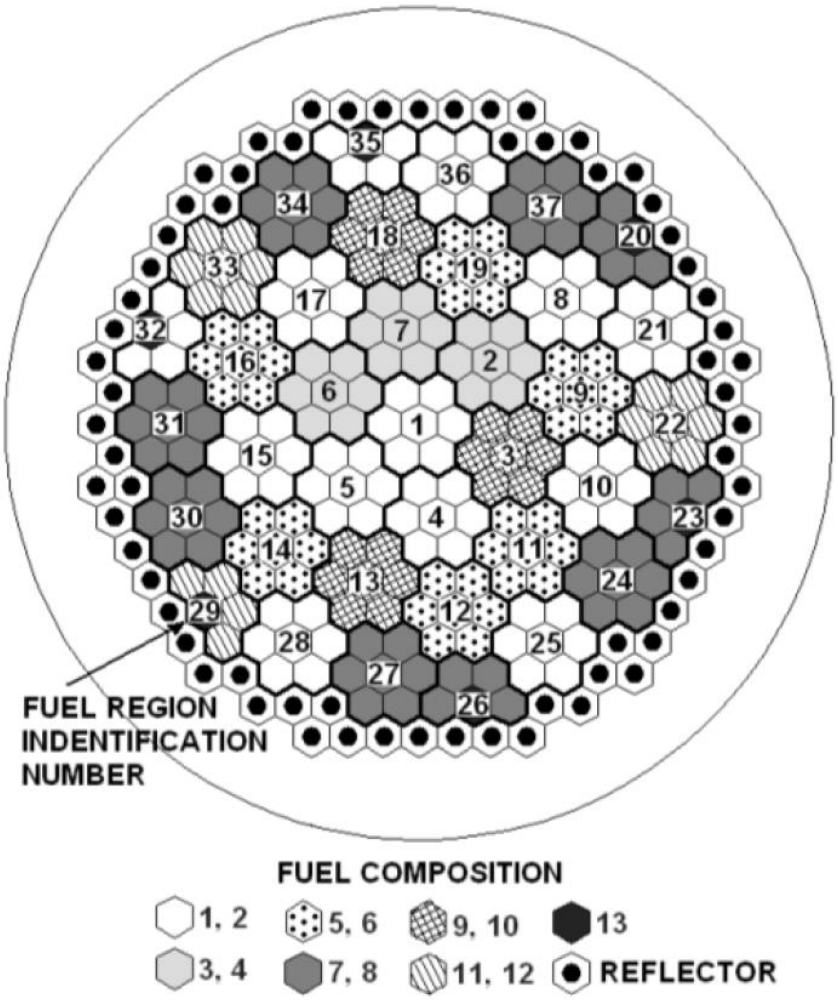

Figure 32. A radial cross-section of the FSV reactor [48].

A steel core barrel and prestressed concrete reactor vessel (PCRV) [49] surrounded the core. The PCRV internal diameter was 31 ft with a 75 ft internal height. The upper and lower heads were nominally 15 ft thick. The PCRV walls had a nominal thickness of 9 ft. It contained coolant at operating pressure and provided radiological shielding. The concrete walls and heads of the PCRV had a carbon-steel liner that is nominally 0.75 inches thick, which provided a helium-tight membrane. The steel core barrel, PCRV, and liner are shown in the vertical cutout diagram in Figure 32.

A standard fuel element had 108 coolant channels and 210 holes for fuel. The pitch between fuel elements was 0.74 inch [47]. The standard hexagonal fuel element block was 14.172 inches across the flats and 31.22 inches high. The fuel holes in the elements had a 0.50 inch diameter. These holes were filled with stacks of fuel compacts. The compacts consisted of TRISO particles dispersed in graphite [50]. There were two types of TRISO kernels, fissile and fertile, consisting of uranium-thorium-carbide and thorium-carbide, respectively. The uranium enrichment was 93 wt%. There were 13 different fuel concentrations in the FSV core, which were varied by changing the proportion of fissile and fertile TRISO particles [47] [44].

Each region of the central column of fuel elements contains three parallel channels. Two channels were for control rods that move as a unit, and the third channel was for shutdown poison balls that are inserted in case of an accident [51] [52].

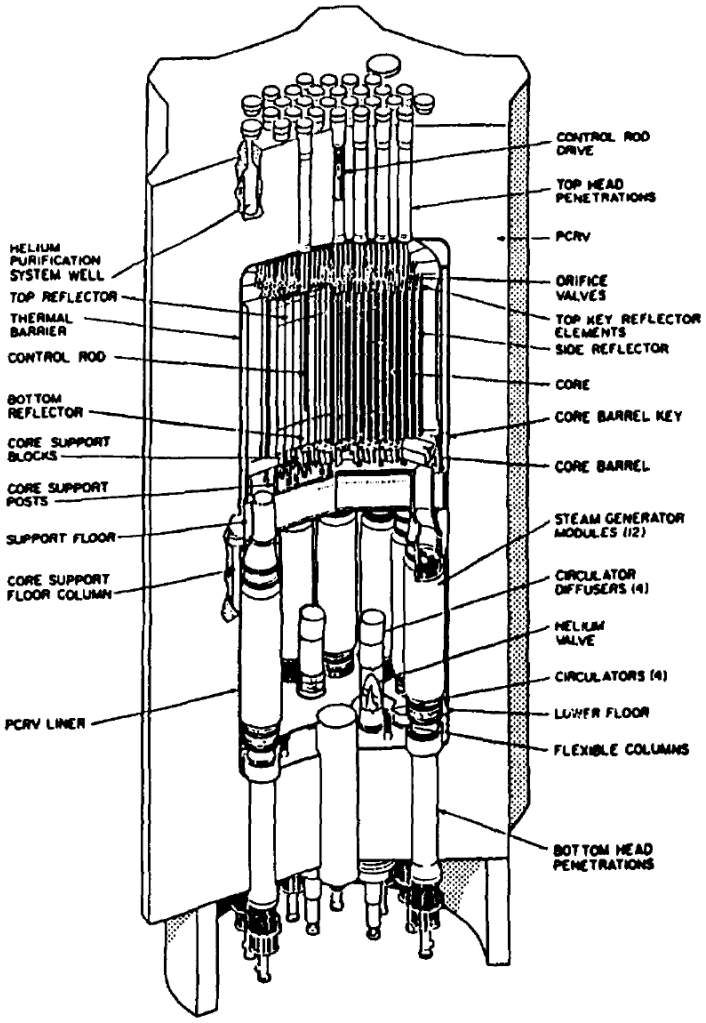

Figure 33. Vertical cross-section of the FSV reactor [53].

Approximately 3.4×10^6 lb/hr of 760°F primary coolant helium entered the core from the upper plenum and passed through orifices in each region. The helium flowed downward through the coolant holes in the reflectors and active core and exited through the core support blocks to the lower plenum at an average outlet temperature of about 1430°F [46] [49]. The helium then flowed through twelve steam generator modules [43]. The steam exited the steam generator modules and entered the high-pressure turbine. Cold reheat steam then left the high-pressure turbine and provided the driving force for the four helium circulators and reheated the upper section of each steam generator module. This reheated steam was then directed back to the intermediate and low-pressure turbines and finally to the condenser [43].

Startup Physics Test Program

The FSV startup testing program was divided into two groups, the low-power physics tests and the rise-to-power tests [54, 43]. A list of the low-power tests is shown in Table 11. Test A1 is the core loading discussed above. In Table 11, two tests are not present, Test A2 was removed and

Test A5, Burnable Poison Loading Adjustment, was not performed [54]. The low-power physics tests include zero-power tests to confirm established core characteristics [55]. A list of the rise-to-power test is given in Table 12. These tests were conducted after FSV was brought to critical and verified the safe performance of the reactor [54].

Table 11. Low-power tests performed for FSV taken from Reference [54].

Test Number	Description of Test
A1	Initial loading of fuel and reflector elements. Loading of fuel elements, temporary absorbers, and reflector elements while a subcritical configuration was maintained.
A3	Pulsed source measurements and initial criticality. Using a pulsed neutron source, the core was repetitively pulsed to determine its shutdown margin at various configurations.
A4	Control rod drive and orifice tests. Temporary absorbers were removed, and the permanent control rod drive and orifice assemblies were installed and tested.
A6	Differential control rod worth measurements. Using a reactivity computer, the worth of rod pairs and groups were calibrated.
A7	Neutron flux distribution measurements. Axial flux distributions were measured for un-rodded, rodded, and partially rodded regions.
A8	Reactivity coefficient measurements. The pressure and temperature coefficients were measured.
A9	Fuel handling machine. Using the computerized fuel handling machine, one region of the core was unloaded from the reactor, transferred to the fuel storage facility, and returned to the reactor.
A10	Low-power helium purification test. The operability of the helium purification system during the initial heating and outgassing of the reactor core was demonstrated.
A11	Helium circulator performance. The operability of the system with water and steam as the motive sources was verified.

Table 12. The rise-to-power tests in the FSV reactor [54].

Test Number	Description of Test
B1	Steam generator performance verification. The performance of an instrumented steam generator module with the simulated plugging of one feedwater tube was evaluated the steady-state and transient performance of the turbine-generator was tested.
B2	Analysis of chemical impurities in the primary coolant. At selected time intervals, analyses were made of primary coolant and helium purification system impurities.
B3	PCRV performance. At steady-state power levels, the effectiveness of both the liner thermal barrier and liner cooling system were evaluated.
B4	Primary system performance. At steady-state power levels, the four helium circulators and their auxiliaries were evaluated.
B5	Plant instrumentation performance. The power range nuclear and feed water instrumentation is calibrated. The permanent thermocouples are compared to calibration thermocouples.
B6	Plant transient performance. The transient performance of the plant protective systems was demonstrated after nine planned trips selected to duplicate those that could occur during plant performance.
B7	Plant automatic control system performance. The responses of 18 separate control subsystems, which operate independent of and are subservient to the plant protection system, were evaluated during steady-state operation and power shafts.

B8	Reactivity coefficient measurements. During increasing or decreasing power shafts, the temperature coefficient of reactivity was measured.
B9	Differential control rod worth measurements. While at steady-state power levels, control rod pairs were calibrated by differential measurements using the reactivity computer and normal plant instrumentation.
B10	Xenon build up and decay measurements. Using control rod worths and temperature coefficient data, the xenon reactivity effect was measured.
B11	Xenon stability. With the power at a steady 100%, the transient response of the power distribution due to xenon following a planned flux perturbation will be evaluated to verify that the power distribution is stable with respect to radial and azimuthal oscillations.
B12	Shielding surveys. The adequacy of the plant shielding was determined at two steady-state power levels and during a rapid regeneration of one of two helium purification systems.
B13	Radiochemistry analysis of the primary coolant. Radioactive gaseous and iodine probe analyses were made at all major steady-state power levels.

Experimental Methods and Results

Several key core parameters were measured and calculated during both core loading and the initial core criticality. To perform these measurements, two different sets of detection instruments were used. One set was six B-10 proportional counters used during the core loading process with changing positions. These instruments were withdrawn after the core loading process [56]. During core startup and normal operations, six wide-range neutron flux detectors located symmetrically around the core in wells in the PCRV [52] were used to measure the neutron flux.

FUEL LOADING AND INITIAL CRITICALITY

The loading of FSV fuel and reflector elements started in December 1973 and the last element was loaded on January 1974 [56]. A 1 curie Pu-Be neutron source was positioned in the reserve shutdown hole of Region 1 of the first fuel layer and remained there throughout the core loading [57]. For most regions, the elements comprising one layer of a region were loaded before the next, and the loading of one entire layer of blocks was completed prior to loading the next layer. The core was loaded radially outward for each sequential vertical layer. To ensure subcritical configurations during fuel loading, temporary absorber rods consisting of steel cans filled with B_4C [56] were installed in the three control channels beyond the first 34 refueling regions. During the loading, the 34 control rod drive assemblies were removed, but three control rod pairs and drive assemblies were installed and available for scram insertion into the core [56]. After fuel loading, pulsed neutron source measurements of control rod worths were performed, the temporary absorber rods were removed, and the permanent control rod drives were installed region by region [57].

While loading the 33 fuel elements around the central fuel element, the detectors were moved to the reserve shutdown holes. A view of the loading pattern of the first seven regions is shown in Figure 34, and the complete listing of the loading pattern is given in the appendix of Reference [56].

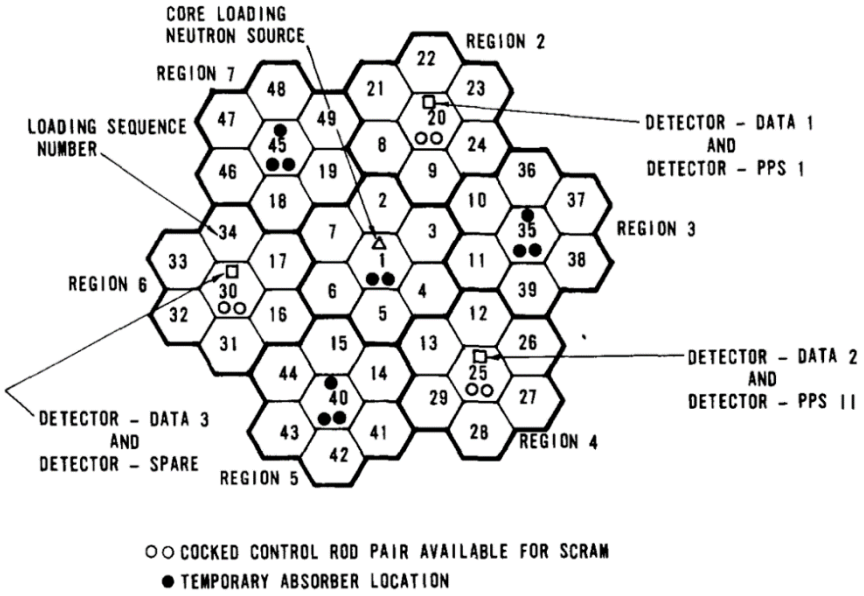

Figure 34. Diagram of the FSV fuel block loading pattern [56].

Inverse multiplication (1/M) measurement and calculations for the detector located in Core Region 2 are shown in Figure 35. The diffusion code GAMBLE calculated both the detector response and 1/M curves shown in Figure 35 [56]. In Figure 35, there are sharp discontinuities as absorbers were added and the detector positions were shifted during loading, and the detector shows a sharp drop when the second layer fuel is added. The detectors were initially in the Central Region 1 location but were shifted as Regions 2, 4, and 6 were loaded. The detectors were moved or added when the fuel block was added to the sequence. In Figure 35, the general shape of the calculated result compares well to the measurement. The measured inverse count rate consistently showed a smaller change than that predicted by the R-Z diffusion theory calculations. However, X-Y diffusion calculations were applied when the presence of strong absorbers and asymmetric detectors were added during the loading sequence. The smaller change and consistent greater value of the measured 1/M curve compared to the diffusion-calculated 1/M curve indicates that the core was more subcritical than calculated [56].

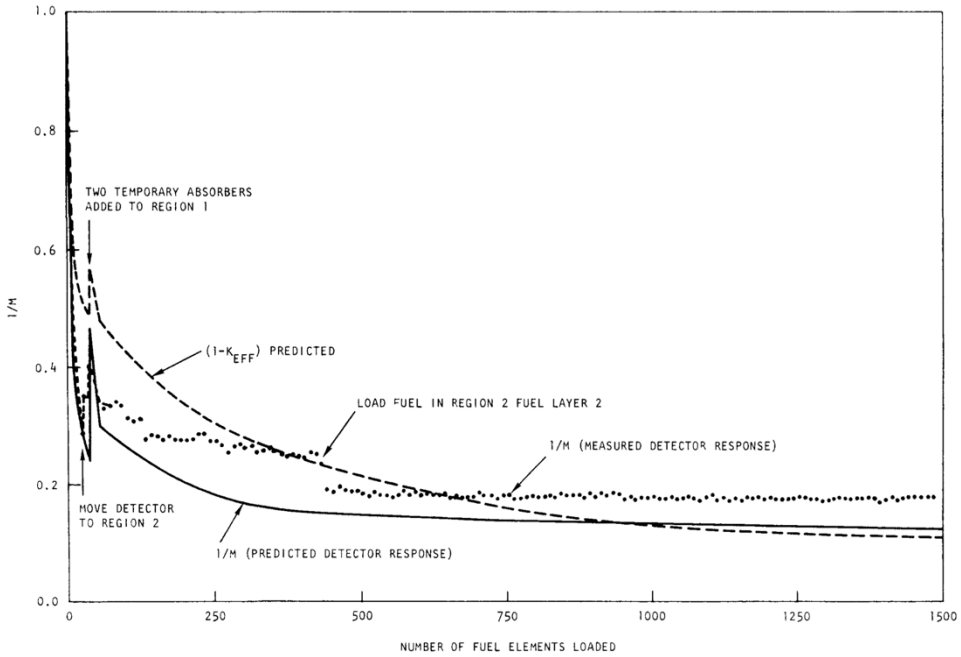

Figure 35. Concave up 1/M plots for in-core detectors located in Region 2 observed during fuel loading of the FSV reactor [56].

Later in the testing program, the six neutron detectors, located at the sides of the PCRV wer found to have a decalibration issue. This was because the detector signal was generated primarily from the flux from the outer portions of the reactor core [58]. Because the two californium-252 startup sources were in the top layer of the fuel, the neutron signal from the detector was affected by the control rod positions. The 1/M curves were not the desired concave-up shape. This was determined to be a result of poor correlation between the measured ex-core flux and the core average flux. The poor correlation was caused by flux distortions created by mismatched control rod insertions between the inner and outer core. The solution was to administratively limit the control rod withdrawal rate [46].

PULSED NEUTRON MEASUREMENTS

Before the core was brought critical, pulsed neutron experiments were performed on the FSV core to determine reactivity for different control rod positions [59] [51]. From the reactivity measurements, control rod worths and shutdown margins were obtained, and for certain configurations near critical, the mean neutron generation time and lifetime were determined. For predictions of the pulsed neutron method, computer simulations were performed to obtain placement of the pulse source and detectors [59]. The pulsed neutron source was a Kaman Model A-801 that produces 14 MeV neutrons by accelerating deuterium atoms into a tritium target [51]. The source was always placed in Region 1, and the detectors were placed in Regions 16, 30, and 31 for all measurement configurations [51]. Pulsing of the core with the temporary absorbers and the three control rods inserted initially showed the core to be more subcritical than calculated. After the initial pulsing experiment, the temporary absorbers were removed and the permanent control rod drives were installed region by region, from a prespecified sequence [57]. A total of 13 distinct control rod configurations were pulsed and included two configurations with a temporary absorber in the core, eight with rods withdrawn in the normal sequence, and three with high-worth rods withdrawn [51].

CONTROL ROD WORTH MEASUREMENTS

During the rise-to-power tests after the initial core criticality, the worths of the control rods were determined and compared to calculated values [60, 52]. The regulating rod worth was determined by the double bump technique while the other control rod worths were determined by a substitution technique. Details of the double bump and substitution techniques are given in Reference [52]. The average signal from three ex-core detectors located in the PCRV provided input to a reactivity computer, which calculated the reactivity change from the control rod movement. The measurements provide data for differential reactivity worth to which a curve was fitted using a least squares technique. The curve was then integrated to obtain the reactivity for the rod position, which then was compared to calculated values.

TEMPERATURE COEFFICIENT MEASUREMENTS

The negative temperature coefficient was measured during the low-power tests and the rise-to-power tests [52]. For the low-power tests, the negative temperature coefficient was obtained by heating the helium coolant to ~148°C with a reactor power under 100 W. The core temperature was allowed to equilibrate after every 28°C increase. The central rod was moved to maintain criticality, and a differential reactivity measurement was made every 254 mm of rod motion. For the rise-to-power tests, the negative temperature coefficient was obtained by measuring the change in reactivity from a successive set of power increase steps. At each new power level, the temperature was allowed to equilibrate over 1 hour. The change in reactivity was obtained from the reactivity change in the measured power level and the known calibrated worth of the control rod bank position. For comparison, the R-Z diffusion code GAMBLE and the hexagonal fine mesh diffusion code BUGTRI were used to calculate the temperature coefficient [61] [52].

RADIAL PEAKING MEASUREMENT

The radial peaking factor (RPF) or the ratio of the power density generated in an individual fuel element relative to that of the average power density of the core was both measured and calculated and gives a radial distribution of the energy generated across the core [52, 45]. The thermal power of each fuel column, Q_r, was calculated from the measured temperature rise, $(\Delta T)_r$, in each column as

$$Q_{r=\dot{m}_r C_p (\Delta T)_r} \quad 3$$

where Cp is the coolant's heat capacity and $\dot{m}_r$ is the mass flow rate through the fuel column. The RPF is then the ratio of the individual fuel column divided by the average of all fuel columns. The flow, $\dot{m}_r$, of the helium coolant was inferred from the positioning of the orifice valve positions. In general, the measured RPFs in the north boundary regions were lower than the calculated RPF, while the measured RPFs in the south boundary regions were higher [62]. After investigation, these differences were attributed to the position of the thermocouple strings and the presence of cool helium in the north boundary region. Details can be found in Reference [52].

AXIAL PEAKING MEASUREMENT

Axial neutron flux shapes were measured during the very low-power test stage in an air environment [57] [52]. At higher powers, the temperature would be too high for the neutron detectors. The axial flux distribution measurements were made after the core was loaded and was at a clean critical state. The core power was less than 1 watt. One detector was kept in place for normalization while another detector was traversed axially to obtain the reading. The measured flux readings and calculated values from the diffusion codes showed good agreement.

Comparison of Predicted and Measured Values

The values in Table 13 are taken from References [52], [57]. [60], [62], and [63]

Table 13. Agreement between test results and predictions for the FSV reactor.

Parameter	Unit	Measurement	Computed	Maximum Difference
Temperature Coefficient	$(\Delta\rho\ [°F]^{-1})*10^{-5}$	-6.9 -7.5	-6.9 -7.5	<4%
Control Rod Worth : 3C	Δk	0.034	0.036	<6%
Control Rod Worth : 2A	Δk	0.037	0.035	<6%
Control Rod Worth : 4B	Δk	0.008	0.008	—
Control Rod Worth : 4F	Δk	0.009	0.010	<12%
Shutdown Margin	Δk	0.096	0.098	<3%
Radial Peaking Factor	Normalized	0.34–2.16	0.36–1.99	18%
Axial Flux Distribution	Normalized	0.35–1.85	0.4–1.8	12.5%
Eigenvalue for Criticality Control Rod Position	—	1.001	1.0	0.1%

High Temperature Engineering Test Reactor

Reactor Design Summary

The HTTR is a graphite-moderated and helium-cooled block-type HTGR designed to demonstrate the hydrogen production and HTGR safety characteristics [64]– [65]. The HTTR first achieved criticality November 10, 1998, and began to produce 30 MWth of power with an outlet coolant temperature of 850°C on December 7, 2001 [66].

The HTTR is designed for a 950°C outlet gas temperature and is composed of different hexagonal block elements [67]. The blocks are categorized into fuel, control rod, and reflector elements and are stacked to form the HTTR core columns [68]. The active core consists of 30 fuel columns and seven control rod guide columns. Twelve replaceable reflector columns, nine reflector region control rod guide columns, and three irradiation test columns surround the active core. Permanent reflector blocks surround the replaceable reflector blocks and are fixed by a core restraint mechanism. The HTTR fuel elements are composed of fuel rods in a hexagonal graphite block also called a pin-in-block design [67]. Each fuel rod consists of 14 fuel compacts. Each compact contains spherical TRISO or coated fuel particles dispersed in graphite with a packing fraction of 30% by volume [69] [70]. Each fuel compact is a circular annulus with an outer diameter of 2.6 cm, an inner diameter of 1 cm, and a height of 3.9 cm. The spherical TRISO fuel particles are 0.92 mm in diameter. The low-enriched TRISO fuel kernels are enriched from 3.4 wt% to 9.9 wt% with about 6 wt% on average. A diagram of a vertical slice of the HTTR is shown in Figure 36 and a horizontal cross section is shown in Figure 37.

The HTTR helium coolant is pumped through the core bottom and flows to the top of the core. As shown in Figure 36, the helium is then forced to flow downwards in the annular spaces between the fuel rods and holes in the graphite [71]. The overall reactor cooling systems is composed of a main cooling system, an auxiliary cooling system, and a vessel cooling system [72]. The main cooling system is used during normal operations and exchanges heat with an intermediate heat exchanger and a pressurized water cooler [66]. The auxiliary cooling system is a safety feature that operates if the reactor undergoes a scram, and it removes heat through the auxiliary heat exchanger. The vessel cooling system is also a safety feature designed to cool the biological shield under normal operations and acts as a cooling system after an accident.

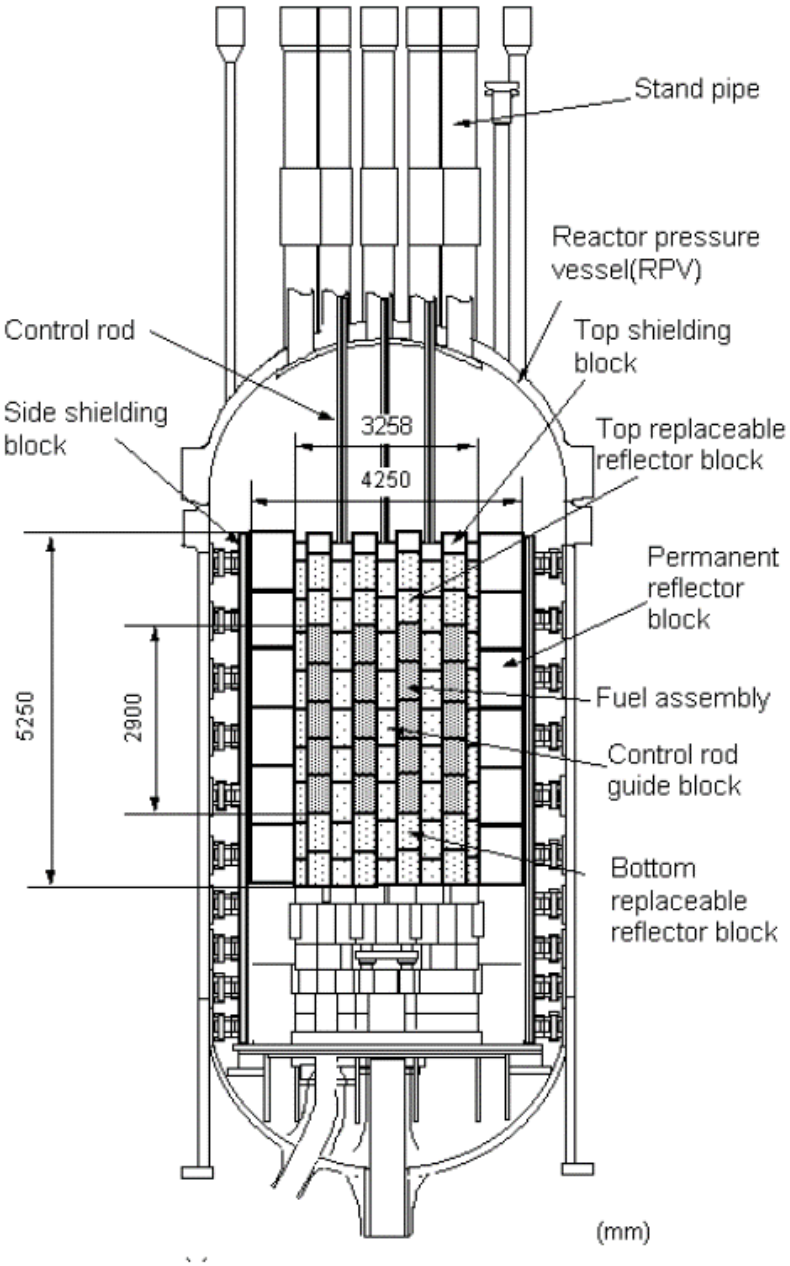

Figure 36. Vertical cross section of the HTTR [73].

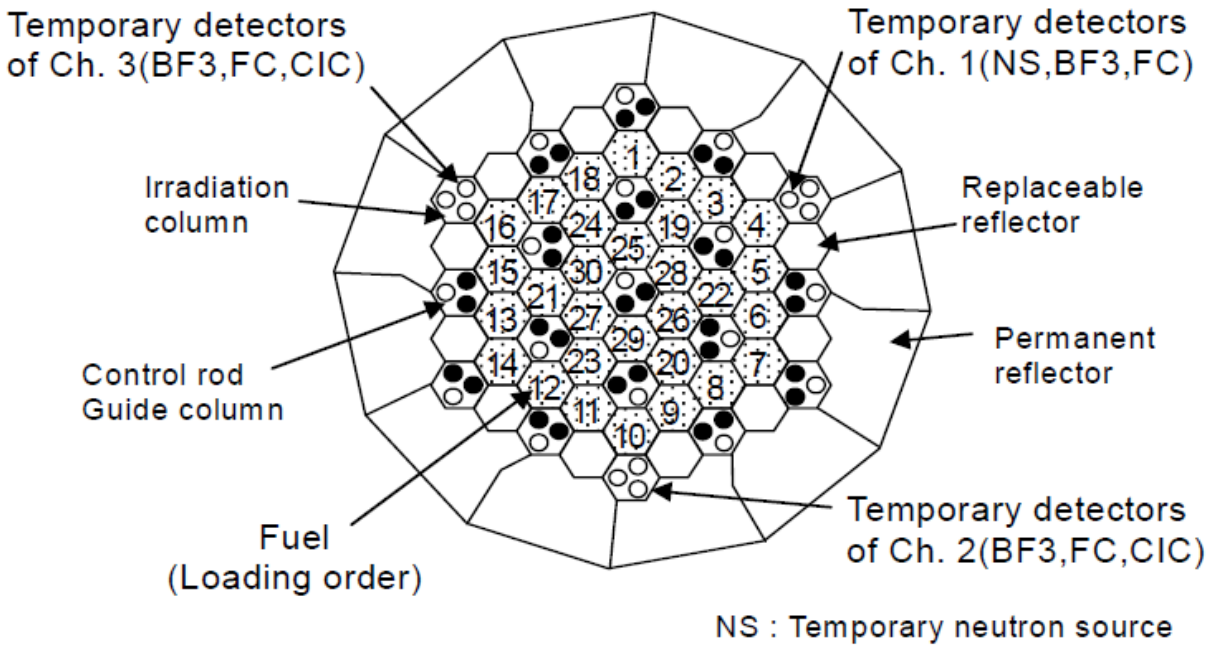

Figure 37. Horizontal cross section of the HTTR [73].

Startup Physics Test Program

Before initial criticality on November 10, 1998, non-nuclear heatup tests were performed in February 1997 [74]. One surprising outcome of the heatup tests was that the temperature of primary upper shielding as well as the helium gas temperature inside reactor standpipes were higher than expected and exceeded design limits. Modifications were made to keep the temperature within acceptable limits, and tests were conducted to verify their effectiveness [74]. Experiments and computer code validation were applied to the standpipe components to ensure safe operation [75].

During and after core loading, measurements were conducted to determine excess reactivity, shutdown margin, control rod worth, temperature coefficients, axial neutron flux distributions, and radial and axial power distributions.

Tests were also conducted to demonstrate the HTTR safety features [72] [76]. A timetable of the conducted low-to-intermediate power tests are shown in Figure 38.These tests demonstrated safe operation up to 850°C, which is useful for demonstrating heat removal features for HTGRs.

During the rise-to-power tests at 20 MW, the reactor core support plate showed a temperature rise that would exceed the design limit temperature of 470°C when the reactor operated at 30 MW [77]. After determining the cause of the unexpected temperature rise and re-evaluating the design limit, the design limit temperature of the support plate was revised to 530°C.

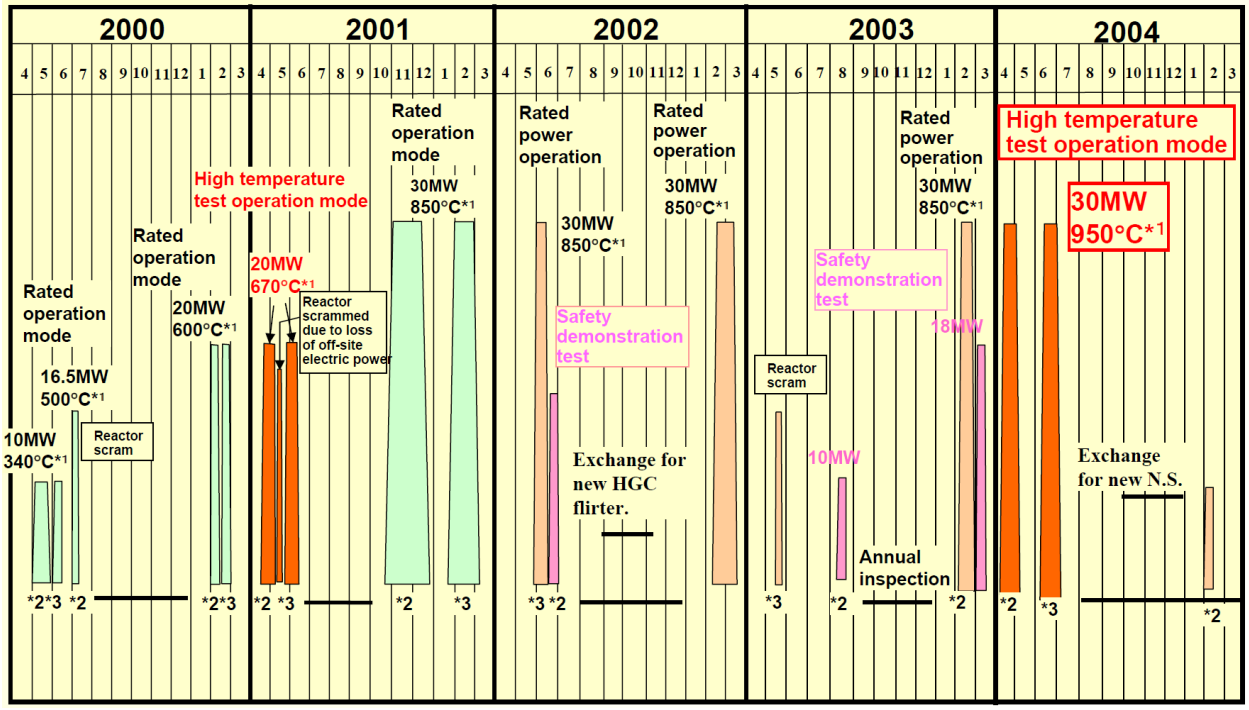

Figure 38. Sequence of testing at HTTR [78].

Experimental Methods and Results

CRITICAL EXPERIMENTS

Although not part of the startup testing, several critical parameters for HTTR safety calculations were first obtained from the Very High Temperature Reactor Critical Assembly (VHTRC). The VHTRC was constructed for measuring neutronics data, such as temperature coefficient and delayed neutron fraction [79] [80], and providing validation data for a suite of neutronics design and analysis codes [81]– [82]. The VHTRC was a reconstruction of the Semi-Homogeneous Experiment. The experiments conducted with Semi-Homogeneous Experiment provided validation data for different codes [83]. At the time of reconstruction, neutronic measurements had been performed for highly enriched fuel HTGRs, but no experimental work for the temperature dependence of reactivity had been reported on a clean HTGR core fully loaded with low-enriched uranium fuel. One of the goals of conducting tests with the VHTRC was to demonstrate a negative overall temperature coefficient and generate validation data [70] [81].

The VHTRC is a low-enriched uranium-fueled and graphite-moderated critical assembly with a hexagonal prism shape, as shown in Figure 39. The prism is 2.4 m across the flats and 2.4 m long and can be horizontally split into two equal half assemblies. One assembly is fixed and the other is movable. Each half is constructed with hexagonal graphite blocks, except the outermost reflector blocks that are trapezoidal. A fuel block has 19 holes into which fuel rods, graphite rods, burnable poison simulation rods, etc. can be inserted. Forty 750 W electric power heaters are distributed in the reflector region to keep the assembly at a uniform temperature. Design details and technical specifications can be found in References [81] and [84].

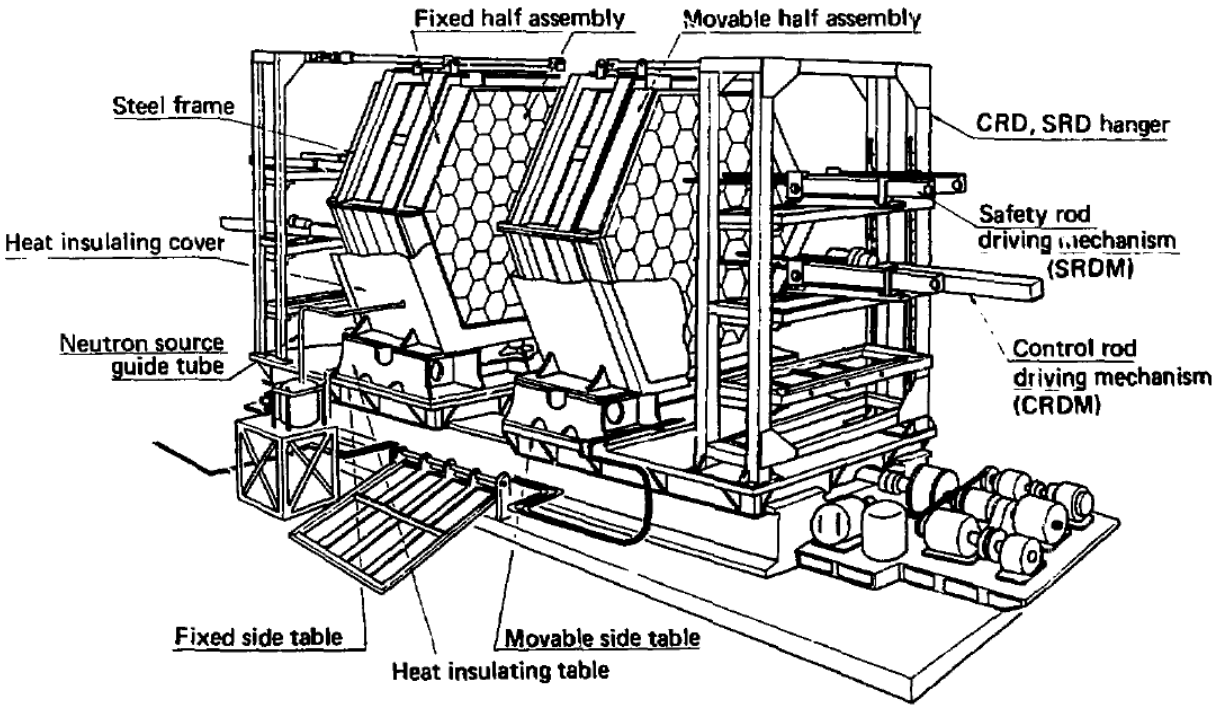

Figure 39. VHTRC side view taken from Reference [85].

FUEL LOADING AND INITIAL CRITICALITY

The initial critical approach was performed using the fuel addition method, in which fuel assemblies replace dummy graphite blocks previously loaded into the core [86]. In every loading step, all control rods were withdrawn from the core after each fuel loading and the inverse multiplication factor was used to predict criticality. Figure 40 shows that the fuel was loaded from the outer ring to the inner ring.

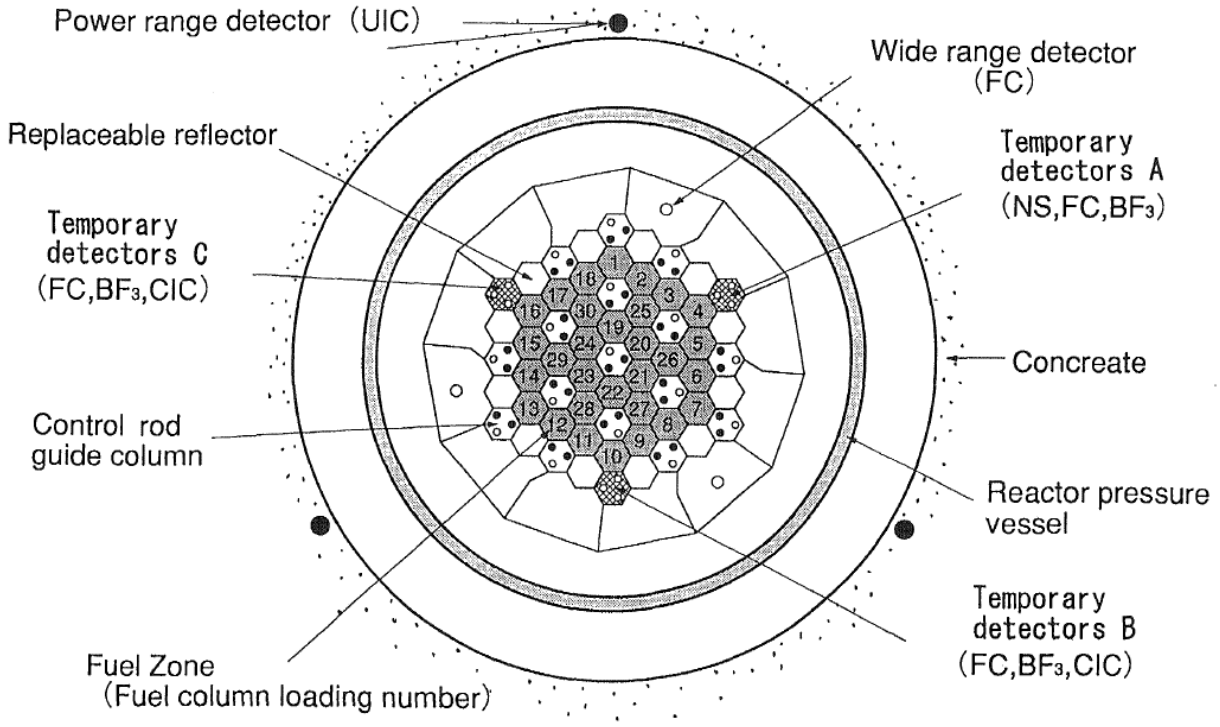

Figure 40. Fuel loading scheme and temporary neutron instrumentation for the HTTR [87].

The number of fuel columns required for initial criticality was calculated using the Monte Carlo MVP code [88] [70] and the deterministic design codes DELIGHT, TWOTRAN-2, and CITATION-1000VP [89]. In both evaluations, the predicted number of fuel columns for initial criticality was 16±1. The actual number of columns needed to reach criticality was 19 [70]. Re-evaluation of the nitrogen content of the graphite, the boron impurity in the graphite dummy blocks, the nuclear data library, and coated fuel particle heterogeneity treatment in the design codes resulted in an updated predicted value of 18±1 columns.

Another explanation for the misprediction is that the design code did not consider neutron streaming effects for control rod insertion holes in the reflector block. Also, the burnable poisons were homogenized in the fuel blocks [88].

SHUTDOWN MARGIN AND EXCESS REACTIVITY MEASUREMENT

The HTTR core excess reactivity was measured at 21, 24, 27, and 30 fuel columns [86] [88]. The excess reactivity was measured using the inverse kinetic method and was corrected for control rod interference [86] [88]. The control rods in the reflector were inserted first followed by control rods in the fuel. These measurements were done under cold clean conditions during the startup tests and agree well with calculated results [86].

CONTROL ROD MEASUREMENTS

The worth of each control rod was measured at cold clean conditions using the inverse kinetics method. The calculated worths agreed well with experimental results [86]. Calculations and measurements agreed for the core power level at different control rod positions.

TEMPERATURE COEFFICIENT MEASUREMENTS

Like the VHTRC, a negative temperature coefficient was measured for the HTTR at constant power by reducing the heat removal by the secondary coolant system [86]. The temperature coefficient was negative and agreed with calculations for average coolant temperatures above, but not below, 400°C.

The power coefficient, which includes the temperature coefficient and xenon worth change, was measured at power levels between 0 and 30 MW [86]. The power coefficient was shown to be negative and agreed well with results obtained from a diffusion code at power levels below, but not above, 10 MW.

POWER DISTRIBUTION MEASUREMENTS

Axial power distributions were measured by a set of fission chamber traverses in loaded and partially loaded core configurations. The measurements matched the calculated values [86] [88]. After the reactor was shut down, the fuel assemblies were removed, their relative power levels were measured using gamma detectors, and they were reinserted into the core [86].

Comparison of Predicted and Measured Values

The values in Table 14 are taken from References [86], [88], and [90].

Table 14. Agreement between test result and predictions for the HTTR.

Parameter	Unit	Measurement	Computed	Maximum Difference
Temperature Coefficient	$\%\Delta k/k\ [K]^{-1}$	-0.02 -0.01	-0.0217 -0.0025	≤75%
Power Coefficient	$\%\Delta k/k\ [K]^{-1}$	-0.1 -0.5	-0.04 -0.24	≤108%
Control Rod Worth	$\%\Delta k/k\ [K]^{-1}$	13.8	12.5	9.4%
Number of Fuel Columns	—	19	18 ± 1	10.5%
Excess Reactivity	$\%\Delta k/k$	12	12.4	3.3%
Shutdown Margin	$\%\Delta k/k$	-43.7	-42.9	1.87%
Radial Power Distribution	Normalized	0.96–1.03	0.97–1.05	1.03%
Axial Power Distribution	Normalized	0.5–1.55	0.5–1.6	3.125%
Eigenvalue at Criticality	—	1.00025	0.99148	0.877%

SODIUM-COOLED FAST REACTORS

Experimental Breeder Reactor (EBR- II)

Reactor Design Summary

EBR-II was a complete sodium-cooled fast reactor (SFR) power plant demonstration, which included a fuel cycle facility for reprocessing spent fuel and a power conversion plant [91, 92]. The core and supporting structures were contained within a single reactor vessel with 86,000 gallons of sodium. A diagram of the reactor primary system is in Figure 41. EBR-II went

dry critical (i.e., critical without sodium coolant) in 1960 and wet critical in 1964. It continued to operate until 1994. The reactor could produce 62.5 MWth (19 Mwe) and supported four major research campaigns: proof of concept for an SFR plant with onsite reprocessing, an irradiation facility for LMR fuels and materials, inherent safety and operability testing for LMRs, and finally a test bed for the integral fast reactor development and plant testing.

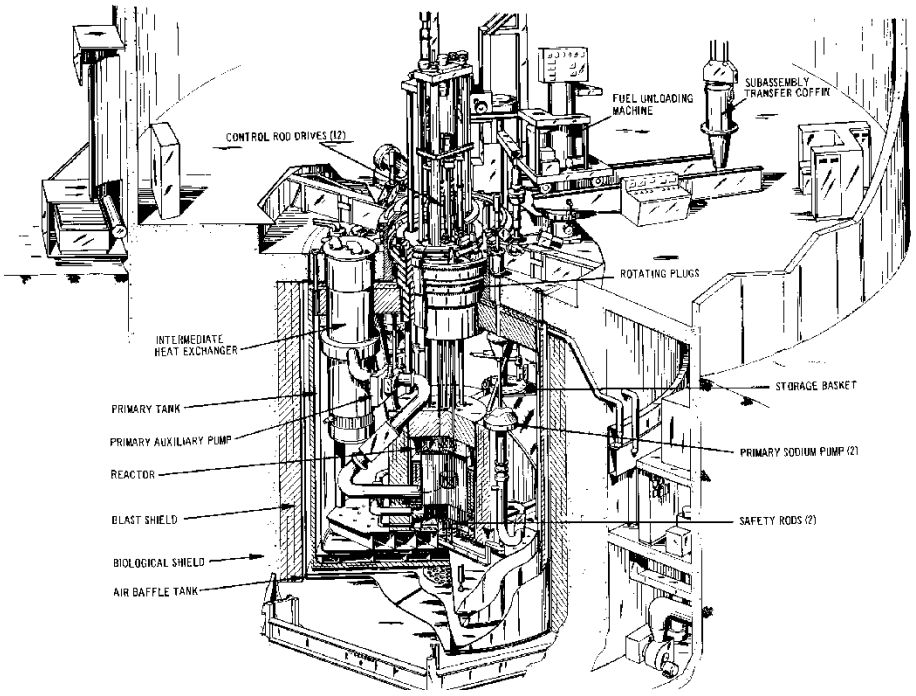

Figure 41. EBR-II primary tank arrangement [93].

The EBR-II contained 637 hexagonal subassemblies that made up the core, inner blanket, and outer blanket regions. Figure 42 shows a slice of the core, showing the three regions. Most of the power was generated in the core region which, because of its high neutron flux, often contained multiple experiments. Subassemblies were categorized as driver, blanket, control, reflector, and experiment [94].

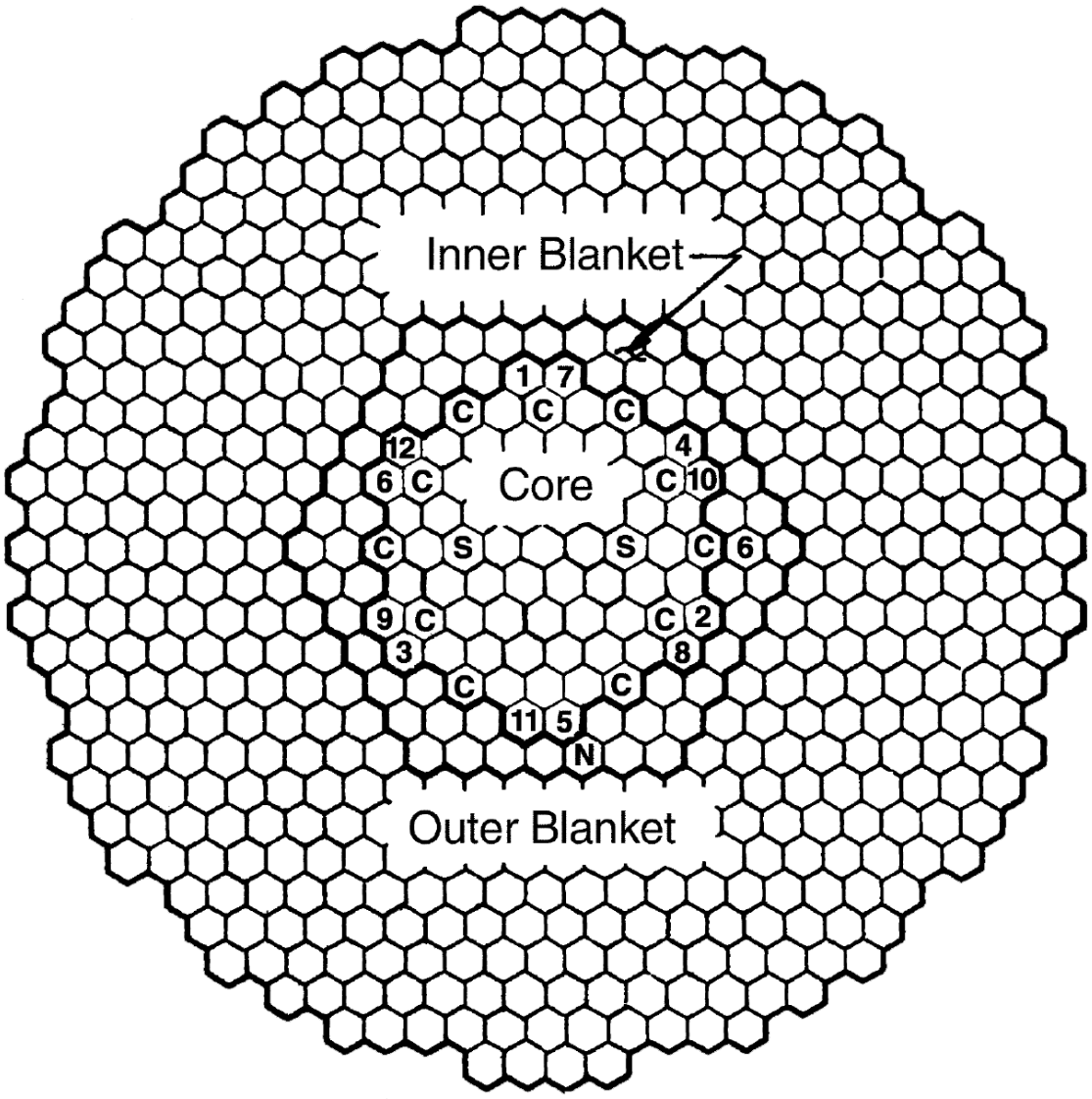

Figure 42. EBR-II subassembly arrangement [95].

Subassemblies were hexagonal with an outer flat-to-flat distance of 5.82 cm and an intersubassembly gap thickness of 0.1 cm. The major exception to this was the control rods, which had inner and outer hexagonal ducts to facilitate rod movement. Each subassembly contained a lower and upper adapter. The upper adapter allowed for ease of movement into and out of the core. The lower adapter ensured subassemblies could only be placed into the correct core region and dictated the amount of coolant flow through the subassembly.

Driver fuel subassemblies underwent multiple design changes throughout EBR-II's lifetime. The MK-II fuel subassembly is described in some detail to provide a description of a typical driver subassembly. Each driver subassembly contained 91 fuel pins in a hexagonal lattice with a 0.56 cm pitch.

Fuel pins contained an extruded metallic fuel slug (outer diameter of 0.33 cm), a sodium bond (outer diameter of 0.38 cm), and a stainless-steel cladding (outer diameter of 0.44 cm). The fuel pin height was 62.04 cm, with a fuel slug height of 33.29 cm. Above the fuel slugs was a helium

plenum that facilitated the collection of fission product gases that migrated out of the fuel. The plenum region also contained a trace amount of xenon to help identify a fuel pin leak. Fuel pins had a stainless-steel wire wrap to prevent rubbing and to facilitate coolant mixing for better heat transfer.

The fuel slugs were a metallic alloy containing 95 wt% uranium and 5 wt% fissium. Fissium was a combination of fission product elements alloyed with uranium to simulate the reactivity of fuel with burnup. The enrichment of the fuel changed throughout the life of EBR-II but typically ranged between 45 wt% and 67 wt% U-235. The fuel pins were relatively short, which provided a flat pancake-like core with inherent safety features.

Blanket subassemblies were often used around the core to promote breeding of plutonium. Each blanket subassembly contained 19 fuel pins, with a pitch of 1.26 cm. Blanket fuel pins contained the fuel slug (outer diameter of 1.1 cm), a sodium bond (outer diameter of 1.16 cm), and a stainless-steel cladding (outer diameter of 1.25 cm). The blanket fuel pins had a height of 1.43 m to encourage breeding.

Safety and control subassemblies were the primary mechanisms for controlling EBR-II reactivity. Twelve control subassemblies had an inner hexagonal duct with 61 fuel pins that would be raised into the core lattice to add reactivity. Two shutdown subassemblies also contained seven B_4C pins above the fuel during operation and to ensure shutdown. Scram signals actuate the rods in accordance with the mode of operation. During "reactor operation," when the reactor was critical, an automatic scram signal would release the 12 control rods. With a pressure assist, the control rods move to their least reactive positions. During "fuel handling," when the reactor was expected to be substantially subcritical, an automatic scram signal released the safety rods. Gravity causes them to move to their least reactive positions below the core. The safety rods may also be manually released during "reactor operation."

Experimental subassemblies were used to test fuel and materials within EBR-II. Often these subassemblies were highly instrumented to monitor the experiment. Experimental subassemblies had a hexagonal duct, and the inner region comprised the experiment.

EBR-II underwent four main phases of research during its 30 years of operation. The first research stage was meant to pick up where EBR-I left off and prove that a liquid metal fast breeder reactor (LMFBR) could breed additional fuel and reprocess the fuel onsite for reuse. The next research phase used EBR-II as an irradiation facility for LMFBR fuels and materials testing. The third stage was to provide proof of the inherent safety features of an LMFBR using sodium as a coolant. The last phase was the inclusion of EBR-II in the integral fast reactor development program designed to help improve the economics and enhanced safety features of LMFBRs [96].

Startup Physics Test Program

The EBR-II startup physics test program consisted of a dry critical program [97] and a wet critical program [98]. Zero-power critical experiments had been previously performed in the Zero Power Reactor III (ZPR-III) to support the reactor design, but they are not considered part of the startup testing. The dry critical experiments included:

- Neutron source and instrument response
- Approach to criticality
- Neutron flux and power calibration
- Reactivity measurements, including the worth of control rods and safety rods and temperature coefficients.

The wet critical program determined the reactivity worth of the sodium coolant. The wet critical program also determined the impact of gradually increasing the reactor power level. Stability and kinetic parameters were measured [99] [98]. The main objectives of the wet critical experiments were to obtain data essential for power reactor operation.

Experimental Methods and Results

DRY CRITICAL EXPERIMENTS

FUEL LOADING APPROACH TO DRY CRITICALITY

The fuel loading sequence to dry criticality is shown in Table 15. As shown in Figure 43, neutron flux measurements were made, and inverse multiplication plotted, with control rods fully inserted and fully withdrawn until criticality was reached. It should be noted that the count rates were corrected for decay of the neutron source, see Table 16. The critical core configuration had 87 fuel subassemblies containing 232.18 kg of U-235 with 11 of the 12 control rods fully inserted (i.e., fueled portion of the control subassembly is in the core). The critical position of the eleventh control rod was not determined.

Table 15. Loading sequence for EBR-II dry critical [100].

TABLE II. FUEL SUBASSEMBLY* LOADING INCREMENTS

Loading No.	Number of Subassemblies Added/Loading	Total Number of Subassemblies	Total Kg of U^{235}
1	15*	15	29.21
2	16	31	74.18
3	9	40	99.49
4	9	49	124.98
5	6	55	141.86
6	6	61	158.81
7	6	67	175.73
8	6	73	192.67
9	4	77	203.95
10	6	83	220.88
11	4	87	232.18

*Including control and safety subassemblies.

CRITICAL MASS

The reactor minimum critical mass was determined using a small neutron source in the outer blanket. The loading to approach criticality resulted in excess reactivity of 176.2 inhours. It is noted in References [97] and [100] that the worth of each fuel subassembly containing 2.81 kg of U-235 was measured to be 115.5 inhours or 41.1 inhours/kg U-235. Dividing the 176.2 inhours of excess reactivity by this conversion converts to 4.28 kg more than the critical mass. The critical configuration contained 232.18 kg. Subtracting the two gives a dry critical mass, with all control rods fully raised (i.e., fueled portion is raised into the core), of 227.9 kg U-235 [100].

Table 16. Source decay correction factors [100].

TABLE IV. SOURCE DECAY CORRECTION FACTORS

(Source Strength ~189 Curies on Sept. 1, 1961)

Loading No.	Date	Correction Factor*
1	Sept. 18, 1961	.824
2	Sept. 20, 1961	.805
3	Sept. 21, 1961	.796
4	Sept. 22, 1961	.787
5	Sept. 23, 1961	.778
6	Sept. 24, 1961	.769
7	Sept. 25, 1961	.760
8	Sept. 26, 1961	.752
9	Sept. 28, 1961	.734
10	Sept. 29, 1961	.726
11	Sept. 30, 1961	.718

CONTROL AND SAFETY ROD WORTH

The reactivity of control and safety rods was measured using a positive period and subcritical methods, as shown in Table 17. These results were noted to have a +/- 10% error. These uncertainties were not discussed in the source document [100].

ISOTHERMAL TEMPERATURE COEFFICIENT

The dry isothermal temperature coefficient was measured by establishing two isothermal conditions—one lowering the reactor temperature to 58°F and one raising the reactor temperature to 99°F [100]. The delta T of +41°F resulted in a reactivity loss of 25 inhours, giving a dry isothermal temperature coefficient of $-0.6\ Ih/°\mathrm{F}$ or $-2.6 \times 10^{-5} \Delta k/k\ /°\mathrm{C}$

POWER CALIBRATION EXPERIMENTS

The fission counters used in the dry critical experiments could not be used in the wet critical experiments because of the temperatures of molten sodium [97]. High-temperature fission counters were calibrated in the Argonne Fast Source Reactor and verified by absolute fission counters [97] [100].

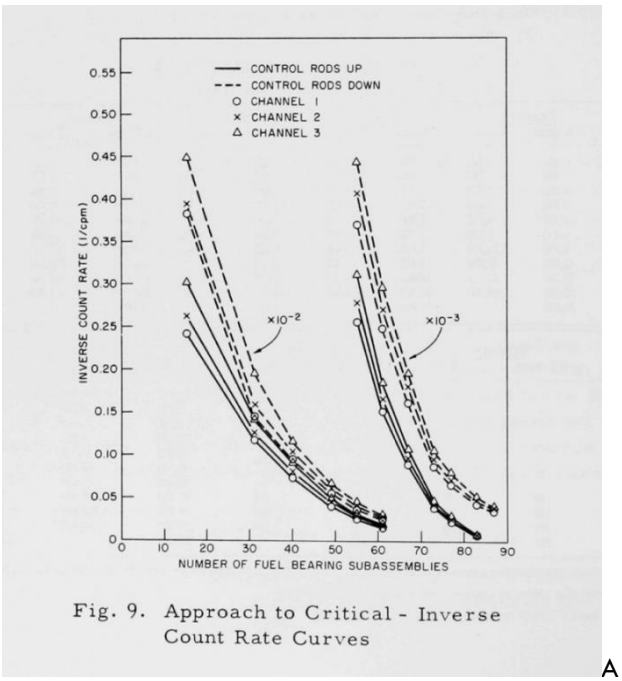

Fig. 9. Approach to Critical - Inverse Count Rate Curves

A

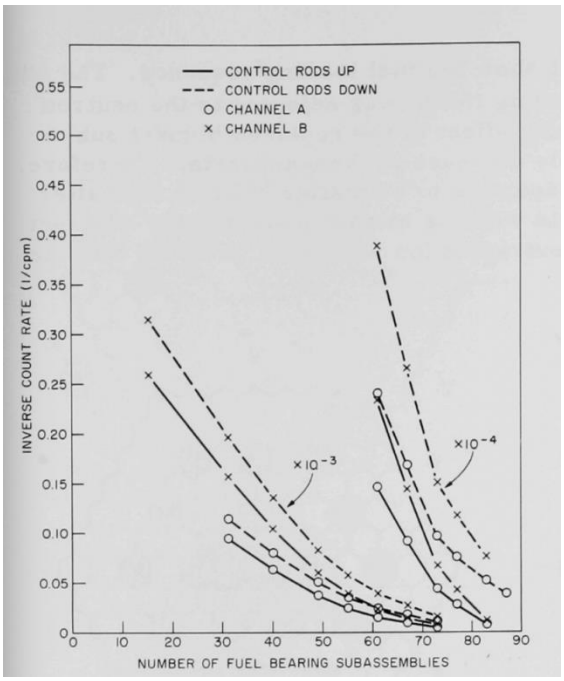

B

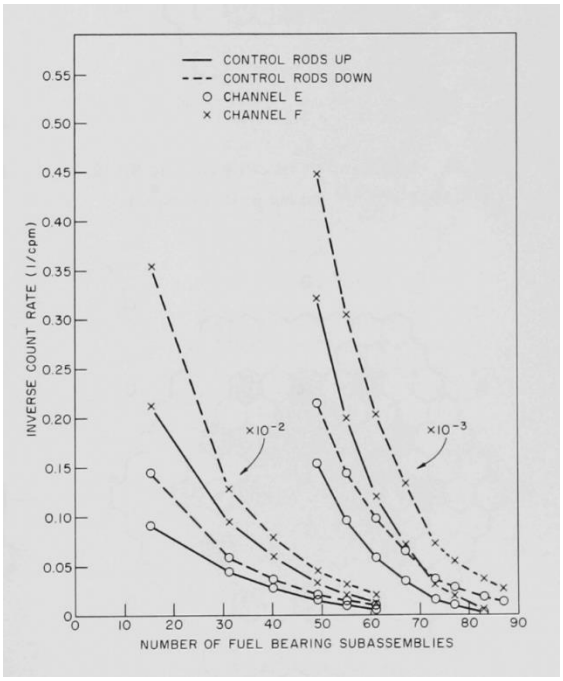

C

Figure 43. Approach to dry criticality curves for the EBR-II [100].

Table 17. The measured reactivity worth of the EBR-II control and safety rods [100].

TABLE V. REACTIVITY WORTHS OF CONTROL AND SAFETY RODS

Rod	Core Loading Figure Number	Reactivity Worth Inhours	Reactivity Worth % Δk/k(3)
Control Rod*			
No. 10	22	154.0(1)	0.37
No. 1	22	137.0(1)	0.33
No. 7 (special)	22	239.0(2)	0.58
No. 9	22	132.5(2)	0.32
No. 6	23	163.0(1)	0.39
No. 2	23	149.5(1)	0.36
No. 2	23	150.1(2)	0.36
All 12 Control Rods	22	1854**(2)	4.37
Two Safety Rods	22	430**(2)	1.04
Two Safety Rods	22	425**(2)	1.02

(1) Period Measurement

(2) Subcritical Measurement

(3) 415 inhours = 1% Δk/k

*Even numbered control rods on "flat" of hexagonal core
Odd numbered control rods on corner of hexagonal core

**Error is ± 10%

Control rods No. 1 and 10 were also calibrated over the 14-in. stroke. The calibration curves are shown in Fig. 24.

†Sb^{124} has a 60-day half-life.

WET CRITICAL EXPERIMENTS

In 1963, the EBR-II core was filled with liquid sodium in preparation for the wet critical experiments [101]. Most of the wet critical experiments were performed at 600°F [98] [101].

UEL LOADING APPROACH TO WET CRITICALITY

The experiment program began with the fuel loading approach to criticality [98] [101] essentially following the same procedures used for the dry critical loading. The loading approach is illustrated in Figure 44. Following the same process as that used to determine the dry critical mass, the minimum wet critical mass with 68.8 subassemblies, including the safety and control rods, was 181.2 kg of U-235 at 600°F.

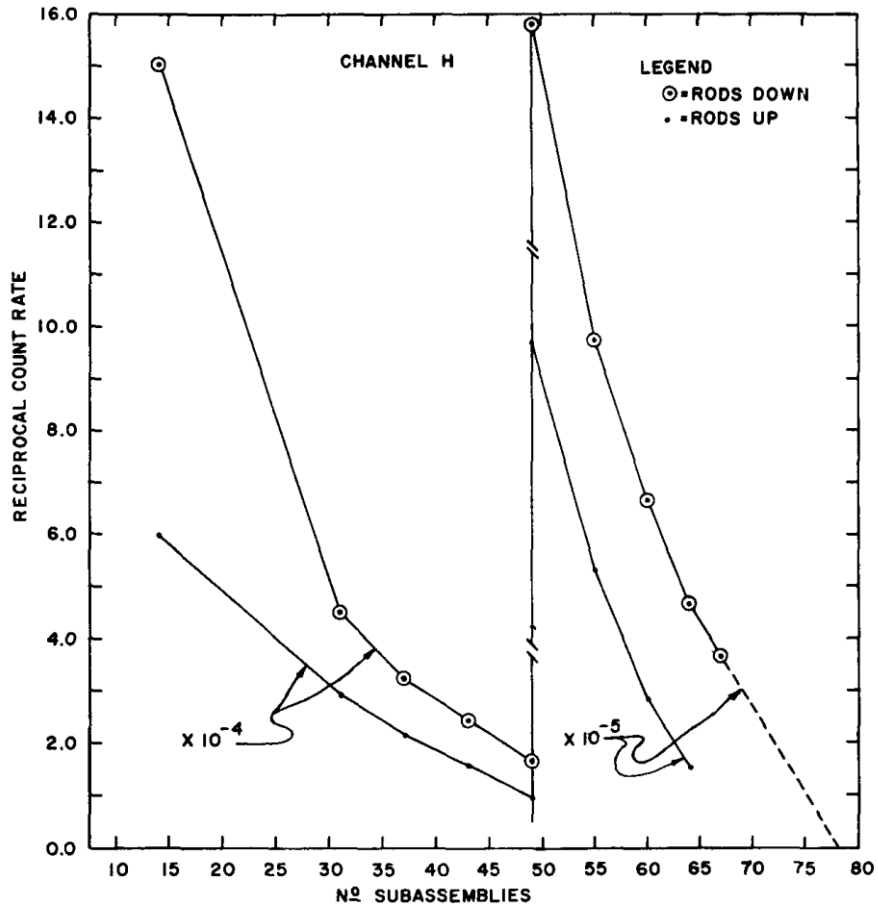

Fig. 15. Inverse Count Rate Versus No. of Subassemblies for Channel H

Figure 44. Approach to wet criticality curves for the EBR-II.

POWER CALIBRATION

To calibrate ex-core detectors for measuring power, foil holders and one wire holder were placed in an inner blanket subassembly and irradiated under normal operating conditions, and the fission products were measured and compared with the output of Detector Channels 1 through 7. Channel 7 was considered the basic power indicator, and all nuclear instruments were calibrated against Channel 7 using the factors shown in Table 18. Two Mo-99 activation spectroscopy measurements were taken. One set was analyzed using beta counting while the other used gamma counting at two different temperatures. The power calibration results are shown in Table 19.

CONTROL ROD WORTH

Individual Control Rods 2 and 7 were calibrated using the period method to obtain the curves shown in Figure 45 [98]. The remaining rods were inserted 50% into the core for comparison with the reactivity curves developed for Rods 2 and 7, as shown in Table 20.

Table 18. Calibration factors for instrumentation calibrations for EBR-II [98].

CALIBRATION OF NUCLEAR INSTRUMENTS

Channel No.	Calibration
1	390 counts/Watt-sec
2	390 counts/Watt-sec
3	400 counts/Watt-sec
4	6.4×10^{-8} Amp/kW
5	5.3×10^{-8} Amp/kW
6	6.1×10^{-8} Amp/kW
7	2.0×10^{-8} Amp/kW

Table 19. EBR-II power calibration in [98].

Table VII

EBR-II POWER CALIBRATION

Temp (°F)	Foil No.*	Foil Weight (mg)	Total Fissions [g (U^{2})]	Channel 7 (Amps)	Irradiation Time (sec)	Calculated Reactor Power Level (Watts)**	Calibration (Amps/kW)
600	401 (I)	54.4	5.06×10^{11}				
	402 (C)	54.2	5.03				
	403 (I)	55.0	5.04				
	404 (I)	53.6	4.84				
			Av 5.01×10^{11}	1.3×10^{-8}	7260	650	2.0×10^{-8}
460	415 (I)	54.3	2.33×10^{12}				
	416 (C)	54.0	2.22				
	417 (C)	54.9	2.19				
			Av 2.21×10^{12}				
			Corr. 1.96×10^{12} †	2.6×10^{-9}	14460	1280	2.03×10^{-8}

*The symbols (I) and (C) refer to foils analyzed in Idaho and Argonne, Illinois, respectively.

**Reactor power level was calculated assuming ZPR-III fission distribution, 3.1×10^{10} fissions per Watt-second, and 85% fission in core.

† This is corrected for contribution to the Mo^{99} fission product due to other operating times while fission foils were in the reactor.

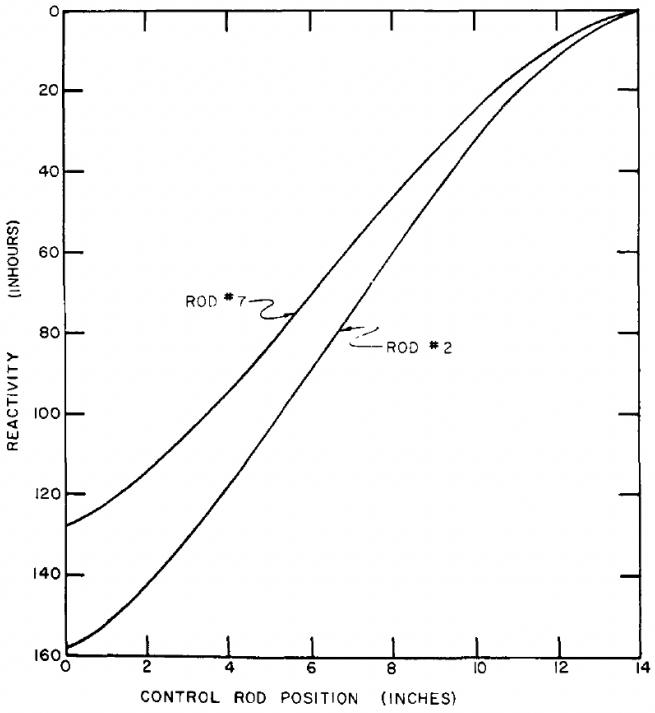

Figure 45. Rod calibration curves for EBR-II Control Rods 2 and 7 [98].

Table 20. EBR-II control rod worth in wet critical experiment conditions [98].

Table X

REACTIVITY WORTH OF CONTROL RODS

Control Rod No.	Reactivity Worth at 7 in.*		Total Reactivity Worth	
	(Ih)	(% Δk/k)	(Ih)	(% Δk/k)
1	59	0.142	127	0.306
2	75	0.176	158	0.381
3	61	0.147	130	0.314
4	76	0.183	158	0.381
5	59	0.142	128	0.309
6	75	0.176	157	0.379
7	58	0.140	128	0.309
8	75	0.176	156	0.376
9	59	0.142	128	0.309
10	77	0.186	161	0.388
11	61	0.147	127	0.306
12	75	0.176	157	0.379
Total Worth of Rods			1715	4.13
7 (Boron loaded)**			235	0.566

*~50% inserted

**Special control rod containing 161 g of B^{10} in the form of B_4C was placed in the upper 7 in. of the follower section.

Additional sub-critical reactivity worth measurements were made for the banked control rods using subcritical counting techniques. The reactor was brought critical with all control rods inserted

to 10.5 inches. Then the rods were lowered as a bank, thus removing reactivity, to positions 9, 7, 4, and 0 inches. From these measurements, the reactivity worth of all control rods "down" (i.e., reactivity is being removed) is approximately 4.4% Δk, while with all safety rods, "down" is approximately 5.6% Δk. The worth of the banked rods is larger than the sum of worth of the individual rods. The report suggested that this could be because, when the rods are "down," the reactor was significantly smaller than when the rods are "up." Since peripheral fuel is being removed by control rod motion, the effective radius of the core is decreased. Therefore, the control rods could exhibit greater reactivity worth. The total reactivity worth of the control rods was measured using the integral count method, a subcritical method involving kinetic response, which resulted in 4.1% Δk [98].

ROD SHADOWING EFFECT

Rod shadowing effects are the impacts of one control rod on the reactivity worths of the adjacent rods. Starting with the reactor critical, subcritical count rate measurements were made with different systematic control rod configurations [98]. The count rate results (shown in Table 21) indicate the interactions between adjacent rods.

Table 21. EBR-II rod shadowing effect results [98].

ROD SHADOWING EFFECT

Rod Positions (in.)			Count Rates (counts/min)	Δk (Ih)
No. 12	No. 7	No. 11		
0	14	14	Critical	0
0	0	14	6924	128
0	14	0	7338	120

ISOTHERMAL TEMPERATURE COEFFICIENT

The isothermal temperature coefficient was measured using critical control rod positions at temperatures of 460°F, 500°F, 550°F, and 600°F. Temperature measurements were taken at the coolant outlet, inlet plenum, and directly above the reactor fuel subassemblies. The isothermal temperature curve with the max ΔT of 140°F is provided in Figure 46. An average isothermal temperature coefficient was determined to be 1.01 + 0.02 Ih/°F based on data obtained at the three locations [98].

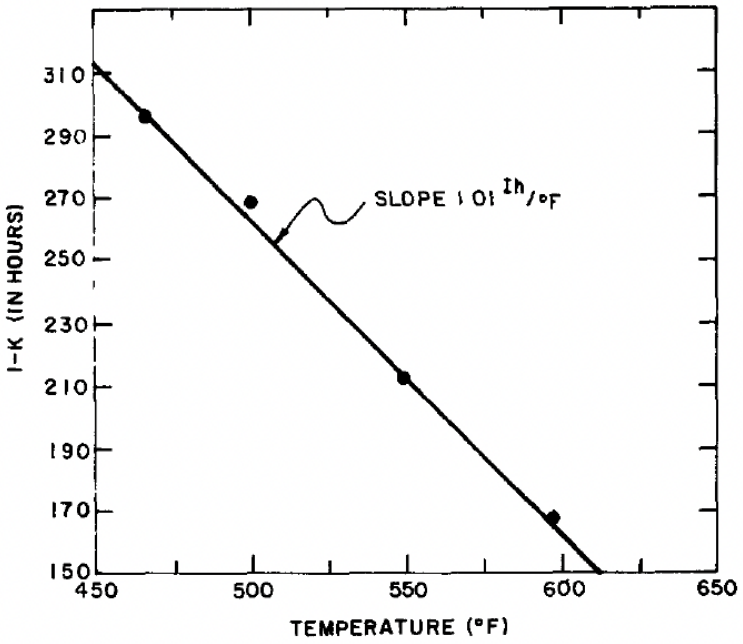

Figure 46. Wet critical core isothermal temperature coefficient in EBR-II [98].

TOTAL REACTIVITY WORTH OF SODIUM

By comparing the wet and dry criticality results, the total worth of sodium was determined to be 5.5% Δk. A second method, based on the difference in subcritical reactivities given the same core loading, gave a worth of approximately 5.7% Δk. The measured value of sodium worth was 6.0 $\pm$ 0.5% Δk, which agrees with the computed values [98].

Comparison of Predicted and Measured Values

The ZPR-III experiments were used to predict values for the dry critical experiment and the results from the dry critical experiments were used to predict results for the wet critical experiments. Table 22 from Reference [98] provides a comparison of predicted versus measured reactor physics parameters in ZPR-III and the EBR-II dry and wet critical experiments.

Table 22. Computed and measured values for the EBR-II dry critical and wet critical experiments [98].

Table XV

CALCULATED AND MEASURED VALUES OF NUCLEAR PARAMETERS FOR EBR-II

(Nominal Temperature = 315°C, Except Where Noted Otherwise)

	Calculated	ZPR-III Mockup	Dry Critical	Final Prediction	Measured
Critical Mass, kg U^{235}	172	165	228	176-184	181 2
Reactivity Worth, % Δk/k					
Control Rod (Av)	0 45	0 37	0 35	0 34	0 345
Control Rods (12-banked)	-	-	-	-	4 4
Poison ($B_4^{10}C$)[a]	-	0 55	0 58	0 55	0 57
Safety Rods (2)	1 5	1 36	1 0	1 3	1 2
Sodium					
Total	-	6 9	-	6 0 ± 0 5	5 7
Core, (% Δk/k)/kg	0 14	0 116	-	0 116	-
Isothermal Temp Coef , [(Δk/k)/°C] x 10^{-5}					
Structure (Including Fuel)	-1 9	-	-2 6	-2 2 ± 0 4	-
Coolant	-1 7	-	-	-1 8	-
Total	-3 6	-	-	-4 0 ± 0 4	-4 3[b]
Power Calibration, Counts/(Watt)(sec)	-	730	-	500	390
Subassembly Substitution, % Δk/k					
Core Center	1 43[c]	1 53[c]	-	1 26[d]	1 2[d]
Row 5 (Radius = 21 cm)	-	0 77[c]	-	0 64[d]	0 56[d]
Row 6 (Radius = 27 cm)	-	-	0 35[d]	-	0 35[d]

[a]Optional control rod containing 253 g of 87% enriched $B_4^{10}C$ in upper 7 in of control rod follower
[b]Measured at 237-315°C
[c]Enriched subassembly versus sodium
[d]Enriched subassembly versus U^{238} subassembly of identical composition

Superphénix

Reactor Design Summary

Superphénix's mission was to breed fuel for France's nuclear fleet and to generate electricity as a commercial nuclear power plant. The initial commissioning of the reactor started in January 1985 and lasted for about 2 years, with the rise to full power and coupling to the electricity grid achieved by the end of 1986. The Superphénix nuclear power plant was the culmination of a multidecade effort intended to commercialize LMFBR technology. Thus, the scope of the commissioning tests cannot be fully isolated from previous LMFBR prototypes and demonstrators. The first prototype was Rapsodie, France's first experimental fast reactor of 40 MWth, followed by Phénix, a small-scale demonstration plant of 560 MWth. The Superphénix design is essentially a scaled-up version of the Phénix reactor. The rated power was 3,000 MWth. Both Rapsodie and Phénix had irradiation capabilities and served as catalysts for proving and maturing the technology that paved the way for the construction of Superphénix. In addition, different Atomic Energy Commission critical facilities were employed, such as Masurca.

An overview of the primary circuit is provided in Figure 47, while the core is depicted in Figure 48. There were four main zones:

- 364 fuel assemblies divided into two zones with different enrichments
- 233 radial breeder assemblies

- 197 steel reflector assemblies to improve neutron economy
- 1,076 shield assemblies, whose purpose is to reduce doses to the internal structures and to intermediate heat exchangers.

Fuel assemblies contain 271 pins with wire wrap spacing in a hexagonal duct. The fuel fissile material consists of mixed oxide $(U,Pu)O_2$ pellets. Depleted uranium pellets were used axially at the bottom and top of the rods.

Reactivity was controlled by 21 control rods, divided in two groups (also known as curtains): an inner curtain of six rods in the central fuel zone and an outer curtain of 15 rods at the boundary between the two fuel zones. Control rods contain three pins with B_4C with B-10 enriched to 90%. These rods were employed to control the power shape and excess reactivity and to shut down the reactor in the event of a scram. Additionally, there were three backup safety rods only used for scram in an accident. These safety rods were axially divided into three zones with a spherical coupling to ensure they can be inserted even in a major core deformation event. Only two positions were available for these safety rods, fully inserted or fully withdrawn.

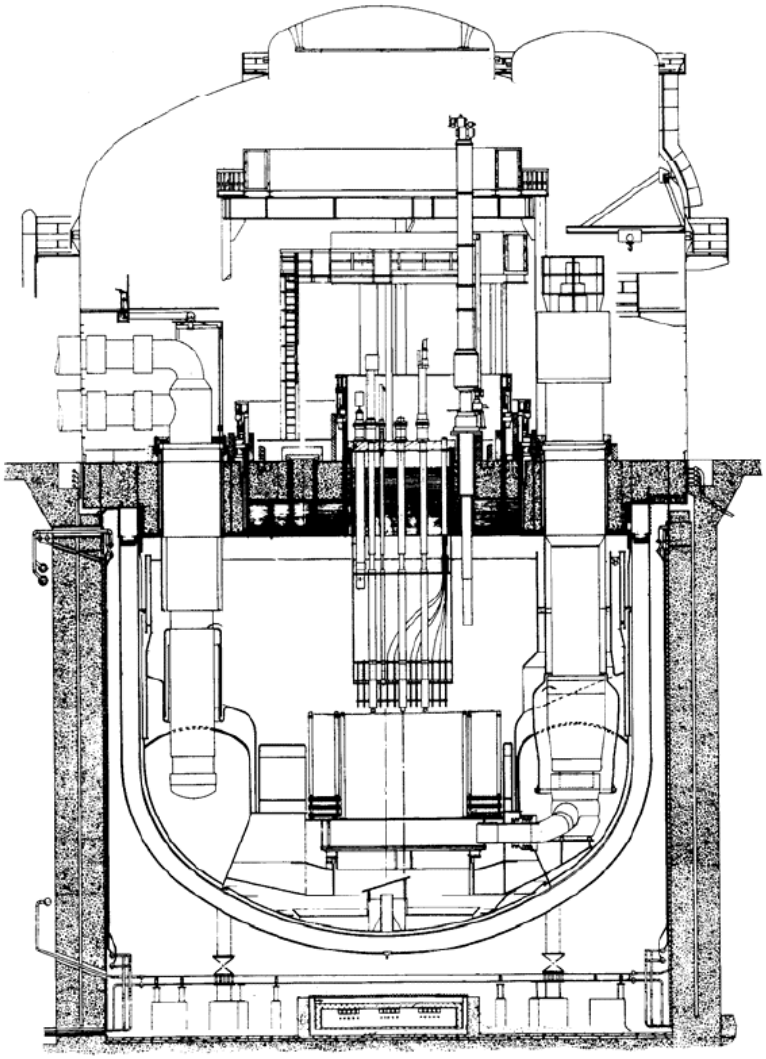

Figure 47. Primary circuit of Superphénix [102].

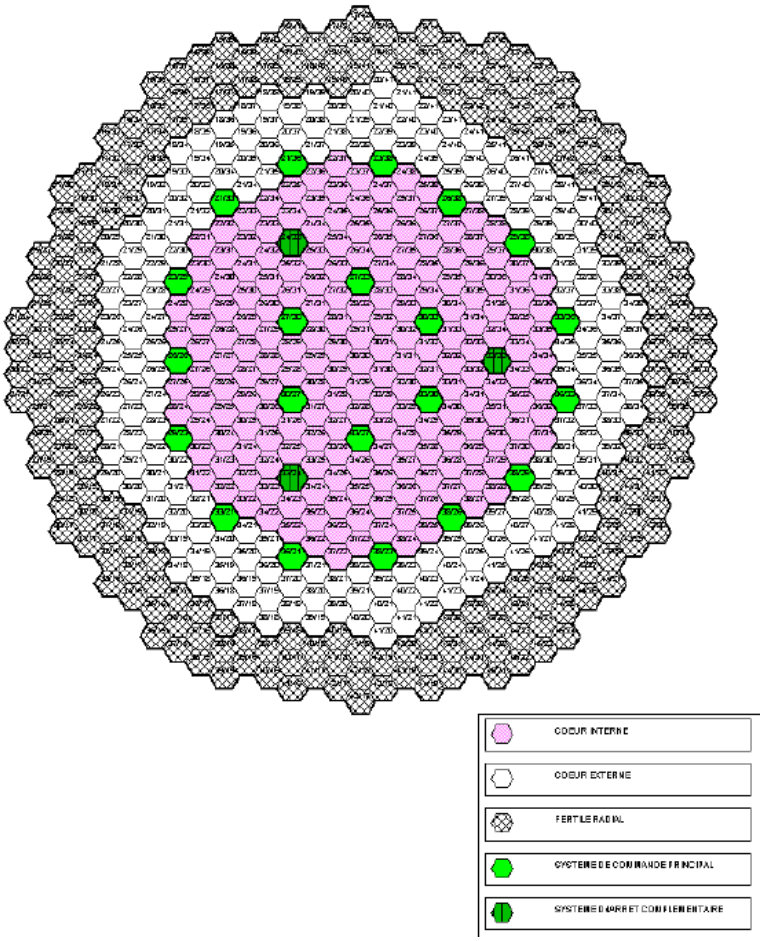

Figure 48. Radial core layout of Superphénix [103].

NEUTRON MONITORING

The neutron monitoring system controls reactor power from startup to full power. Three intermediate and power range neutron monitors were placed under the vessel and receive neutrons from three neutron guide tubes, located 120 degrees apart at the periphery of the core. These neutron guides act as collimators to facilitate neutron transport and increase neutron flux under the vessel by several decades, thus ensuring measurement from shutdown to full power. Helium counters were used for low-power control (1 W–10 kW), while fission chambers were used for low, intermediate, and high-power control (10 kW–3,000 MW). Additionally, for core loading and initial startup, three temporary source range channels were used to monitor the subcritical approach and reactivity measurements. These in-core chambers were located at the core center in a special assembly thimble handled by a telescopic device. The in-core chambers were used because the fixed in-core neutron guide tubes did not provide sufficient signals at startup and low-power conditions.

TEMPERATURE MEASUREMENTS

Thermocouples were placed at the inlet and outlet of the central fuel assemblies (376), the control rods (21), and the first row of the breeder assemblies (72). These thermocouples provide continuous monitoring of the cooling conditions of the assemblies within the core that are particularly important for SFRs in case of flow blockage. Peak fuel and cladding temperatures

were deduced from these measurements by an online computer program, and a scram signal is actuated if temperature limits were exceeded. Additional thermocouples were located at the pump outlets to provide the core inlet temperature, as well as within the primary and secondary circuits, primary vessel, grid plate, intermediate heat exchangers, and hot plenum.

REACTIVITY MONITORING

An online computer was available to measure and record reactivity, control rod position, neutron power, core temperature, and inlet sodium flow rate.

PRESSURE MEASUREMENT IN THE DIAGRID

During the initial startup phase, two 20 m long rigs were temporarily installed in the diagrid, also referred to as a core support plate, to measure pressure at the core entry by comparing it with an argon gas supply. The measurement was performed online as a function of primary pump speed and was used to deduce the sodium flow rate in the core.

TEMPERATURE AND NEUTRON FLUX MEASUREMENT IN THE CORE

An 18 m long telescopic tube was placed in the central channel of the reactor. The lower part of the tube was placed in a special fuel assembly in which the 19 central fuel pins were replaced by a guide tube. This instrument tube was used for handling the three fission chambers mentioned above and was also intended for holding a temperature probe.

SPECIAL ASSEMBLIES FOR IN-CORE MEASUREMENTS

Special assemblies were made with guide tubes instead of central pins for different core locations (10 fuel, three blanket, two steel reflector, and three shielding assemblies). These guide tubes were loaded with fission and activation foils to determine the neutron flux distribution inside and around the core.

SPECIAL DEVICES FOR MEASUREMENTS

Probes fitted with thermocouples were installed in the primary vessel, particularly in the hot plenum and in the sodium cavity between the core lateral shielding and the inner tank to study the temperature distribution and sodium stratification. Two IHXs were equipped with tubes located near their axes, with foil holders to determine neutron flux at full power.

Startup Physics Test Program

The commissioning test results were published in a Superphénix dedicated edition of Nuclear Science and Engineering in 1990 (Volume 106, see References. [104] [105] [106] [107] [108] [109] [110] [111]). These papers provide a wealth of information relative to the core physics testing that occurred during the commissioning tests.

The commissioning tests were conducted in three main phases:

- January–July 1985: isothermal tests up to 425°C
- July–December 1985: core loading and zero-power tests, first criticality achieved in September 1985
- December 1985–December 1986: power raising, coupling to the grid (first coupling on January 14, 1986, rise to full power on December 12, 1986).

Phase 1 consisted of isothermal tests intended to verify the thermal-hydraulic behavior of the core, the efficiency of the sodium purification system, overall equipment behavior, and component and structures at preset temperature levels (250°C, 345°C, 395°C, 425°C). The core was loaded with dummy steel assemblies. Sodium was heated by the heat from the primary and secondary

pumps. Additional tests were performed during this phase on control rod operation and calibration of temperature instrumentation.

Phase 2 initially consisted of fuel loading, which was performed using a checkerboard pattern of assembly batches, with fuel assemblies gradually replacing dummy assemblies. During loading, the reactor core was switched from a fuel handling configuration to an operational configuration. Neutron monitoring was performed after each batch loading, with all control rods inserted. No neutron source was necessary, as sufficient spontaneous fission from heavy nuclides (Pu, Cm) and (α,n) reactions from heavy nuclides on oxygen were present in the mixed oxide fuel assemblies. The inherent neutron source induced noise in the instrumentation at the shutdown condition and varied depending on the plutonium content. The loading pattern was optimized to maximize neutron counts in the temporary central instrumented neutron detector, in the fixed neutron instrument tubes at the periphery of the fueled core, and to maximize control rod worth. The first critical core was obtained after six batches, and the core was fully loaded after another batch.

Once the core was fully loaded, a series of control rod reactivity worth measurements was performed for different combinations of control rod insertion, and different isothermal temperatures ranging from 185°C to 395°C. The purpose of the tests was to quantify spatially distorted flux effects, which are important in such a large core. These control rod spatial effects required different experiments, such as:

- A local criticality configuration (a subcritical reactor with all rods inserted and adjacent control rods successively withdrawn up to criticality)
- Criticality achieved with one control rod curtain up and the other remaining fully inserted
- A handling error configuration, where all rods were inserted except one, representing an inadvertent insertion of a fuel assembly in a control rod position.

Neutron flux and fission rate distributions were also measured during these low-power isothermal conditions. The goal was first to determine the core reaction rate distribution to determine axial and radial power profiles and their sensitivity to rod insertion (local peak power), and for regions outside the core, to determine secondary sodium activity and damage to the internal structure.

The calibration of the neutron monitoring channels against thermal power was performed at 30 MW using an efficient calorimetric method.

Tests were performed to measure and verify temperature feedback coefficients. While the reactor was critical at zero power, the flow rate was increased to nominal to verify the coolant worth was negligible. Then, sodium was heated up to 400°C and then cooled at a rate of 10°C/hour while maintaining the critical reactor. The reactivity measurements allowed the measurement of the temperature and thermal expansion reactivity coefficients.

Phase 3 consisted of the rise to full power, with the commissioning of the steam side of the power plant. Feedback coefficients were measured for at-power conditions. Fuel assembly outlet temperature distributions and the impact of different control rod insertions on the core power distribution were also measured. The dynamic behavior and the stability of the plant were validated, with different power and flow ramp transients performed. The data was then used to validate the safety codes used for the design and licensing. Several modeling improvements were identified as necessary to reduce computed divided by experiment (C/E) discrepancies.

Experimental Methods and Results

CORE LOADING STRATEGY

The traditional loading approach to criticality used batches of fuel assemblies. Neutron counts were taken after each batch loading with all control rods in, using the special fission chambers located temporarily in the center position of the core and the permanent fission chambers located under the core and fed by the neutron collimators. The minimum number of fuel assemblies for a critical core was then extrapolated from the inverse count rate plots for different control rod insertions.

CONTROL ROD WORTH

Different control rod worth techniques were employed:

- Modified source multiplication method (MSM), which enables subcritical reactivity levels to be derived from measured subcritical counting rates, with computed spatial correction factors.
- Rod drops from a critical configuration, using computed correction factors for capturing spatial effects.
- Balancing of two rods while the reactor is critical (i.e., the standard in-hour approach).
- Temperature compensation method, where the reactor is maintained critical while the sodium temperature is increased. The reactivity change is compensated by withdrawing the control rod to be measured.

POWER AND NEUTRON FLUX DISTRIBUTIONS IN THE CORE AND SHIELDING

Thirty-three experimental assemblies containing fission or activation foils were loaded into the core, radial blanket, and neutron shield. Fission foils consisted of U-235, U-238, or Pu-239, while activation foils consisted of gold, sodium, or nickel. The measurements were made when the reactor was critical for a few hours at a power between 10 and 20 MW.

REACTIVITY COEFFICIENTS

Three types of experiments were carried out during the commissioning to measure reactivity coefficients. First, isothermal expansion and Doppler coefficients were measured at zero power. Second, reactivity coefficients k, g, and h, defined below, were measured at different power levels. Third, burnup reactivity loss was measured after some operating time.

Three separate at-power feedback coefficients, termed k, g, and h, which represented, respectively, a reactivity change due to a 1°C change at the inlet of the core temperature, a 1°C change in the sodium temperature rise through the core, and a 1% change in power, were measured. The experiments consisted of making perturbations on each of the three parameters around a steady-state point. The reactivity changes recorded by the reactivity meter allowed for the calculation of the values for each of the coefficients. The same method was also used in other SFRs such as Phénix, Joyo, EBR-II, and the Fast Flux Test Facility. These measured parameters lump together many different feedback effects, such as sodium volume expansion, axial and radial expansion of the fuel, radial expansion of the grid plate, differential expansion in the control rods, and fuel Doppler. Neutronic calculations provided an estimate of these k, g, and h coefficients through combination of these separate feedback coefficients.

TRANSIENT TESTS

The dynamic behavior of the core following a reactivity step insertion was measured at zero power and at low power, which also included a verification of the nuclear steam supply system behavior. The acquired data helped validate the dynamic code DYN, which was used for design

and safety analyses. For the zero-power case, the core was at near critical condition at an isothermal temperature of 180°C and the control rods were withdrawn to insert a positive reactivity of around 0.0030%δk/k. The power increased slowly until Doppler feedback compensated for the reactivity insertion, leading to a peak power around 20 MW.

Both reactivity step and inlet flow perturbations were performed at power, which in this case included the dynamic behavior of the core coupled with the nuclear steam supply system, for a reactivity insertion at 50% of rated power.

Comparison of Predicted and Measured Values

CORE LOADING STRATEGY

There was good agreement between predicted and measured critical loading for the fully loaded core. The minimum critical loading was predicted to be 236±5, but was actually 321.5±0.5 Some improvements in the codes were deemed necessary for the partially loaded first critical core. Correction factors were introduced to capture heterogeneity effects and are summarized in Reference [105].

CONTROL ROD WORTH

Calculated rod worths were overestimated by around 10% with the computational scheme employed at the time, a known issue for fast reactor neutronic codes. Having rod worths smaller than designed was an issue for the program that led to the creation of a task force. Various techniques were developed to correct these deficiencies by calibrating the calculational scheme to the measurement values. So called "transport equivalent cross sections" to account for heterogeneous and transport effects, as well as nuclear data adjustments, were introduced to reduce discrepancies.

POWER AND NEUTRON FLUX DISTRIBUTIONS

Calculated flux and power map distributions were found to be impacted by mispredictions of the control rod worths. Experimentally derived correction factors and rod cross-section adjustment were introduced, which enabled a posteriori validation of the computational scheme. The agreement between the calculated and measured U-235, U-238 and Pu-239 reaction rates was approximately 2-3%.

REACTIVITY COEFFICIENTS

Considering the 20%–30% uncertainty in the calculated values, predicted reactivity coefficients were found to be in reasonable agreement with measured values. Both calculated and measured reactivity coefficients required detailed work to separate the different feedback mechanisms (rod worth, core thermal-hydraulics and mechanical expansion of the core structure). Also, reactivity coefficients were calibrated on a control rod value that was not well predicted, which required further investigation.

TRANSIENT TESTS

The agreements between calculations and experiments were satisfactory (i.e., the dynamic behavior) and stability of the core were well calculated by the system analysis code, DYN. The code had to be modified to better calculate vessel temperatures, and thus vessel thermal expansion, which in turn impacted control rod drive differential expansion. These comparisons were only focused on global parameters, such as thermal power and inlet and outlet temperature, and lacked an assessment for local (spatial) effects. Also, since the feedback mechanisms are intertwined, some error compensation was likely to affect the calculated values.

REFERENCES

[1] W. Jackson, L. Moss, L. Blue, K. Medeiros, M. Boling, J. Miller, M. Dunenfeld, D. Paddleford, W. Green, A. Schmalz, E. Hammond, M. Tarpinian and M. Hoffman, "Analysis of SNAPTRAN-1 and -2 Reactor Kinetics Experiments," Atomics International, NAA-SR-11850, Canoga Park, CA, USA, 1967.

[2] K. Buttrey, D. Paddleford, A. Weitzberg and J. Zane, "Analysis of SNAPTRAN-3 Destructive Experiment," Atomics International, NAA-SR-9780, Canoga Park, CA, USA, 1965.

[3] "SNAP Reacror Overview, AFWL-TN-84-14," Albuquerque, NM, August 1984.

[4] "SNAP Power for Hardened Bases, NAA-SR-Memo-7260(Del.)," Canoga Park, CA, 1962.

[5] "SNAP 4 Summary Report, Volume I, Applications and Summary, AI-AEC-13069, Vol. 1," Canoga Park, CA, 1973.

[6] "SNAP 4 Summary Report, Volume II, System Description, AI-AEC-13069, Vol. II," Canoga Park, CA, 1973.

[7] "Thermal Analysis of the SNAP-6 Reactor, AI-Memo-7840," Canoga Park, CA, 1962.

[8] *SNAP Power for Hardened Bases, NAA-SR-Memo-7260(Del.),* Canoga Park, CA: Atomics International, 1962.

[9] "SNAP Programs Summary Report, AI-AEC-13067," Canoga Park, CA , 1973.

[10] "SNAP 10A Test Program, Energy Technology Engineering Center," Canoga Park, California, 1988.

[11] "SNAP 10A Reactor Design Summary, Revision 1, NAA-SR-Memo-8679, Revision 1," Canoga Park, California, 1964.

[12] "Interim Report on the Critical Assemby 4A (SCA-4A) Experimental Results, NAA-SR-10245," Canoga Park, California, 1965.

[13] "Experiments with Water Reflected, Undermoderated, Zirconium, Hydride Critical Assemblies, NAA-SR-8490," Canoga Park, California, 1963.

[14] D. Clifford, "Final Report on the SNAP10A Prototype Critical Assembly Studies," Atomics International, NAA-SR-8613, Canoga Park, CA, USA, 1964.

[15] "SNAP 10A Summary Report, NAA-SR-12073," Canoga Park, California, 1967.

[16] R. Gimera and R. Johnson, "SNAP 10A Reactor Quarterly Progress Report," Atomics International, NAA-SR-9594, Canoga Park, California, 1964.

[17] "Final Snapshot Performance Report, NAA-SR-11934," Canoga Park, California, 1966.

[18] G. a. Sesonsky, Nuclear Reactor Engineering, New York, NY: D. Van Nostrand Company, 1963.

[19] Reactor Physics Constants, ANL-5800, Lemont, Illinois, 1951.

[20] "Preliminary Test Results - SNAP 10A FS-3, NAA-SR-11206," Canoga Park, California, 1965.

[21] "SNAP 10A FS-3 Reactor Performance, NAA-SR-11397," Canoga Park, California, 1966.

[22] SNAP Critical Assembly-4B, Phase III Water Immersion Experiments, NAA-SR-9871, Canoga Park, California, 1964.

[23] "SNAPTRAN 10A/2 Kinetics Testing and Destruct Reactor Experiments, NAA-SR-11906," Canoga Park, California, 1966.

[24] "Measurment of SNAP 10A SNAPTRAN Klnetics Parameters by Reactor Noise Techniques, NAA-SR-9160," Canoga Park, California, 1963.

[25] SNAP 10A Thermoelectric Pump Dcevelopment, NAA-SR-9486, Canoga Park, California, 1964.

[26] W. Cotrrell, H. Hungerford, J. Leslie and J. Meem, "Operation of the Aicraft Reactor Experiment," Oak Ridge National Laboratory, ORNL-1845, Oak Ridge, Tennessee, 1955.

[27] E. Bettis, "The Aircraft Reactor Experiment Design and Construction," *Nuclear Science and Engineering,* vol. 2, no. 6, pp. 804-825, 1957.

[28] R. Briggs, "Molten-Salt Reactor Program Semiannual Progress Report," Oak Ridge National Laboratory, ORNL-3626, Oak Ridge, TN, USA, 1964.

[29] M. Rosenthal, P. Kasten and R. Briggs, "Molten-Salt Reactors - History, Status, and Potential," *Nuclear Applications and Technology,* vol. 8, no. 2, pp. 107-117, 1970.

[30] P. Haubenreich and J. Englel, "Experience with the Molten-Salt Reactor Experiment," *Nuclear Applications and Technology,* vol. 8, no. 2, pp. 118-136, 1970.

[31] R. Robertson, "Conceptual Design Study of a Single-Fluid Molten-Salt Breeder Reactor," Oak Ridge National Laboratory, ORNL-4541, Oak Ridge, TN, USA, 1971.

[32] R. Robertson, "MSRE Design and Operations Report, Part I, Description of Reactor Design," Oak Ridge National Laboratory, ORNL-TM-728, Oak Ridge, TN, USA, 1965.

[33] P. Haubenreich, J. Engle, B. Prince and H. Claiborne, "MSRE Design and Operations Report, Part III, Nuclear Analysis," Oak Ridge National Laboratory, ORNL-TM-730, Oak Ridge, TN, USA, 1964.

[34] R. Kedl, "Fluid Dynamic Studies of The Molten-Salt Reactor Experiment (MSRE) Core," Oak Ridge National Laboratory, ORNL-TM-3229, Oak Ridge, TN, USA, 1970.

[35] R. Steffy, "Inherent Neutron Source in MSRE with clean 233U Fuel," Oak Ridge National Laboratory, ORNL-TM-2685, Oak Ridge, TN, USA, 1966.

[36] R. Thoma, "Chemical Aspects of MSRE Operations," Oak Ridge National Laboratory, ORNL-4658, Oak Ridge, TN, USA, 1971.

[37] B. Prince, J. Engel, S. Ball, P. Haubenreich and T. Kerlin, "Zero-Power Physics Experiments on the Molten-Salt Reactor Experiment," Oak Ridge National Laboratory, ORNL-4233, Oak Ridge, Tennessee, USA, 1968.

[38] B. Prince, "Period Measurements on the Molten-Slat Reactor Experiment During Fuel Circulation: Theory and Experiment," Oak Ridge National Laboratory, ORNL-TM-1626, Oak Ridge, TN, USA, 1966.

[39] P. Haubenreich, "Predictions of Effective Yields of Delayed Neutrons in the MSRE," Oak Ridge National Laboratory, ORNL-TM-380, Oak Ridge, TN, USA, 1962.

[40] M. Rosenthal, R. Briggs and P. Kasten, "Molten-Salt Reactor Program Semiannual Progress Report for Period Ending February 28, 1969," Oak Ridge National Laboratory, ORNL-4396, Oak Ridge, TN, USA, 1969.

[41] J. Engle and P. Haubenreich, "Temperature in the MSRE Core During Steady-State Power Operation," Oak Ridge National Laboratory, ORNL-4396, Oak Ridge, TN, USA, 1962.

[42] R. Steffy, "Experimental Dynamic Analysis of the MSRE with 233U Fuel," Oak Ridge National Laboratory, ORNL-TM-2997, Oak Ridge, TN, USA, 1970.

[43] H. Brey, "Fort St. Vrain Operations and Future," *Energy,* pp. 47-48, 1991.

[44] H. Brey and H. Olson, "The Fort St. Vrain High Temperature Gas Cooled Reactor XIII: Radiological and Sheilding Performance of Fort St. Vrain," *Nuclear Engineering and Design,* pp. 147-152, 1982.

[45] H. Olson, "The Fort St. Vrain High Temperature Gas-Cooled Reactor," *Nuclear Engineering and Design,* pp. 117-123, 1979.

[46] H. Olson, H. Brey and D. Warembourg, "The Fort St. Vrain High Temperature Gas-Cooled Reactor: IX Rise-to-power physics tests," *Nuclear Engineering and Design,* pp. 71-77, 1983.

[47] L. Taylor, "Fort Saint Vrain HTGR (Th/U carbide) Fuel Characteristics for Disposal Criticality Analysis," Unitied States Department of Energy , Idaho Falls, 2001.

[48] W. Martin, J. Lee, B. Betzler, T. Burk, W. Pappo, A. Pavlou and E. Sunny, "Creation of a Full-Core HTR Benchmark with the Fort St Vrain Initial Core and Assessment of Uncertainties in the FSV Fuel Composition and Geometry," University of Michigan, Project No. 09-771, Report No. DE-AC07-05ID14517, Ann Arbor, MI, USA, 2012.

[49] A. HABUSH and R. WALKER, "FORT ST. VRAIN NUCLEAR GENERATING STATION CONSTRUCTION AND TESTING EXPERIENCE," *Nuclear Engineering and Design,* vol. 26, no. 1, pp. 16-26, 1974.

[50] C. Scott and D. Harmon, "IRRADIATION PERFORMANCE OF FORT ST. VRAIN HIGH-TEMPERATURE GAS-COOLED REACTOR FUEL IN CAPSULE F-30," *Nuclear Technology,* vol. 35, no. 2, pp. 442-454, 1977.

[51] W. Pfeifffer, J. Btown and A. Marshall, "Analysis and Results of Pulsed-Neutron Experiments Performed on the Fort St. Vrain High-Temperature Gas-Cooled Reactor," *Nuclear Technology,* vol. 27, no. 3, pp. 352-375, 1975.

[52] J. Brown, R. Hackney, V. Malakhof and W. Simon, "A Review of Fort St. Vrain - A Review," *Nuclear Science and Engineering,* vol. 97, no. 2, pp. 104-122, 1987.

[53] H. Brey, "Fort St Vrain Circulator Operating Experience," in *International Atomic Energy Agency, International Working Group on Gas-Cooled Reactors*, Sandiego, California, USA, November 30 - December 2, 1987.

[54] H. Olson, H. Brey and F. Swart, "The Fort St. Vrain High Temperature Gas-Cooled Reactor IV Rise to power test program," *Nuclear Engineering and Design,* vol. 61, pp. 295-302, 1980.

[55] G. Blockk, "HTGR STARTUP EXPERIENCE AT FT. ST. VRAIN," in *IEEE Transactions on Nuclear Science*, San Deigo, 1975.

[56] A. Marshal and J. Brown, "Loading of Fuel and Reflector Elements in the Fort St. Vrain Initial Core (Results of Start-Up Test A-1)," General Atomic Company, GA-A13101, San Diego, California, 1974.

[57] H. Olson, "The Fort St. Vrain High Temperature Gas-Cooled Reactor I. Low Power Physics Tests," *Nuclear Engineering and Design,* pp. 117-123, 1979.

[58] D. Hoppes, A. Baxter, D. McEachern and W. Arnold, "The effect of Nuclear Detector Decalibration on the Fort St. Vrain Reactor and Suggested Corrective Measures," General Atomics Company, GA-A13954, 1978.

[59] W. Pfeiffer, J. Brown and A. Marshall, "Analysis and Results of Pulsed-Neutron Experiments Performed on the Fort St. Vrain High-Temperature Gas-Cooled Reactor," *Nuclear Technology,* pp. 352-375, 1975.

[60] R. Walker, "Experience with Fort St. Vrain Reactor," *Journal of Nuclear Energy,* pp. 337-356, 1978.

[61] A. Marshall, "TEMPERATURE COEFFICIENTS FOR THE FSV INITIAL CORE," Gulf General Atomics Company, San Deigo, California, 1973.

[62] D. McEachern, J. Brown, R. Heller and W. Franek, "Fort St. Vrain Core Performance," in *American Nuclear Society*, Chattanooga, Tennessee, 1977.

[63] J. Cadwell, D. McEachern, J. Read, W. Simon and R. Walker, "Operational Testing Highlights of Fort St. Vrain," General Atomics, GA-A13602, Denver, Colorado, USA, 1975.

[64] Y. Tachibana, S. Nakagawa, T. Takeda, A. Saikusa, T. Furusawa, K. Takamatsu, K. Sawa and T. Iyoku, "Plan for first phase of safety demonstration tests of the High Temperature Engineering Test Reactor HTTR," *Nuclear Engineering and Design,* vol. 224, 2003.

[65] M. Ogawa and T. Nishihara, "Present Status of Japan's HTTR Status," *Nuclear Engineering and Design,* vol. 233, 2004.

[66] S. Shiozawa, S. Fujikawa, T. Iyoku, K. Kunitomi and Y. Tachibana, "Overview of HTTR design features," *Nuclear Engineering and Design,* vol. 233, 2004.

[67] T. Iyoku, S. Ueta, J. Sumita, M. Umeda and M. Ishihara, "Design of Core Components," *Nuclear Engineering and Design,* vol. 233, 2004.

[68] J. Sumita, M. Ishihara, S. Nakagawa, T. Kikuchi and T. Iyoku, "Reactor internals design," *Nuclear Engineering and Design,* vol. 233, pp. 81-88, 2004.

[69] K. Yamashita, R. Shindo, I. Murata, S. Maruyama, N. Fujimoto and T. Takeda, "Nuclear Design of the High Temperature Test Reactor (HTTR)," *Nuclear Science and Engineering,* vol. 122, pp. 212-228, 1996.

[70] N. Fuijimoto, N. Nojiri and K. Yamashita, "Validation of the nuclear design code system for the HTTR using the criticality assembly VHTRC," *Nuclear Engineering and Design,* vol. 233, pp. 155-162, 2004.

[71] E. Takada, S. Nakagawa, N. Fujimoto and D. Tochio, "Core thermal-hydraulic design," *Nuclear Engineering and Design,* vol. 233, no. 1, pp. 37-43, 2004.

[72] S. Nakagawa, K. Takamatsu, Y. Tachibana, Y. Sakaba and T. Iyoku, "Safety Demonstration Test using High Temperature Engineering Test Reactor," *Nuclear Engineering and Design,* no. 233, pp. 301-308, 2004.

[73] I. A. E. Agency, "Evaluation of High Temperature Gas Cooled Reactor Performance: Benchmark Aanlysis Related to Initial Testing of the HTTR and HTR-10," International Atomic Energy Agency, IAEA-TECDOC-1382, Vienna, Austria, 2003.

[74] Y. Tachibana, K. Hontani, T. Takeda, A. Saikusa, M. Shinozuki, I. Minoru, T. Yyoku and K. Kuitomi, "Procedure to prevent temperature rise of primary upper shielding in high temperature engineering test reactor," *Nuclear Engineerig and Design,* vol. 201, no. 2-3, pp. 227-238, 2000.

[75] S. Takada, "Research and development of passibe cooling system," *Nuclear Engineering and Design,* vol. 233, no. 1-3, pp. 185-195, 2004.

[76] S. Nakagawa, Y. Tachibana, S. Ueta and S. Hanawa, "Performance test of the HTTR," *Nuclear Engineering and Design,* vol. 233, no. 1-3, pp. 291-300, 2004.

[77] N. Fujimoto, Y. Tachibana, A. Saikusa, M. Shinozaki, M. Isozaki and T. Iyoku, "Experience of HTTR construction and operation - unexpected incidents," *Nuclear Engineering and Design,* vol. 233, no. 1-3, pp. 273-281, 2004.

[78] N. Fujimoto, N. Nojiri, Y. Tachibana and T. Mizushima, "Operation of the High-Temperature Engineering Test Reactor (slide presentation)," in *Non-Electric Applications of Nuclear Power: Seawater Desalination, Hydrogen Production and other Industrial Applications*, Oarai, Japan, April 16-19, 2007.

[79] K. Sumita, Y. Kaneko, R. Kurokawa and T. W. Park, "Reactivity Measurement on the Reflected Semi-Homogeneous Critical Assembly by Pulsed Neutron Technique," *Nippon Genshiryoku Gakkai-Shi,* vol. 4, no. 12, 1962.

[80] Y. Kitamura and Y. Eguchi, "Uncertainty Analysis of Temperature Effect on Reactivity in Very High Temperature Reactor Critical Assembly and Establishment of Biases for Benchmark Models," *Nuclear Science and Engineering,* vol. 174, no. 1, pp. 4001-413, 2014.

[81] T. Yamane, H. Yasoda, F. Akino and Y. Kaneko, "Measurement of Overall Temperature Coefficient of Reactivity of VHTRC-1 Core by Pulsed Neutron Method," *Journal of Nuclear Science and Technology,* vol. 27, no. 2, pp. 122-132, 1990.

[82] F. Akino, M. Takeuchi, T. Ono and Y. Kaneko, "Experimental Verification and Analysis of Neutron Streaming Effect through Void Holes for Control Rod Insertion in HTTR," *Journal of Nuclear Science and Technology,* vol. 34, no. 2, pp. 185-192, 1997.

[83] Y. Koneko, "Reactor Physics esearch Activities Related to the Very High Temperature Reactor in Japan," *Nuclear Science and Engineering,* vol. 97, no. 2, pp. 145-160, 1987.

[84] K. Yamashita, I. Murata and R. Shindo, "Analysis of Overall Temperature Coefficient of Reactivity of the VHTRC-1 Core with a Nuclear Design Code System for the High-Temperature Engineering Test Reactor," *Nuclear Science and Engineering,* vol. 110, no. 2, pp. 177-185, 1992.

[85] H. Yasuda, F. Akino, T. Yamane, F. Yoshira, K. Kitadate, H. Yoshifuji, M. Takeuchi, T. Ono and Y. Kaneko, "Construction of VHTRC," Japanese Atomic Energy Research Institute, JAERI-1305, Tokyo, Japan, 1987.

[86] N. Nojiri, S. Shimikawa, N. Fujimoto and M. Goto, "Characteristic Test of Initial HTTR Core," *Nuclear Engineering and Design,* pp. 283-290, 2004.

[87] N. Nojiri, M. Nakano, M. Takeuchi, P. Pohl and K. Yamashita, "Characteristics of HTTRs Startup Physics Tests," in *High Temperature Gas Cooled Reactor Development, Proceedings of Technical Committee Meeting, International Atomic Energy Agency, IAEA-TECDOC-988*, Johannesburg, South Africa, November 13-15, 1996.

[88] N. Fujimoto, Kiyoobu Yamashita, Naoki Nojiri, Mituo Takeuchi, Shingo Fujisaki and Masoaki Nakano, "Annular Core Experiments in HTTR's Start-Up Core Physics Tests," *Nuclear Science and Engineering,* vol. 150, no. 3, pp. 310-321, 2005.

[89] M. Nakano, Nozomu Fujimoto and Kiyonobu Yamashita, "Analytical Estimation of Control Rod Shadowing Effect for Excess Reactivity Measurement of HTTR," in *The 6th Asian Symposium on Research Reactors (ASRR-VI)*, Makaasaar, Indonesia, 1999.

[90] N. Fujimoto, N. Nojiri, H. Ando and K. Yamashita, "Nuclear Design," *Nuclear Engineering and Design,* pp. 23-36, 2004.

[91] C. Till and Y. I. Chang, plentiful energy: the story of the integral fast reactor, the complex history of a simple reactor technoloogy, with emphasis on its scientific basis for non-specialists, CreateSpace, 2011.

[92] C. Stevenson, The EBR-II Fuel Cycle Story, American Nuclear Society, 1987.

[93] C. Pope, R. Stewart and E. Lum, "Experimental Breeder Reactor II," in *Nuclear Reactors - Spacecraft Propulsion, Research Reactors, and Reactor Analysis Topics*, IntechOpen, 2022.

[94] E. Lum, C. Pope, R. Stewart, Byambadorj and Q. Beaulieu, "Evaluation of Run 138B at Experimental Breeder Reactor II, A Prototypic Liquid Metal Fast Breeder Ractor," in *International Handbook of Evaluated Reactor Physics Benchmark Experiments*, OECD/NEA, 2018.

[95] R. Stewart, "Sensitivity and Uncertainty Analysis in the Homogenization of the EBR-II Core," Idaho State University, Pocatello, 2017.

[96] L. Koch, "Experimental Breeder Reactor II (EBR-II) An Integrated Experimental Fast Reactor Nuclear Power Station," Argonne National Laboratory, 2008.

[97] L. Koch, W. Loewenstein, A. Lovoff, H. Hooker, H. Monson, R. Ramp and E. Hutter, "EBR-II Dry Critical Experiments - Experimental Program, Experimental Procedures, and Safety Considerations," Argonne National Laboratory, ANL-6299, Argonne, Illinois, USA, 1961.

[98] F. Kirn and W. Loewenstein, "EBR-II Wet Critical Experiments," Argonne National Laboratory, ANL-6864, Argonne, Illinois, USA, 1964.

[99] W. Loewenstein, "The Physics of the EBR-II," Argonne National Laboratory, ANL-6383, 1961.

[100] R. McVean, G. Brunson, B. Cerutti, W. Loewenstein, F. Thalgott and G. Whitman, "EBR-II Dry Critical Experiments - Experimental Results," Argonne National Laboratory, ANL-6462, 1962.

[101] "EBR-II Sixteen Years of Operations, Summary Repoort," Argonne National Laboratory - West, Idaho Falls, 1980.

[102] I. A. E. Agency, "Liquid Metal Cooled Reactors: Experience in Design and Operation," International Atomic Energy Agency, IAEA-TECDOC-1569, Vienna, Austria, 2007.

[103] J. Tommasi, G. Czernecki, F. Rimpault and F. Varaine, "Analysis of Super-Phenix and Phenix Neutron Physics Experiments with Eranos Code and Data System," in *International Atomic Energy Agency, Technical Meeting on Operational and Decommissioning Experience with Fast Reactors, IAEA-TECDOC-1405*, Cadarache, France, March 11-15, 2002.

[104] J. Gourdan, B. Mesnage, J. Voitellier and M. Suescun, "An Overview of Superphenix Commissioning Tests," *Nuclear Science and Engineering,* vol. 106, no. 1, pp. 1-10, 1990.

[105] G. Flamenbaum, R. de Wouters, A. Le Bourhis, T. Newton and G. Vambenepe, "Superphenix Core Loading Strategy Using teh Checkerboard Pattern," *Nuclear Science and Enginieering,* vol. 106, no. 1, pp. 11-17, 1990.

[106] J. Gauthier, J. Cabrillat, G. Palmiotti, M. Salvatores, M. Giese, M. Carta and J. West, "Measurement and Predictions of Control Rod Worth," *Nuclear Science and Engineering,* vol. 106, pp. 18-29, 1990.

[107] M. Vanier, P. Bergeonneau, J. Gauthier, M. Jacob, J. de Antoni, E. Gesi, P. Peerani and J. Adam, "Superphenix Reactivity and Feedback Coefficients," *Nuclear Science and Engineering,* vol. 106, no. 1, pp. 30-36, 1990.

[108] J. Cabrillat and M. Martini, "Power and Neutron Flux Distributions in the Core and Shielding," *Nuclear Science and Engineering,* vol. 106, no. 1, pp. 37-46, 1990.

[109] J. Grouiller, J. Perrigueur and A. Le Bourhis, "Neutron Monitoring and the Inherent Source of Superphenix," *Nuclear Science and Engineering,* vol. 106, no. 1, pp. 81-87, 1990.

[110] G. Flamenbaum, A. Zaetta, M. Martini, M. Michenot, T. Newton and H. Sztark, "Analysis of Specific Control Rod Experiments Involving Highly Distorted Flux Distributions," *Nuclear Science and Engineering,* vol. 106, no. 1, pp. 64-68, 1990.

[111] P. Bergeonneau, M. Vanier, M. Favet, J. De Antoni, K. Essig and J. Adam, "An Analysis of the Dynamic Behavior of the Core," *Nuclear Science and Engineering,* vol. 106, no. 1, pp. 69-74, 1990.